ANTARCTIC CLIMATE & ECOSYSTEMS CRC

climate futures for tasmania

TECHNICAL REPORT

Extreme Events

White CJ, Grose MR, Corney SP, Bennett JC, Holz GK, Sanabria LA, McInnes KL, Cechet RP, Gaynor SM & Bindoff NL

December 2010

Climate Futures for Tasmania
Extreme Events Technical Report

ISBN 978-1-921197-09-3

The Manager
Communications
Antarctic Climate & Ecosystems Cooperative Research Centre

Private Bag 80
Hobart Tasmania 7001
Tel: +61 3 6226 7888, Fax: +61 3 6226 2440
Email: climatefutures@acecrc.org.au

Disclaimer

The material in this report is based on computer modelling projections for climate change scenarios and, as such, there are inherent uncertainties in the data. While every effort has been made to ensure the material in this report is accurate, Antarctic Climate & Ecosystems Cooperative Research Centre (ACE) provides no warranty, guarantee or representation that material is accurate, complete, up to date, non-infringing or fit for a particular purpose. The use of the material is entirely at the risk of a user. The user must independently verify the suitability of the material for its own use.

To the maximum extent permitted by law, ACE, its participating organisations and their officers, employees, contractors and agents exclude liability for any loss, damage, costs or expenses whether direct, indirect, consequential including loss of profits, opportunity and third party claims that may be caused through the use of, reliance upon, or interpretation of the material in this report.

Science Reviewers

Dr Albert Klein-Tank (Royal Netherlands Meteorological Institute), Paul Fox-Hughes (Bureau of Meteorology), Dr Lisa Alexander (University of NSW) and Dr Sarah Perkins (CSIRO).

The reviewers listed in this report have offered all comments and recommendations in good faith and in an unbiased and professional manner. At no time was the reviewer asked to verify or endorse the project conclusions and recommendations nor was the reviewer privy to the final draft of the report before its release.

The reviewers' role was solely advisory and should not be construed as an endorsement of the project findings by the reviewer or his /her employing organisation. Neither the reviewer nor his/her employing organisation provides any representation or warranty as to the accuracy or suitability of any project findings. Responsibility for all work done in connection with the project remains with the project team.

Photo Credits: Melanie Webb (coverpage), Jennifer Sheridan (p 9), Malcolm Hibberd (pp 32/33) Chris White (pp 47, 63), Shaun Gaynor (p 55), Andrew Wood (p 69), Rachel Brown (p 73) Suzie Gaynor (pp 2, 5, 15, 18/19, 22, 28/29, 35, 38/39, 74, 84)

Graphic Design: Suzie Gaynor

Graphic Layout: Epiphany Public Relations

Citation

White CJ, Grose MR, Corney SP, Bennett JC, Holz GK, Sanabria LA, McInnes KL, Cechet RP, Gaynor SM & Bindoff NL 2010, *Climate Futures for Tasmania: extreme events technical report,* Antarctic Climate and Ecosystems Cooperative Research Centre, Hobart, Tasmania.

TECHNICAL REPORT

Climate Futures for Tasmania: extreme events

White CJ, Grose MR, Corney SP, Bennett JC, Holz GK, Sanabria LA, McInnes KL, Cechet RP, Gaynor SM & Bindoff NL

December 2010

Foreword

The Climate Futures for Tasmania research project is the key source of information for the Tasmanian Government's Climate Change Strategy and a number of the outputs from the project will have long-term strategic implications for emergency management in Tasmania.

The outputs from the Extreme Weather Events module of the project will be helpful in supporting evidence based policy and decision-making in emergency management and emergency responses to more frequent and intense events, including bushfires, floods and storms.

The LiDAR (Light Detection and Ranging) Dataset produced by the project has been an enormous improvement to the quality and quantity of information about the vulnerable coastlines of Tasmania. The LiDAR Dataset is being used to improve mapping and understanding of how certain hazards interact with communities, particularly regarding storm surges and tidal changes due to climate change.

This unique and leading research will enable the Tasmanian Government to work in partnership with stakeholders to assist communities around the State to minimise the adverse effects of climate change by preparing and responding to extreme weather events.

The extreme weather events around the country in early 2011 have highlighted the importance of this project. No longer can we assume that we are immune from the damaging impacts of extreme weather events. Tasmanian communities have to be prepared for these events by obtaining a high level understanding of the impacts of climate change.

This collaborative research project, lead by Professor Nathan Bindoff and authored by Dr Chris White and his team from the University of Tasmania, has demonstrated innovative leadership by involving and engaging external stakeholders on all levels. The outputs from the project are strong and robust, meaning the research is directly applicable to our decision-making processes.

The report has passed the rigours of an external scientific review process. I appreciate the efforts of the respected scientists who provided their expertise and time to confirm the research outcomes. In particular, thank you to Albert Klein-Tank (Royal Netherlands Meteorological Institute), Paul Fox-Hughes (Bureau of Meteorology), Lisa Alexander (University of NSW) and Sarah Perkins (CSIRO).

Tasmanian communities will benefit from this Extreme Weather Events module from the Climate Futures for Tasmania research project and all those involved in the project are to be congratulated for their valuable contribution to emergency management in Tasmania.

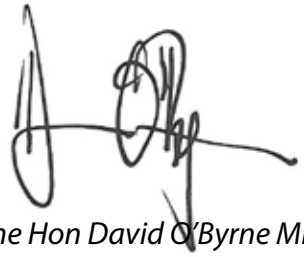

The Hon David O'Byrne MP
Minister for Police and Emergency Management

Executive Summary

The Climate Futures for Tasmania project is the most complete regional climate change study of Tasmania for the 21st century.

Climate Futures for Tasmania is a unique, externally-funded collaborative research project that has generated improved climate change information for Tasmania. We used a dynamical downscaling method to generate climate projections over Tasmania at a resolution of about 10 km. Six global climate models from the IPCC Fourth Assessment Report were used, each for a high and low emissions scenario. The downscaled simulations of mean annual temperature and rainfall produced a spatial correlation of 0.93 and 0.63 respectively when compared to observations for the 1961-1990 reference period. The successful validation of climate simulations gives confidence in projections of future temperature and rainfall and their application to the analysis of extremes.

Hot summer days and heat waves are projected increase.

For most regions of Tasmania under the high A2 emissions scenario, the number of summer days warmer than 25 °C is projected to double or triple, relative to what we have experienced. Some areas of Tasmania will see 40 additional summer days per year by the end of the 21st century. The largest increases in extreme temperatures are projected to occur in the spring and autumn months, with increases of greater than 4.0 °C. This increase is substantially greater than the projected mean temperature change. The greater temperature changes in these seasons imply an extension of the summer season. Heat waves (where maximum temperatures exceed 28 °C for more than three days) will occur more frequently. For example, the number of heat waves at Launceston is projected to increase progressively throughout the century, occurring on average twice per year by 2070-2099, approximately four times more frequent than what we have experienced.

Cold waves are projected to decline.

The frequency of cold waves (defined as three or more consecutive days below 5 °C) show a sharp decrease by the end of the centruy. In the central highlands, the projections show an eight-fold decrease in the number of cold waves.

There will be more frequent and more intense extreme rainfall events interspersed with more dry days.

Extreme wet days will increase in the south-west and north-east with up to seven days (or about 25% more events) per year. The projected increases in the south-west are driven predominantly by the number of winter events, with smaller increases in autumn and spring. For the central highlands, there are projected decreases in extreme wet days in all seasons.

The results show a projected increase in peak intensity rainfall events across the whole of Tasmania, with an increase of up to 60% in some seasons, in some coastal regions. Paradoxically, the number of rain days across the whole of Tasmania is likely to decrease. This decrease will be felt most in the north-west.

Drier conditions and wetter conditions on 6-month and 12-month intervals are both likely to increase in the coming century.

Both cumulative rainfall deficits (drier conditions) and surpluses (wetter conditions) are likely to increase towards the end of the century, with normal conditions likely to occur less often in some regions. The patterns of drier and wetter conditions are distributed unevenly over Tasmania; however, the tendency is for an increase of the occurrence of wetter and drier in all regions on these two time intervals. Where annual rainfall increases, there is a lower level of occurrence of drier conditions and greater occurrence of wetter conditions. Where rainfall decreases, there is increased tendency for drier conditions and a decrease in wetter conditions.

Extreme and record rainfall events will become more frequent in the coming century, consistent with a warmer climate.

The broad consistency between the estimates of the average recurrence intervals for 24-hour rain events and those from the observations is notable, providing confidence that the future projections to the changes in the risk of the most extreme rainfall events are plausible. The projections show a substantially greater frequency of events, with the recurrence intervals likely to decrease substantially relative to the 1961-1990 reference period.

The nature of Tasmania's climate will adjust progressively in a manner that is consistent with our understanding of the drivers of Tasmanian weather.

For Tasmania, the pattern of extreme weather is likely to change across a broad range of climate indices by the end of the century. Across these indices, the emerging pattern of change represents a consistent and progressive adjustment of the current climate and its weather patterns to a new climate where there will be more hot days and warm nights, more extreme wet days, an increase in the size of heavy downpours, and more dry days. The intensifying of rainfall events also leads to a tendency for increased drier and wetter conditions on seasonal and annual bases and the reduced occurrence of normal conditions.

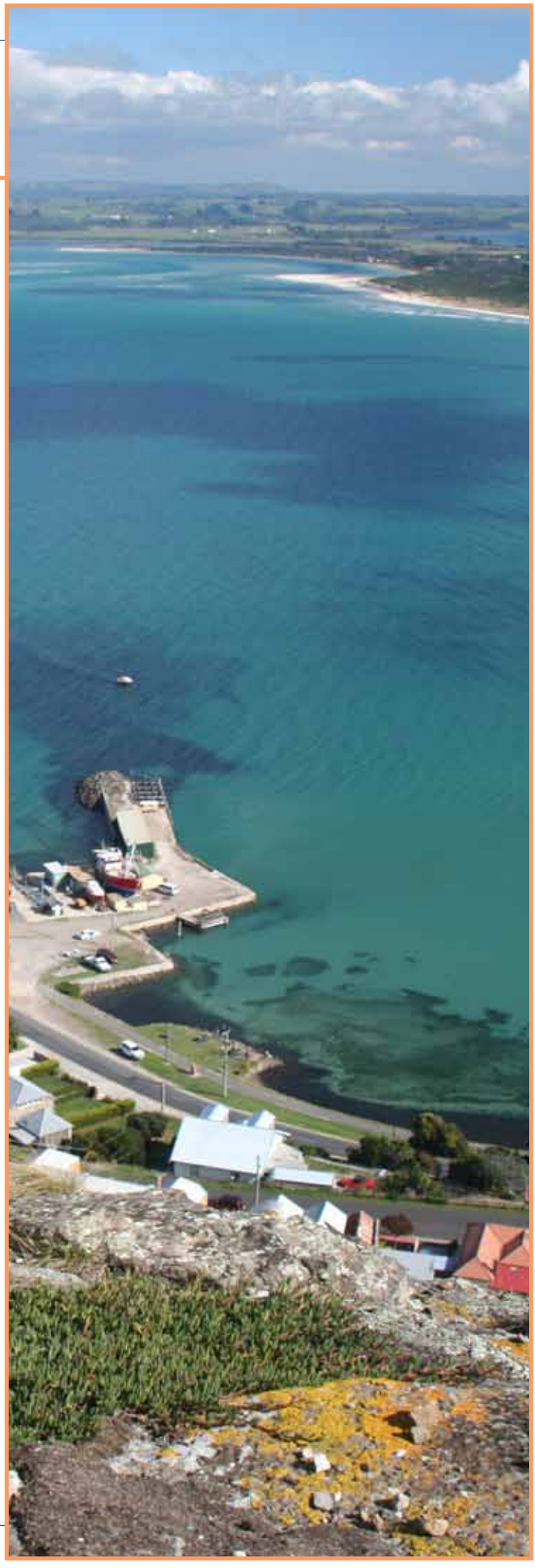

FREQUENTLY USED ABBREVIATIONS

Australian Water Availability Project	AWAP
Fourth Assessment Report	AR4
Average Recurrence Intervals	ARI
Conformal Cubic Atmospheric Model	CCAM
Expert Team on Climate Change Detection and Indices	ETCCDI
Global Climate Model	GCM
Generalized Extreme Value	GEV
Intergovernmental Panel on Climate Change	IPCC
Probability density function	PDF
Standardised Precipitation Index	SPI
Special Report on Emissions Scenarios	SRES
Sea Surface Temperature	SST
Tasmanian Partnership for Advanced Computing	TPAC

ABBREVIATIONS USED FOR GLOBAL CLIMATE MODELS

Australia's CSIRO GCM	CSIRO-Mk3.5
Germany developed GCM	ECHAM5/MPI-OM
USA developed GCM	GFDL-CM2.0
USA developed GCM	GFDL-CM2.1
Japan developed GCM	MIROC3.2(medres)
UK Hadley Centre's GCM	UKMO-HadCM3

Table of Contents

1 Introduction

Scientific evidence that the Earth is warming is unequivocal. There is overwhelming evidence that increased concentrations of greenhouse gases caused by human activity are contributing to this warming (IPCC 2007a). The Intergovernmental Panel on Climate Change (IPCC) concluded that the observed warming over the 20th century of approximately 0.7 °C is consistent with our knowledge of the physical climate system (the atmosphere, oceans, land and sea ice) and its response to increasing greenhouse gases in the atmosphere. Anthropogenic greenhouse warming is caused by a change to the radiative balance of the earth's atmosphere. Global warming also causes changes to precipitation, wind, evaporation, cloudiness and other climate variables. Climate change is also not restricted to changes in the mean state of the atmosphere. Some of the most notable impacts of climate change result from a shift in the frequency and strength of climatic extremes. For example, climate change may lead to a change in the frequency of heatwaves, heavy rains, floods, severe frosts and tropical cyclones.

The projected effects of global climate change are unevenly distributed over the globe. It is because of this spatial variation that local or regional studies are required to understand the effects of climate change on specific areas. Tasmania has a temperate maritime climate with a complex set of influences from nearby oceans. It lies on the border between a region to the north where most global climate models project a drying trend and to the south where most global climate models project a wetting trend (Meehl et al 2007; Christensen et al 2007).

In 2004 Hydro Tasmania commissioned a study to examine the impact of climate change on Tasmania to 2040 (McIntosh et al 2005). The pilot study was undertaken by the Tasmanian Partnership for Advanced Computing (TPAC) and CSIRO. That project served as an initial exploration of the impact of climate change over Tasmania and was fundamental to the creation of the Climate Futures for Tasmania project. A major recommendation of the pilot study was to use multiple climate models and multiple emissions scenarios. These recommendations were adopted in the Climate Futures for Tasmania project. In addition, there was a widening of the scope to include the impact of climate change on agriculture, water and catchments, and extreme events. Climate Futures for Tasmania also feeds into a number of other climate impact studies and also makes climate projection outputs freely available at www.tpac.org.au.

Climate Futures for Tasmania generated climate projections specific to Tasmania through fine-scale climate modelling using a dynamical downscaling method. The study used the CSIRO Conformal Cubic Atmospheric Model (CCAM) to dynamically downscale outputs from global climate models to simulate the Tasmanian climate to 2100. The downscaling method used two IPCC emissions scenarios (SRES A2 and B1) and six global climate models (GCMs) for each emissions scenario (see Corney et al 2010 for full details of the modelling strategy). The A2 emissions scenario better represents observed emissions since 2000 (The Copenhagen Diagnosis 2009) and thus we concentrate on the A2 emissions scenario in this report. By using two emissions scenarios and multiple downscaled simulations of the climate from the six GCMs, it is possible to better quantify the uncertainty in the projections and reduce the effect of model errors on the projections of the future climate. The aim of the study was to produce projections of climate change for the Tasmanian region of sufficient spatial resolution to allow the analysis of climate impacts at different locations within Tasmania (Corney et al 2010). In addition, it aimed to produce projections at sufficient temporal resolution to allow the analysis of changes in seasonality and extreme events.

The project significantly expanded the involvement of end-users from the pilot study. We were driven by the information requirements of end-users, including local and state governments, business, industry and agriculture.

The project complements climate analysis and projections done at the continental scale for the IPCC Fourth Assessment Report (Christensen et al 2007), at national scale in the Climate Change in Australia report and data tool (CSIRO and Bureau of Meteorology 2007), as well as work done in the southeast Australia region in the South Eastern Australia Climate Initiative (SEACI). It also complements projections done specifically on water availability and irrigation in Tasmania by the Tasmania Sustainable Yields Project (CSIRO 2009).

This extreme events technical report represents one of five major components of research undertaken as part of the Climate Futures for Tasmania project. The other four components are presented as a series of reports on climate modelling (Corney et al 2010), general climate impacts (Grose et al 2010), water and catchments (Bennett et al 2010) and impacts on agricultural impacts (Holz et al 2010). In addition,

as part of the extreme events component, further reports are presented covering tidal surges and coastal inundation (McInnes et al in prep) and severe wind hazards (Cechet et al in prep).

The Extreme Events Technical Report covers projected changes to the frequency, magnitude and duration of temperature and precipitation extremes across Tasmania for the 21st century. Section 2 describes extreme events in the Tasmanian region. Section 3 assesses aspects of the performance of models to simulate extremes. Section 4 describes projected changes to temperature extremes up to the end of the 21st century, and Section 5 presents projected changes to precipitation extremes for the same period, including the likely drivers of the projected changes. Section 6 gives a description of projected changes to cumulative precipitation totals and meteorological drought, followed by Section 7 that examines extreme precipitation average recurrence intervals.

Box 1
About the project

Climate Futures for Tasmania is the Tasmanian Government's most important source of climate change data at a local scale. It is a key part of Tasmania's climate change strategy as stated in the Tasmanian Framework for Action on Climate Change and is supported by the Commonwealth Environment Research Facilities as a significant project.

The project used a group of global climate models to simulate the Tasmanian climate. The project is unique in Australia: it was designed from conception to understand and integrate the impacts of climate change on Tasmania's weather, water catchments, agriculture and climate extremes, including aspects of sea level, floods and wind damage. In addition, through complementary research projects supported by the project, new assessments were made of the impacts of climate change on coastal erosion, biosecurity and energy production, and the development of tools to deliver climate change information to infrastructure asset managers and local government.

As a consequence of this wide scope, Climate Futures for Tasmania is an interdisciplinary and multi-institutional collaboration of twelve core participating partners (both state and national organisations). The project was driven by the information requirements of end users and local communities.

The Climate Futures for Tasmania project complements climate analysis and projections done at the continental scale for the Fourth Assessment Report from the Intergovernmental Panel on Climate Change, at the national scale in the *Climate Change in Australia* Report and data tool, as well as work done in the south-east Australia region in the *South Eastern Australia Climate Initiative*. The work also complements projections done specifically on water availability and irrigation in Tasmania by the *Tasmania Sustainable Yields Project*.

2 Defining extreme events

2.1 What are extreme events?

The Intergovernmental Panel on Climate Change (IPCC) Fourth Assessment Report (AR4) (IPCC 2007b) defines an extreme climatic event as one that is rare at a particular place and time of year. On the other hand, Easterling et al (2000) defines an extreme event as one that causes extraordinary economic and social damage and disruption. In this report, we define a climatic extreme as an event (or series of events) with a low (or rare) probability of occurrence, one that occurs with greater intensity or frequency than most climate events. Every region of the world experiences extreme events from time to time. Natural climate variability already produces such events across Tasmania, including heat waves, floods, droughts and storms. Some historical examples of these are listed in Box 2 (Table 2.1). Extreme events can have devastating and wide-ranging effects on society and the environment, including infrastructure, agriculture, utilities, water resources and emergency planning.

Australia suffers more from meteorological disasters (storms) and climatological events (such as drought and heat waves) than other types of natural disaster (Munich Re Geo Risks Research NatCatSERVICE). Munich Re has also reported an increase in both the number of extreme meteorological storms and the rising costs associated with damage claims in Australia since 1980 (Figure 2.1). Note the values shown in Figure 2.1 were not corrected for increased vulnerability when counting the number of events.

It is often difficult to determine whether an extreme event falls within the normal range of variability or is truly a rare event. Instrumental records of climate observations extend to a maximum of 150 years across Australia, so there is limited information to establish the probability of a particular extreme event. Also, extreme events occurring simultaneously are likely to increase the damage than would result from a single event. For example in coastal areas, tidal surges caused by the passage of deep low-pressure systems may also occur at the same time as high-tide events, increasing the likelihood of coastal inundation (McInnes et al 2009). Some research has been undertaken on the current risk of joint occurrences (Svensson and Jones 2004; White 2007).

The focus of this report uses definitions of extreme events in the context of Tasmania, and determines how climate change might alter the characteristics of these events occurring over the rest of this century. This is explored further in the following section.

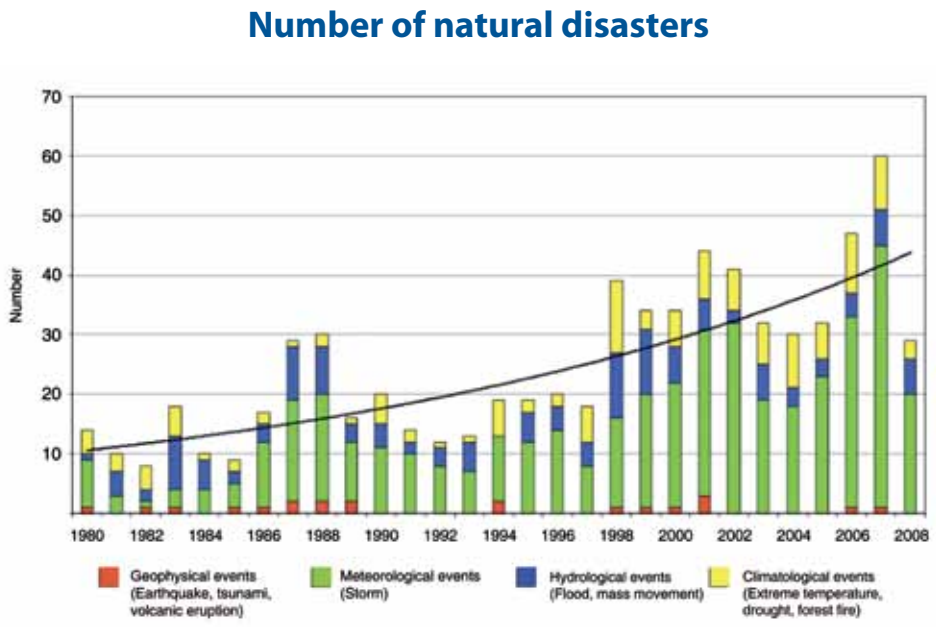

Figure 2.1 Number of natural disasters observed per annum in the Australian region (1980-2009). Reproduced with permission from Munich Re Geo Risks Research NatCatSERVICE. Sourced: May 2009.

Box 2
Historical extreme events in Tasmania

Event type	*Description*
Hot and cold spells	Although Tasmania does not regularly see extreme temperatures like those seen in many parts of the Australian mainland, it does still experience high temperature events. On 30 January 2009 the Bureau of Meteorology recorded the highest temperature on a single day, with 42.2 °C observed at Scamander in the state's north-east (Bureau of Meteorology 2010a). The lowest temperatures observed in Tasmania were on 30 June 1983 in the central highlands at Butlers Gorge, Shannon and Tarraleah, with recorded temperatures as low as -13.0 °C (Bureau of Meteorology 2010a).
Droughts and dry spells	The last century in Australia was characterised by droughts during the 1900s, the 1930s and the 1940s, interspersed with widespread wet conditions in the 1950s and 1970s (Hennessy et al 2008). In Tasmania, while the areas experiencing long-term exceptionally low rainfall have actually decreased slightly since 1900, the shorter-term period 1998-2007 has seen an above average percentage area of exceptionally low rainfall across the state (Hennessy et al 2008). Hobart recently experienced its driest seven months on record (January – July 2010), with just 5.8 mm of rain falling in the month of July compared to an average of 52.0 mm (Bureau of Meteorology 2010b).
Flooding and high rainfalls	The worst flood disaster in Tasmania occurred in northern and eastern regions of the state from 4-6 April 1929. Launceston was particularly affected, resulting in 22 deaths (Bureau of Meteorology 2008). The state record for the highest rainfall in one day occurred at Cullenswood in the north-east, which received 352 mm of rain on 22 March 1974 (Bureau of Meteorology 2010a).
Bushfires	The most devastating bushfire in Tasmania occurred on 7 February 1967. Widespread fires caused 64 deaths and destroyed 1400 homes and structures in the south and east of the state (Haynes et al 2008). Similar extreme bushfire conditions occurred recently on 12 October 2006, causing bushfires across the Meehan Range to the east of Hobart. Fortunately, these were contained and no lives were lost.

Box 3
Defining changes to climatic extremes

Climate change projections indicate that significant changes to the frequency and magnitude of extreme events may result from a relatively small shift in the distribution (Nicholls and Alexander 2007). Further, changes to the variance (or shape) of the distributions may have a larger effect on the frequency of extremes than just a simple shift in the mean (Groisman et al 1999).

To demonstrate this concept, the probability of occurrence of a climatic variable such as temperature can be represented by a probability density function (PDF), commonly referred to as a bell-curve. Figure 2.2 shows example PDFs of daily maximum temperature at Launceston Airport in the north of the state, fitted to the Generalized Extreme Value (GEV) family of distributions. The solid lines represent the baseline (1961-1990) and future (2070-2099) PDFs, with the majority of values near the mean and fewer occurrences at the extreme ends. The shading indicates the extreme parts of the distributions, highlighting events that occur relatively infrequently.

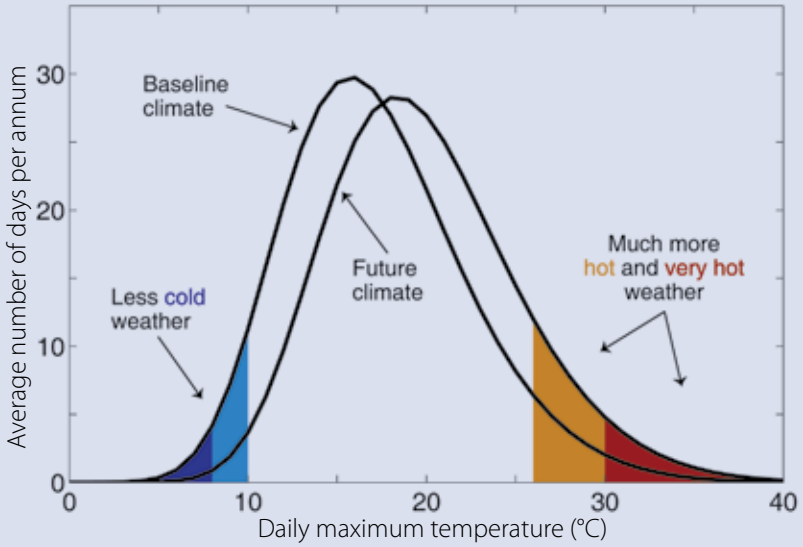

Figure 2.2 Probability density functions (PDF) for simulations daily maximum temperature at Launceston Airport, depicting the effect of changes to the mean and variance. PDF's are fitted to the Generalized Extreme Value (GEV) family of distributions. Average number of days per annum are calculated using the bias-adjusted SRES A2 30-year multi-model projections (six models) for the baseline (1961-1990) and future (2070-2099) climate. Dark blue and light blue shading represents the baseline 1st and 5th percentiles; dark orange and red shading represents the baseline 95th and 99th percentiles respectively.

The effect of a changing climate on temperature extremes is likely to be marked. The projected changes to both the mean and the variance of the PDFs in a future climate demonstrates that there will be a substantial increase in the occurrence of high temperature extremes at one end of the distribution coupled with a more moderate decrease in cold extremes at the other. For example, an increase in the number of hot days will be accompanied by a decline in the number of cold days, with many more hot days and relatively fewer cold days. The projected changes to the variance of the distributions are therefore likely to have a greater effect on the severity and frequency of future extreme events than a shift in the mean alone.

2.2 Impact of climate change on extreme events

During the last decade there has been significant research investigating historical trends in climate events and the possible links between extreme events and observed climate change (for example, Groisman et al 1999; Griffiths et al 2005, Alexander et al 2006, Nicholls and Alexander 2007). These papers and the IPCC (IPCC 2007) concluded that higher maximum and minimum temperatures, more hot days and fewer cold days, and more intense precipitation events have been observed in the latter half of the 20th century. Heat waves can have a significant impact on societies that are not used to coping with such extremes. About 1100 heat-related deaths currently occur each year in Australian temperate cities (McMichael et al 2003). The projected rise in global temperatures, together with anticipated demographic changes, are likely to result in more heat-related deaths in all Australian cities (McMichael et al 2003). Cold-related deaths are expected to decrease, these deaths being greatly outnumbered by additional heat-related deaths (McMichael et al 2003). Climate change may also lead to increased bushfire risk across Australia (Williams et al 2001; Hennessy et al 2005).

The IPCC fourth assessment evaluated extreme climate events in the context of climate change on a global basis. The global climate model (GCM) simulations demonstrated that a gradually warming world would be accompanied by changes in the variability, intensity and frequency of extreme climate events. These changes could occur even with relatively small variations to the mean climate (Meehl et al 2007). In other words, a small change of the mean of a climate variable (such as temperature) can cause a disproportionally larger change in the variability and frequency of extreme events. This phenomenon is described in Box 3 (Figure 2.2).

3 Modelling the Tasmanian climate

3.1 Climate Futures for Tasmania

Projections of the likely future changes to extreme events, in terms of their frequency, magnitude and duration, is typically calculated using simulations from global climate models (GCM) (often on a global or continental scale) or from perturbed observations (either gridded or point data). However, for the accurate assessment of vulnerability to the changing nature of extreme events at the local scale (for locations such as Tasmania), it is critical to give proper consideration of fine-scale climate processes (Diffenbaugh et al 2005). Most extreme events are of a relatively small spatial scale and often short in duration. Due to the coarse resolution of GCMs, they are often unable to simulate adequately the characteristics of extremes. Kiktev et al (2003), Kharin et al (2005) and Alexander et al (2006) all note that coarse-resolution GCMs simulate temperature extremes reasonably well. However, Kiktev et al (2003), Kharin et al (2005), Sun et al (2006) and Kharin et al (2007) all show that GCMs have less success in simulating precipitation extremes, with most GCMs found to underestimate high-intensity precipitation events and simulate too many days of light precipitation (Sun et al 2006).

Recent advances in climate modelling techniques have developed high-resolution downscaled GCMs that allow for the simulation of extreme climatic events at an appropriate scale. The Climate Futures for Tasmania project has produced high-resolution dynamically downscaled GCM projections of the Tasmanian climate to the year 2100. The project provides a unique opportunity to use downscaled climate change projections to produce likely changes to extreme events at the regional scale for the state. The use of dynamical downscaling in this project to increase the spatial and temporal resolution of the simulated climate allows for increased fidelity of the extremes relative to the low-resolution GCMs, and this is important for accurate simulation of extreme precipitation events (Corney et al 2010).

This chapter provides the context and framework for the interpretation of the downscaled projections of extreme events for Tasmania. A full account of the modelling strategy, methods used and an evaluation of the modelling from the project can be found in Corney et al (2010).

3.2 Dynamical downscaling

Climate models are designed to simulate the main components of the earth's climate system in a simplified but robust manner. These components are the atmosphere, ocean, sea ice and land surface. For climate change studies, global climate models are run as a closed system, and once initialised they operate independently from observations. This analysis considered the atmospheric composition under two scenarios of anthropogenic emissions of greenhouse gases and aerosols over the next century. These scenarios are known as the A2 and the B1 emissions scenarios, created for the special report of emissions scenarios (SRES) of the IPCC (Nakićenović and Swart 2000). The A2 scenario has higher emissions than the B1 that result in a stronger climate response; the B1 scenario has lower emissions that result in a weaker climate response. It is worthwhile adding that the current anthropogenic emissions over the last decade have tracked above the A2 emissions scenario (Le Quéré et al 2009).

The downscaling was performed using the CSIRO stretched grid global Conformal Cubic Atmospheric Model (CCAM) (McGregor and Dix 2008). The only forcing taken from GCMs was sea surface temperature (SST) used as a bottom boundary condition. Persistent biases in the mean seasonal climate of the SST for the reference period of each GCM in the current climate were assessed against the Reynolds SST dataset (Reynolds 1988), and these biases were quantified and removed from the forcing SSTs prior to the downscaling process. The SST was also interpolated on to the relevant grid scale to characterise more accurately the ocean-land interface at a higher resolution. The downscaling process was carried out in two stages: firstly from the original grid resolution (200 to 300 km) down to a 0.5-degree latitude/longitude grid, and secondly from this 0.5-degree grid down to a 0.1-degree (about 10 km) grid across Tasmania.

A single simulation using a prescribed emissions scenario gives a single projection analogous to a single replication of an experiment. More simulations give further replications of that experiment and help to give an estimate of the range of possible outcomes for a given emissions scenario. For this reason, the project has undertaken the maximum number of simulations that time and resources allowed, with the downscaling of six GCMs (CSIRO-Mk3.5, GFDL-CM2.0, GFDL-CM2.1, ECHAM5/MPI-OM, UKMO-HadCM3 and MIROC3.2(medres)) for both A2 and B1 emissions scenarios. The six GCMs were chosen for their performance over the Australian region (Corney et al 2010). Multi-GCM ensemble simulations also generally provide more robust information than simulations from any single model (Meehl et al 2007). As such, a multi-GCM mean calculated from the six

downscaled simulations is typically used in this report, with an associated range of uncertainty for the future projections of the extremes (Appendix B).

3.3 Topography

The process of downscaling using CCAM allows for interactions of synoptic weather patterns with a more realistic topography of Tasmania, resulting in improved simulations of extreme events. The topography in the high-resolution downscaled GCMs (for example, the elevation of each grid cell) is based on the elevation of the area within each 0.1-degree cell using a 250 m digital elevation model (DEM) (Appendix A). In Tasmania, there are often sharp altitudinal gradients within each of the 0.1-degree grid cells, therefore there may be substantial topographical variations within each grid cell that are not represented in the downscaled GCM topography. This issue of model resolution means that, for example, the highest points in the models occur to the east around the central plateau where the land is uniformly high. Thus, when a grid cell covers a region containing strong altitudinal gradients, a specific point of interest within that cell may not necessarily be well represented by the average value of that cell.

3.4 Bias-adjustment

While the downscaled GCMs displayed a high level of skill in simulating most variables across the majority of the state (Corney et al 2010), some errors and persistent biases with a distinct spatial pattern were identified at certain high and low ranges of the frequency distribution when compared to observations. Capturing the correct magnitudes of events are important for extreme events analyses requiring daily datasets that replicate the absolute scale and range of observations with a high level of precision. This is particularly relevant for precipitation extremes that are typically localised phenomena, resulting from the complex interaction between temperature, moisture, winds and topography. As such, the magnitudes of extreme precipitation events can vary greatly over relatively short distances and elevations. For reporting trends in climate extremes, the slight bias in the climate simulations does not adversely affect the output (for example, the frequency of extreme events). However, to enable the simulations to be used for the specific assessment of changes to the magnitude and duration of extreme events (for example, the count of days exceeding a given threshold) the small biases in the simulations are removed.

A series of bias-adjusted simulations were created using the period 1961-2007 where both observations and simulations are available. The bias-adjustment process modified the absolute magnitudes of the downscaled simulations, while retaining the frequency and trends in the projections. The bias-adjustment process was based on a percentile binning method (Corney et al 2010), using the Australian Water Availability Project (AWAP) 0.05-degree grid of daily data as the observations (Jones et al 2009; Raupach et al 2008). The adjustment process was applied on a daily, cell-by-cell basis for each of the land cells for five climate variables, including daily minimum temperature, daily maximum temperature and daily precipitation. The bias-adjustment forced the adjusted probability density functions (PDFs) to have a very similar distribution to the AWAP gridded observations at all the percentile levels for 1961-1990.

Figure 3.1 shows four examples of the bias-adjusted data from a range of locations across Tasmania with distinctly different rainfall patterns. Raw and bias-adjusted PDFs of daily minimum and maximum temperature, and daily precipitation, at four representative locations are compared with AWAP gridded observations for the 1961-1990 period. The amount of adjustment from the raw simulations to the bias-adjusted data simulations was, as expected, greater at some locations than at others. For example, Launceston (Figure 3.1) has a proportionately higher level of adjustment applied to the magnitudes compared to other locations; this is particularly the case for the daily precipitation events exceeding the 90th percentile that were typically too high in the raw simulations compared with the AWAP gridded observation dataset (Corney et al 2010).

A key objective of the bias-adjustment process was to maintain the distributions present in the individual downscaled GCMs, while adjusting the magnitudes of the variables to the same absolute scale as observations. To assess the success of the bias-adjustment process, a sample of the results of the bias-adjusted projections for daily temperature and precipitation compared with AWAP gridded data for 1961-1990 is shown in Table 3.1 at four representative locations across the state using simple temperature and precipitation indices important for extremes. The results show that the bias-adjustment process described in Corney et al (2010) was largely successful in adjusting the magnitudes of the daily downscaled simulations relative to AWAP for the 1961-1990 hindcast period, such that the observed and simulated values are generally within the range of the six downscaled simulations (Table 3.1).

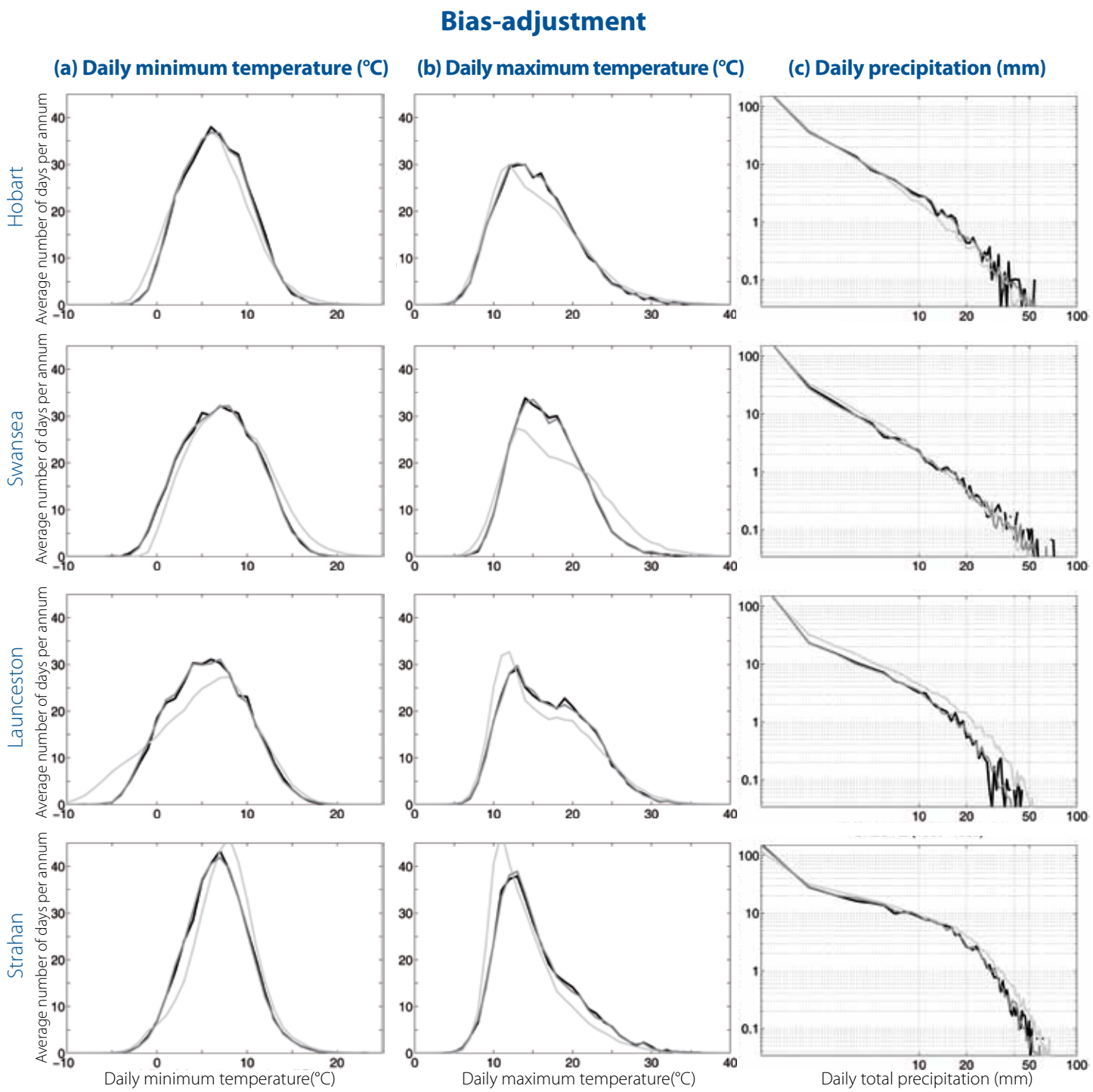

Figure 3.1 Histograms of a) daily minimum temperature, b) daily maximum temperature, and c) daily precipitation at four selected locations across Tasmania for the 1961-1990 period. Plots compare histograms of the raw simulations (light grey lines), bias-adjusted simulations (dark grey lines) and AWAP gridded observations (black lines). All histograms show values calculated using the multi-GCM mean of the six downscaled-GCMs for the A2 emissions scenario. Location of sites is shown in Appendix A.

Table 3.1 Summary results of the bias-adjusted extreme temperature and precipitation at four locations across Tasmania, comparing AWAP gridded observations and the bias-adjusted downscaled simulations of the six downscaled-GCMs for 1961-1990. Multi-GCM range in brackets (). Location of sites is shown in Appendix A.

Location	Count of days <0 °C per annum		Count of days >25 °C per annum		Maximum daily precipitation per annum (mm)	
	AWAP	Multi–GCM mean	AWAP	Multi–GCM mean	AWAP	Multi–GCM mean
Hobart	5	5 (4/5)	18	18 (17/19)	44	49 (44/56)
Swansea	9	8 (7/10)	17	17 (17/18)	52	59 (54/64)
Launceston	29	30 (28/33)	29	29 (28/31)	33	34 (31/36)
Strahan	6	5 (5/6)	19	19 (18/19)	49	49 (49/50)

The bias-adjusted simulations have been used for the future projections of temperature and precipitation extremes in this report up to 2100 using predefined extreme indices (Section 4 and Section 5). However, for the most extreme values in bias-adjusted simulations (for example, below the 0.5th and above the 99.5th percentiles) the extreme indices were found to be distorted slightly through the bias-adjustment process (Corney et al 2010) and are therefore unsuitable for the estimation of average recurrence intervals that have shorter return periods than is represented in the bias-adjusted simulations. In this case, the average recurrence intervals (Section 7) were estimated directly from the unadjusted downscaled simulations and applied to AWAP as percentage-change anomalies to provide consistent results to the extreme indices. This is discussed further in Section 7.

3.5 Uncertainties in the future projections

Uncertainties in the future temperature and precipitation extreme projections are associated with the downscaling process, the resolution and topography in the downscaled GCMs and the selection and composition of the emissions scenarios. Haylock et al (2006) examined the ability of both statistical and dynamical downscaling of GCMs to simulate extreme precipitation, concluding that no single downscaling system consistently outperformed the others, and urging the use of as many different types of downscaling models, GCMs and emissions scenarios as possible to assess changes in extremes at the regional scale.

While we used only one downscaling system (see Section 3.2), the projections presented in this report have been based on the best available understanding of dynamic climate processes. Further, there has been a calibration of the simulations with observations through the bias-adjustment process, thus the persistent biases in the simulations have been removed. The scenario uncertainty is considered by modelling two possible climate futures (A2 and B1 emissions scenarios) in order to present a credible range of future climate. The model uncertainty is included through the use of the six downscaled-GCM projections. All six simulations for extremes (that is, estimates of indices or average recurrence intervals) have been typically averaged to provide a 'most likely' future scenario, together with an associated range of uncertainty (discussed further in Sections 4.2.2 and 5.2.2). While every effort has been taken to include the uncertainty of future extremes as part of this report, there still remains a measured and plausible level of uncertainty around the future projections of extremes.

4 Projected changes to extreme temperatures

4.1 Extreme temperature indices

Extreme events can be categorised by the number of events above a (historical) percentile or threshold value (frequency), by the total amount or magnitude (intensity), by the percentage of time of occurrence or length of events (duration), and by seasonal patterns or distributions (timing). A suite of extreme temperature indices, developed by the Expert Team on Climate Change Detection and Indices (ETCCDI), provides a comprehensive description of changes to extremes using these categories. These indices are summarised in Table 4.1.

Definitions for temperature-based and precipitation-based indices, first suggested in Frich et al (2002) for the estimation of climatic extremes, were submitted to the World Climate Research Programme's (WCRP) Coupled Model Intercomparison Project phase 3 (CMIP3) archive at the Program for Climate Model Diagnosis and Intercomparison (PCMDI). Tebaldi et al (2006) demonstrated the application of 10 indices to historical and future projections of extreme events from GCMs. A larger suite of 27 definitions of extreme indices was subsequently developed for the measurement and characterisation of extreme climate variability and climate change using observations and modelled GCM outputs by the CCI/CLIVAR/JCOMM ETCCDI panel. Alexander et al (2006) used the ETCCDI definitions for the estimation of observed trends in global climatic extremes. Trends in observed and modelled future projections across the Australian region were also analysed in Alexander and Arblaster (2009) using the CMIP3 archive.

The ETCCDI indices have been used in this chapter to demonstrate projected future changes to the magnitude, frequency and duration of extreme temperature events across Tasmania using the bias-adjusted dynamically downscaled GCM projections. Consistent with the IPCC assessments and many other previous studies, the projections of each of the extreme temperature indices are presented as 30-year mean values. The future climate is described using three 30-year periods (2010-2039, 2040-2069 and 2070-2099), each relative to the 30-year baseline period (selected as 1961-1990). The projections for each index are summarised in Appendix B as a statewide value and at eight representative locations across Tasmania for each of these periods. The results are presented as a multi-GCM mean index, calculated for each of the six downscaled-GCM simulations independently from each other and the results averaged (for each 30-year period) to give the central estimate (referred to as a multi-GCM mean in this report). The range of uncertainty associated with a multi-GCM mean is summarised for each index in Appendix B, presented as a maximum and minimum range estimated from each of the bias-adjusted downscaled GCM simulations.

4.2 Evaluation of temperature indices

4.2.1 Performance for temperature extremes

The ability of our dynamically downscaled GCMs to simulate current temperature extremes with some degree of fidelity is a necessary (but not wholly sufficient) condition to project future climates reliably. Poor skill in simulating present climatic extremes could indicate that some physical or dynamical processes have not been sufficiently well included (Meehl et al 2007).

Corney et al (2010) found the bias-adjusted simulations produced for the Tasmanian climate displayed a high level of skill in reproducing the recent climate across a range of climate variables, noting for example that the downscaled multi-GCM mean of average daily maximum temperature for the 1961-1990 baseline period was within 0.1 °C of the Bureau of Meteorology observed value of 10.4 °C for the state.

Summary tables in Appendix B present results for each of the extreme temperature indices for the 1961-1990 baseline period as 30-year means. The temperature indices have been calculated for both the Australian Water Availability Project (AWAP) dataset and the bias-adjusted dynamically downscaled simulations to enable evaluation of the downscaling performance for temperature extremes. Table B.1 to Table B.9 (in Appendix B) show there to be a high degree of agreement between AWAP dataset and the range of the six downscaled simulations for each of the temperature indices at the eight representative locations across Tasmania. For the majority of temperature indices calculated, including both the high-temperature extreme indices (such as summer days (SU) and warm-spell duration index (WSDI)) and the cold-temperature extreme indices (such as frost days (FD)), the range of the downscaled simulations for the 1961-1990 baseline period includes values estimated from the AWAP dataset. In many cases, the multi-GCM mean displays a precise match with the corresponding AWAP value, providing confidence in the ability of the dynamical downscaling and bias-adjustment processes in reproducing the baseline climate indices for temperature extremes. This level of skill in describing the baseline climate indices provides confidence that the models are able to make realistic projections of temperature extremes up to the end of the century.

Extreme temperature indices

Table 4.1 Summary of extreme temperature indices developed by the ETCCDI panel. Precise index definitions can be viewed at cccma.seos.uvic.ca/ETCCDI. Extreme temperature indices were calculated using daily maximum (***TX***) and minimum (***TN***) temperature values in °C.

Index name	Code	Index definitions	Units
Frost days	***FD***	Annual count of days when daily minimum temperature (***TN***) <0 °C	days
Number of summer days	***SU***	Annual count of days when daily maximum temperature (***TX***) >25 °C	days
Number of icing days	***ID***	Annual count of days when daily maximum temperature (***TX***) <0 °C	days
Number of tropical nights	***TR***	Annual count of days when daily minimum temperature (***TN***) >20 °C	days
Max value of daily max temperature	***TXx***	Monthly maximum value of daily maximum temperature (***TX***)	°C
Max value of daily min temperature	***TNx***	Monthly maximum value of daily minimum temperature (***TN***)	°C
Min value of daily max temperature	***TXn***	Monthly minimum value of daily maximum temperature (***TX***)	°C
Min value of daily min temperature	***TNn***	Monthly minimum value of daily minimum temperature (***TN***)	°C
Cold nights	***TN10p***	Percentage of time when daily minimum temperature (***TN***) <10th percentile of daily minimum temperature for the 1961-1990 baseline	%
Cold days	***TX10p***	Percentage of time when daily maximum temperature (***TX***) <10th percentile of daily maximum temperature for the 1961-1990 baseline	%
Warm nights	***TN90p***	Percentage of time when daily minimum temperature (***TN***) >90th percentile of daily minimum temperature for the 1961-1990 baseline	%
Warm days	***TX90p***	Percentage of time when daily maximum temperature (***TX***) >90th percentile of daily maximum temperature for the 1961-1990 baseline	%
Warm spell duration index	***WSDI***	Annual count of days for periods of >5 consecutive days when daily maximum temperature (***TX***) >90th percentile of daily maximum temperature for the 1961-1990 baseline	days
Cold spell duration index	***CSDI***	Annual count of days for periods of >5 consecutive days when daily minimum temperature (***TX***) <10th percentile of daily maximum temperature for the 1961-1990 baseline	days
Diurnal temperature range	***DTR***	Monthly mean difference between daily maximum temperature (***TX***) and daily minimum temperature (***TN***)	°C
Extreme temperature range	***ETR***	Difference between the highest and lowest temperature values per annum	°C

4.2.2 Uncertainties and limitations

Factors such as the dynamical downscaling process, the topography in the downscaled GCMs, the skill of bias-adjustment process and uncertainties associated with the future emissions scenarios all need to be taken into account when applying the future projected changes to the temperature extremes presented in this chapter (see Section 3.5). Although the central estimate from multiple simulations generally provides more robust information than simulations from any single model (Meehl et al 2007), there remains a range of uncertainty with it. Therefore, the multi-GCM mean for each index (summarised in Table B.1 to Table B.9 in Appendix B) is calculated with an associated range of uncertainty, presented as a maximum and minimum range from the six individual bias-adjusted dynamically downscaled GCM simulations. The maximum and minimum range of uncertainty for each temperature index shows a consistent spatial pattern across the state. For example, the index for frost days (FD) displays a small maximum and minimum range (typically ±1 day relative to the multi-GCM mean for both A2 and B1 emissions scenarios) for the statewide mean (Table B.1) and at the majority of locations across the state (Table B.2 to Table B.9) throughout the century. Similarly, the index for warm days (TX90p) also shows a consistent spatial pattern across the selected locations, with the maximum and minimum range typically ±2 days relative to the multi-GCM mean at most of the representative locations across the state. However, the scale of the ranges of uncertainty across the indices suggest that, in general, the warmer end of the temperature distribution (for example, indices calculated using daily maximum temperature) has a larger range of uncertainty in the projections than the colder end of the distribution (for example, indices calculated using daily minimum temperature). The results suggest that while the six downscaled simulations are largely in agreement and provide consistent and plausible projections of the future range of possible temperature extremes, greater uncertainty is likely in the upper end of the extreme temperature distributions compared with the lower end.

4.3 Results

The extreme temperature indices presented in this section are for the A2 emissions scenario only. However, each index has been calculated for both A2 and B1 emissions scenarios and are summarised in Appendix B. Note that for the temperature index figures, white-to-blue colour bars demonstrate the cold extremes (for example, indices using daily minimum temperatures, or to signify projected cooling trends) and white-to-red colour bars show the hot extremes (for example, indices using daily maximum temperatures, or to signify projected warming trends).

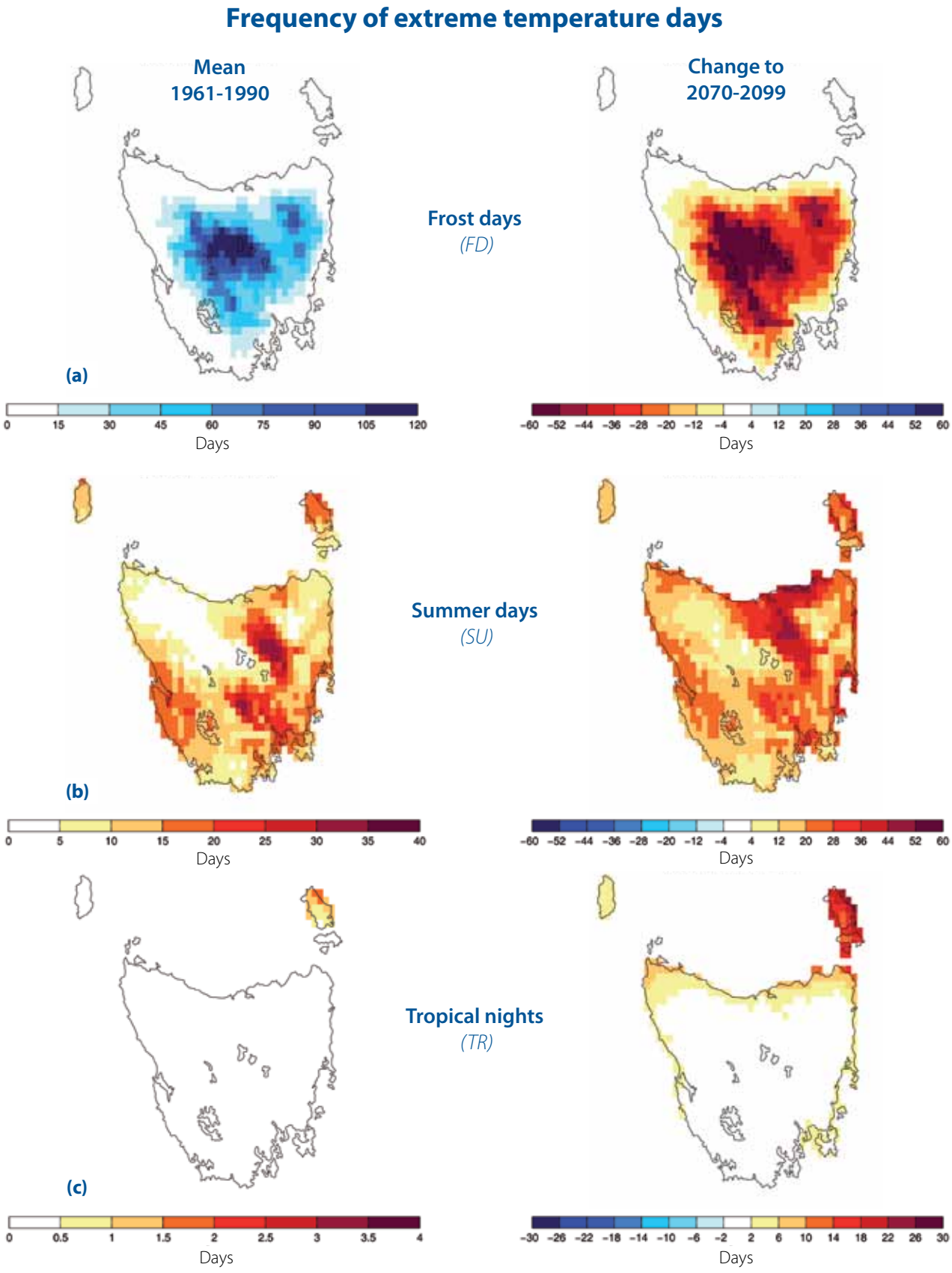

Figure 4.1 Annual number of extreme temperature days, showing a) the number of frost days (*FD*) below 0 °C, b) the number of summer days (*SU*) above 25 °C, and c) the number of tropical nights (*TR*) above 20 °C. Left panels show the mean annual number of days for the baseline 1961-1990 period for each index; right panels show the change in the mean annual number of days for the future 2070-2099 period relative to the 1961-1990 baseline. All plots show values calculated using the multi-GCM mean of the six downscaled- GCMs for the A2 emissions scenario. Definitions for indices are shown in Table 4.1.

4.3.1 Changes to the frequency of extreme temperature events

Using the ETCCDI indices, changes to the frequency (that is, how often an event occurs) of extreme temperature events has been calculated using the bias-adjusted downscaled simulations (Figure 4.1). Projected changes to the distributions of daily maximum and minimum temperature have a large effect on the frequency of both cold and hot extreme events.

The results show a large decrease can be expected in the number of frost day events (where daily minimum temperature is less than 0 °C), which will change progressively throughout the century (Figure 4.1a). The greatest decreases are projected at higher elevations across the state that currently experience the highest number of frosting events. For example, at Miena/Liawenee in the central highlands, the frequency of frost days is projected to decrease by approximately 63 days per annum on average (or about 50%) under the A2 emissions scenario by 2070-2099 (Figure 4.1a and Table B.9 in Appendix B).

At the other end of the temperature distribution, there is an increase in the number of summer days (where daily maximum temperature is greater than 25 °C) and tropical nights (where daily minimum temperature is greater than 20 °C) by the end of the century (Figure 4.1b,c). The projected increase in the number of summer days (Figure 4.1b) occurs across the whole ofTasmania, with the larger increases occurring at lower elevations, particularly throughout the midlands. The pattern of change of summer days is largely an enhancement of the baseline distribution of summer days, with many regions experiencing up to a threefold increase in the number of summer days relative to the 1961-1990 baseline period. At Launceston for example, the frequency of summer days is projected to increase by approximately 46 extra days per annum on average under the A2 emissions scenario by 2070-2099 (Figure 4.1b and Table B.5 in Appendix B), from an average of 29 days in the 1961-1990 baseline period.

In contrast to summer days, there are few tropical nights in the 1961-1990 baseline period (mainly being limited to Flinders Island). However, by the end of the 21st century, tropical nights are projected to occur about 10 times per year in the western, eastern and northern coastal regions of Tasmania and across the Bass Strait islands (Figure 4.1c). The increase in the number of tropical nights from less than 1 night per year to 10 times per year (with up to 30 additional days per annum on average on Flinders Island) is part of a significant increase in the frequency of warmer nights. The projected decreases in the occurrence of frosts, combined with the increase in summer days and tropical nights, reflects a change in the distribution of the temperature relative to the baseline period. To demonstrate this change to the temperature distribution, Figure 4.2a-d shows projections of the average percentage of time in the 2070-2099 period that is likely to experience temperatures above and below the daily minimum and maximum 10th and 90th percentiles calculated from the 1961-1990 baseline period. These are referred to as cold and warm nights, and cold and warm days.

Progressively throughout the century, there is likely to be a substantially greater percentage of time above the warm baseline 90th percentile values (for example, more warm days and nights) compared to a more moderate change in the percentage of time below the corresponding cold baseline 10th percentile values (for example, fewer cold days and nights). As an example, the number of warm nights (Figure 4.2b) is projected to increase in frequency by two-three times relative to the baseline period across the state by 2070-2099. In contrast, cold nights (Figure 4.2a) are projected to decrease in frequency in parts of the central highlands and south-west to the extent that the future 10th percentile value has no overlap with the reference period. These projections are particularly noteworthy. The frequency of warm days (Figure 4.2d) exceeding the 90th percentile value in the baseline 1961-1990 period occurs (by definition) on about 36 days per year; by the end of 21st century however, warm days are projected to occur between 58 days per year (in the south-west) and 102 days per year (in northern coastal regions). These results for 10th and 90th temperature percentiles correspond to the result illustrated in Box 3 where the warmer end of the distribution is more affected than the colder end.

It is also useful to determine whether the frequency of events that extend over multiple days is also likely to change, particularly with reference to heat waves. In addition to the ETCCDI indices (Table 4.1), more appropriate definitions of cold and heat waves have been defined for the Tasmanian region. Heat waves have been defined for Tasmania as events where three or more consecutive days exceed 28 °C, a critical threshold used to model agricultural pasture growth stress (Holz et al 2010), and cold waves for Tasmania have been defined as events where three or more consecutive days are below 5 °C.

Hot and cold days and nights

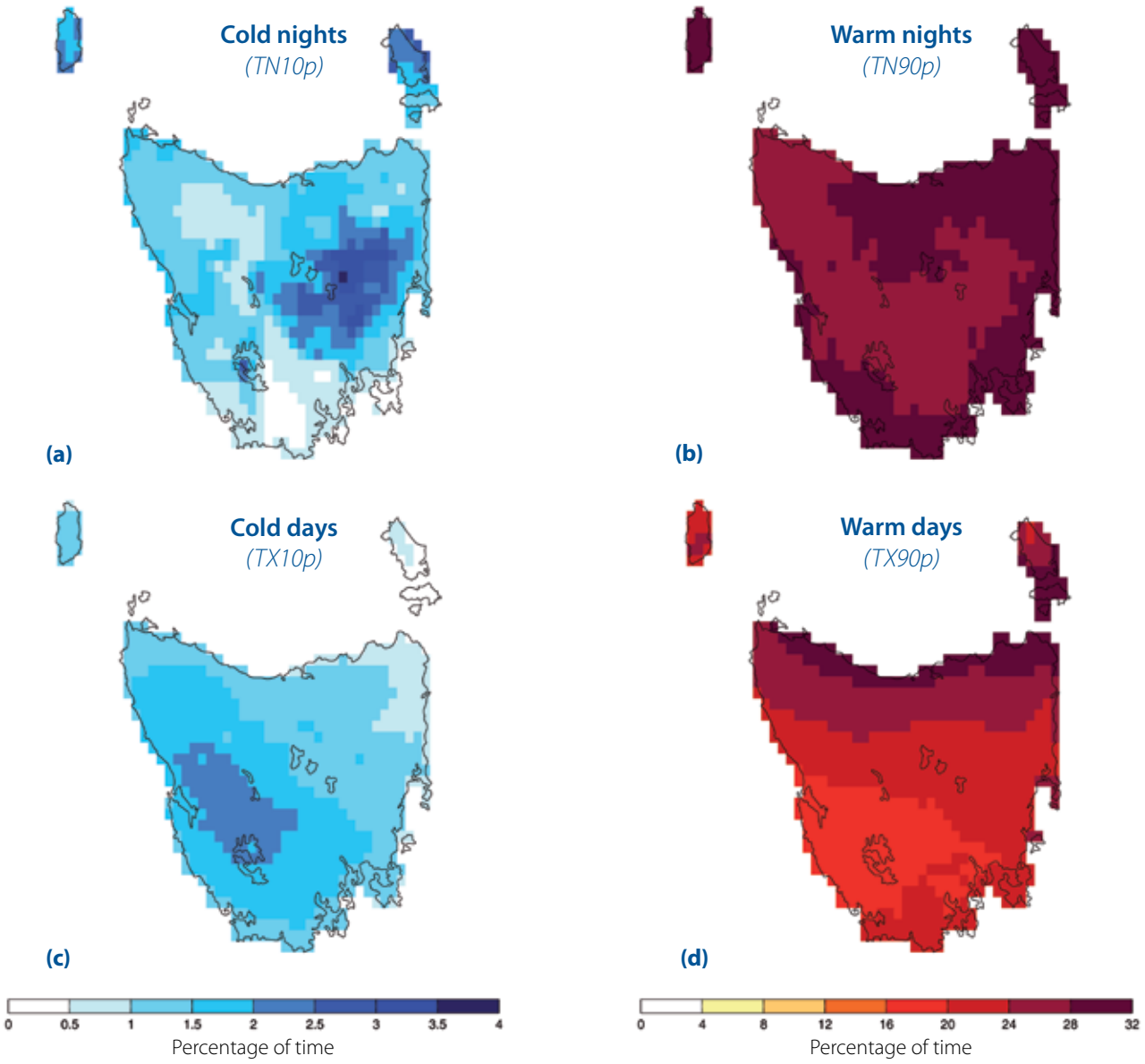

Figure 4.2 Hot and cold days and nights, showing a) cold nights (*TN10p*) defined as the percentage of time (in %) for the future 2070-2099 period where daily minimum temperature <10th percentile of daily minimum temperature of the 1961-1990 baseline, b) warm nights (*TN90p*) defined as the percentage of time (in %) for the future 2070-2099 period where daily minimum temperature >90th percentile of daily minimum temperature of the 1961-1990 baseline, c) cold days (*TX10p*) defined as the percentage of time (in %) for the future 2070-2099 period where daily maximum temperature <10th percentile of daily maximum temperature of the 1961-1990 baseline, and d) warm days (*TX90p*) defined as the percentage of time (in %) for the future 2070-2099 period where daily maximum temperature >90th percentile of daily maximum temperature of the 1961-1990 baseline. All plots show the 2070-2099 mean calculated using the multi-GCM mean of the six downscaled-GCMs for the A2 emissions scenario. Definitions for indices are shown in Table 4.1.

Figure 4.3a compares the frequency of heat waves between the 1961-1990 baseline period and the 2070-2099 future period. Areas that are projected to have increases in the frequency of heat waves through the 21st century include the midlands up to the northern coast, the Derwent Valley and the south-west around Macquarie Harbour. An example time series of the frequency of heat wave events at Launceston for 1961 to 2100 (Figure 4.4a) suggests heat waves will continue to increase in frequency and on average may occur twice per annum by the end of the 21st century, approximately four times more frequently than during the 1961-1990 baseline period. This is greater than the future projections of individual summer days, which show a threefold increase in the frequency by the end of the century in the same region (Figure 4.1b and Table B.5 in Appendix B).

In contrast, the frequency of cold-wave events shows a sharp decrease from the 1961-1990 baseline period to the 2070-2099 future period (Figure 4.3b), mainly across regions with high elevations, including the central highlands and Ben Lomond. The projected decline in the frequency of cold-wave events from 1961 to 2100 at Miena/Liawenee (Figure 4.4b) suggests that there is likely to be less than 0.25 cold-wave events per annum on average by the end of the century, a greater than 10 reduction in the frequency of cold waves. These changes are consistent with the projected decreases in the frequency of individual frost days (see Figure 4.1a).

Results for the temperature frequency indices are summarised for the A2 and B1 emissions scenarios (including the range of uncertainty in the projections) for three future 30-year periods in Appendix B.

4.3.2 Changes to the magnitude of extreme temperature events

With an increase in the frequency of high-temperature events projected across the state throughout the century, this section describes where and how the intensities (that is, the magnitudes) of extreme temperature events are projected to change.

Figure 4.5a shows the values of the 99th percentile of daily maximum temperature for the 1961-1990 baseline period, and the relative change annually (Figure 4.5b) and seasonally (Figure 4.5c) for the 2070-2099 future period (the 99th percentile corresponds to a frequency of three to four days per annum in the reference period). The annual changes show an almost uniform change across the state of between 2.0 °C and 3.5 °C, with a tendency for the larger changes to occur inland from the coast across the western half of the state. However, the seasonal pattern of change has more spatial variations broadly consistent with the climate drivers (Grose et al 2010).

The largest increases (greater than 4.0 °C) tend to occur in the spring and autumn seasons, particularly in the midlands and north-east regions. These larger increases in 99th percentile correspond to where the daily mean temperature is also projected to have the largest increases (see Section 6.1 in Grose et al 2010). The larger temperature changes in these seasons imply an extension of higher summer temperatures into the shoulder seasons.

Although percentiles can be a useful statistic, mean annual maximum and minimum temperatures are more often used by planners and engineers to quantify changes to the magnitudes of extremes. Figure 4.6a shows the mean annual maximum temperatures for the 1961-1990 baseline with the change by the 2070-2099 future period. Figure 4.6b shows the equivalent plots of mean annual minimum temperatures using daily minimum temperature projections. The greatest increases to the magnitudes of mean annual maximum temperatures closely correspond to the higher elevations across the state, particularly in the more mountainous western half and around the Ben Lomond area in the north-east. In these regions, the mean annual maximum and minimum temperatures are projected to increase by more than 3 °C relative to the 1961-1990 baseline period. The magnitudes of annual maximum temperatures are projected to increase more evenly across Tasmania and on average with larger magnitudes than annual minimum temperatures, particularly in the regions with lower elevations. This result is an example of the increased frequency of events at the upper end of the distribution relative to the more moderate decrease in the lower end of the frequency distributions (see Box 3 and Figure 4.2).

Results for the temperature magnitude indices are summarised for the A2 and B1 emissions scenarios (including the range of uncertainty in the projections) for three future 30-year periods in Appendix B, shown as a statewide mean and at eight representative locations across Tasmania.

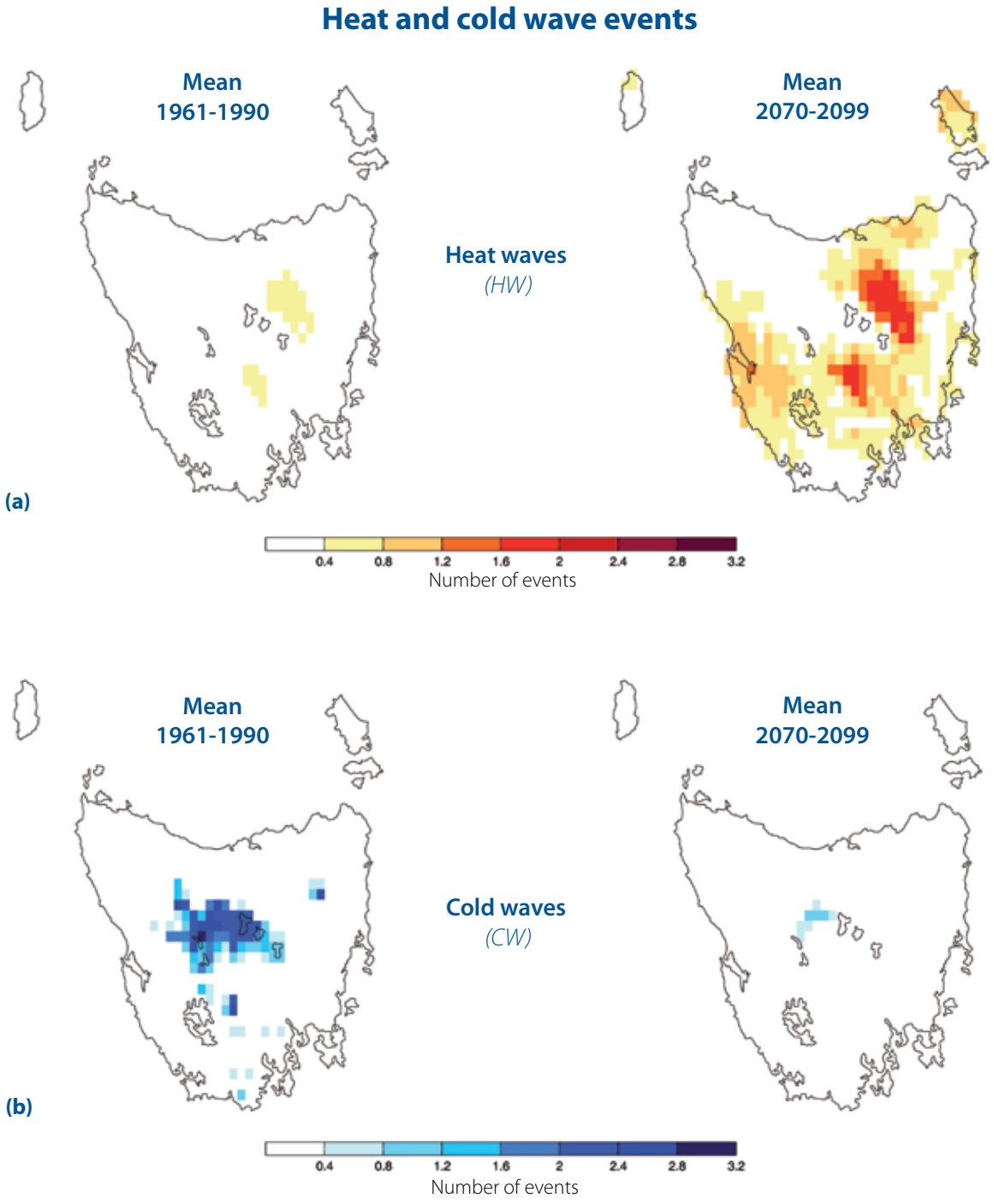

Figure 4.3 Heat and cold wave events, showing a) the average number of heat-wave events (HW) per annum where >3 consecutive days exceed 28 °C, and b) the average number of cold-wave events (CW) per annum where >3 consecutive days are below 5 °C. Left panels show the average number of events per annum for the baseline 1961-1990 period for each index; right panels show the corresponding average number of events per annum for the future 2070-2099 period for each index. All plots show values calculated using the multi-GCM mean of the six downscaled-GCMs for the A2 emissions scenario.

Heat and cold wave events

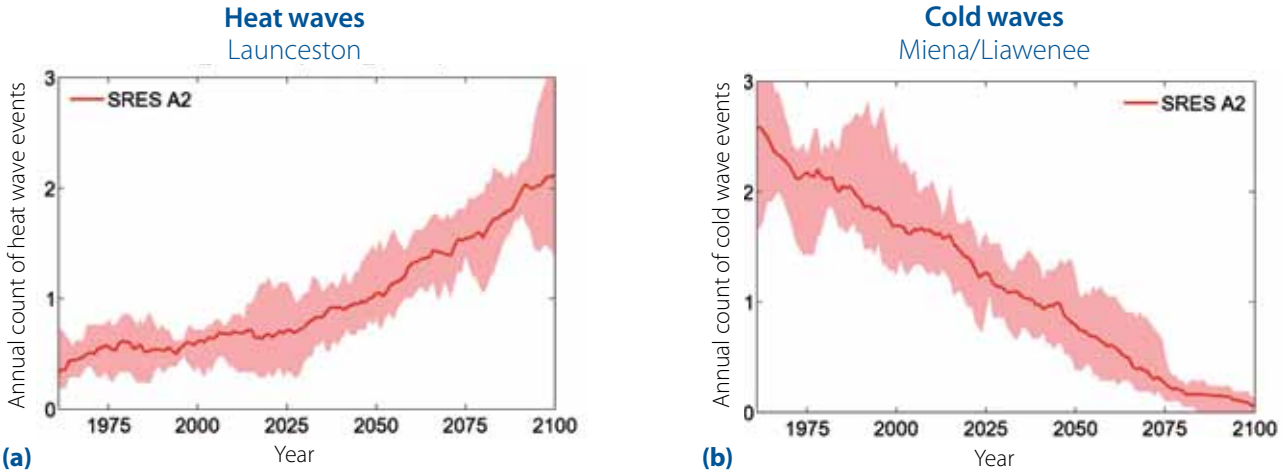

Figure 4.4 Time series of heat- and cold-wave events, showing a) the average number of heat wave events (*HW*) per annum at Launceston where >3 consecutive days exceed 28 °C for 1961-2100, and b) average number of cold wave events (*CW*) per annum at Miena/Liawenee where >3 consecutive days are below 5 °C for 1961-2100. Bold red lines show 11-year running multi-GCM means with the range of the six downscaled-GCMs (light red shading). All plots show indices calculated from the six downscaled-GCMs for the A2 emissions scenario. Location of sites is shown in Appendix A.

4.3.3 Changes to the duration of extreme temperature events

In addition to the projected changes to both the frequency and magnitude of extreme temperature events, it is useful to determine changes to the duration of events (that is, are extreme temperature events likely to get longer or shorter when they occur?). The warm-spell duration index (Figure 4.7a) is defined here as the annual count of days with a duration of five or more days exceeding the 90th percentile of daily maximum temperature for the 1961-1990 baseline period. The warm-spell duration index shows an enhancement of the baseline spatial pattern, with a projected increase in the duration of events through the century. This increase in duration is particularly apparent in the northern half of the state where the average number of days per annum may increase by as much as four times that of the 1961-1990 baseline levels in coastal regions. For example, at Devonport, the warm-spell duration index is projected to increase by approximately 19 extra days per annum on average under the A2 emissions scenario by 2070-2099 (Table B.6 in Appendix B) from the average of six days during the 1961-1990 baseline period.

A corresponding decline in the cold-spell duration index (Figure 4.7b), defined as the annual count of days with a duration of five or more days below the 10th percentile of daily maximum temperature for the 1961-1990 baseline period, is also projected by the end of the century. At Miena/Liawenee in the central highlands, the cold-spell duration index is likely to decrease to less than two days per annum on average under the A2 emissions scenario by 2070-2099 (Table B.9 in Appendix B), corresponding with the projected decline in the frequency of frost days in the region (see Figure 4.1).

Results for these two temperature duration indices are summarised for A2 and B1 emissions scenarios (including the range of uncertainty in the projections) for three future 30-year periods in Appendix B, shown as a statewide mean as well as duration indices at eight representative locations across Tasmania.

Extreme daily maximum temperatures

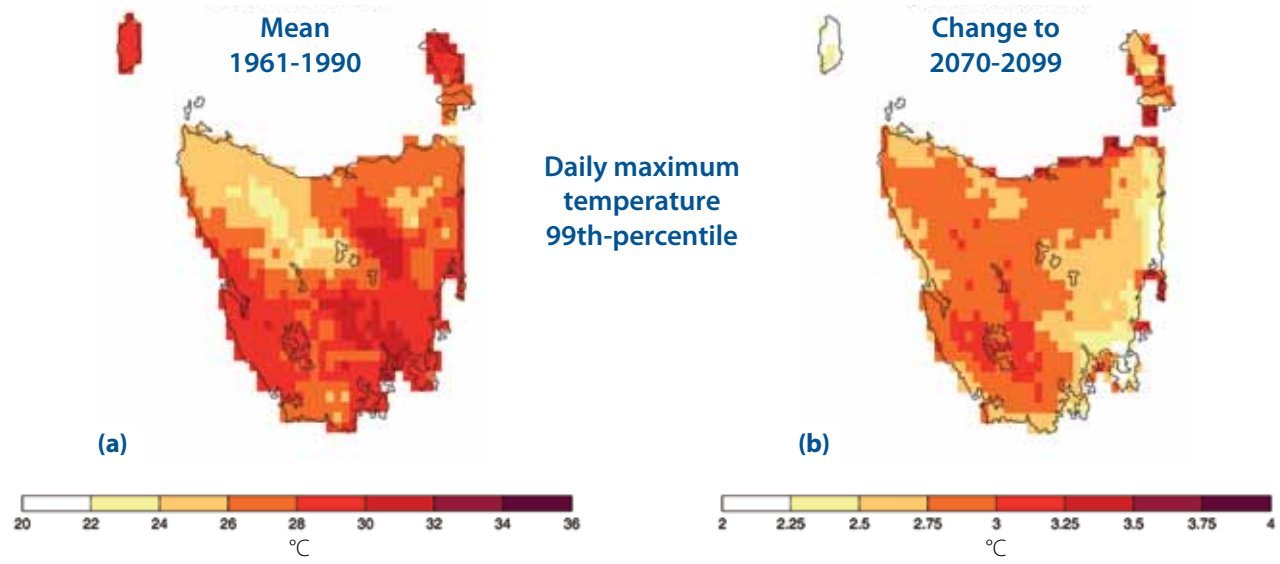

Seasonal changes to 2070-2099

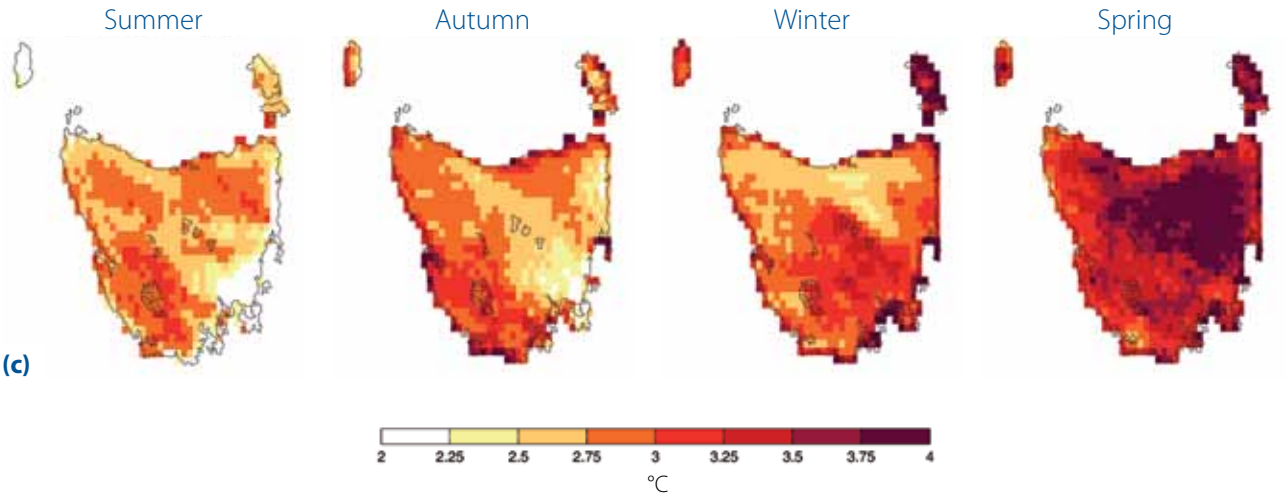

Figure 4.5 Magnitudes of the 99th percentiles of daily maximum temperature, showing a) annual 99th percentile (in °C) for the 1961-1990 baseline period, b) the mean annual change (in °C) for the 2070-2099 future period relative to the 1961-1990 baseline, and c) mean seasonal changes (in °C) for the 2070-2099 future period relative to the 1961-1990 baseline. All plots show values calculated using the multi-GCM mean of the six downscaled-GCMs for the A2 emissions scenario.

4.3.4 Changes to the range of temperature extremes

The projections indicate that magnitudes of both daily minimum and maximum temperatures will increase across the state throughout this century. However, minimum and maximum temperatures are not projected to increase by the same amount (see Figure 4.6), thus it is of interest to consider indices, which measure whether the temperature frequency distribution is narrowed or expanded. The diurnal temperature range and the extreme temperature range indices are two measures that reflect changes in the shape of the frequency distribution (Table 4.1).

The extreme temperature range is defined as the difference between the highest and lowest temperature values per annum. Figure 4.8 shows that the extreme temperature range is projected to increase from the 1961-1990 baseline period progressively through the century across most areas of the state, particularly the south-east and west coast. There is slight projected decrease in the extreme temperature range along the north coast. For example, Hobart displays an increase in the extreme temperature range of around 3 °C for the future 2070-2099 period relative to the 1961-1990 baseline period (Table B.2 in Appendix B), whereas Devonport on the north coast shows a projected decrease of 1 °C for the same period (Table B.6 in Appendix B).

To assess whether the changes to the extreme temperature range are likely to affect particular seasons, changes to the diurnal temperature range (defined as the monthly mean difference between daily maximum temperature and daily minimum temperature) were explored. Figure 4.9 shows the projected changes to the diurnal temperature range for 2070-2099 relative to the 1961-1990 baseline.

The results suggest that there is likely to be a decrease in the diurnal temperature range across much of the state throughout most of the year, consistent with our understanding of greenhouse warming and global projections (Meehl et al 2007).

The projected decrease in the diurnal range is particularly strong in the winter and early spring months in western Tasmania, which is counteracted to some degree by an increase in this region in the diurnal range in the early summer months, driving the prominent increases in the extreme temperature range shown in Figure 4.8. The increase in the diurnal temperature range in the west of Tasmania in the summer months (November to February, Figure 4.9) can be related to the change in the mean sea-level pressure pattern, the weakening of the westerlies and decreased cloud during the summer period by 2100 (Grose et al 2010).

The changes in the diurnal range are likely to result in substantially fewer nights where the temperature drops below freezing (in winter) and more nights where temperatures remain high (particularly in summer) (see also Figure 4.1). It is interesting to note however, that almost without exception, the central highlands shows a projected increase in the diurnal range across every month (up to 1 °C), combined with an increase in annual maximum temperatures (up to 3 °C) (see Figure 4.6). The patterns of reduction to the monthly diurnal temperature range largely reflect the projected changes in the distribution of cloud cover over Tasmania (see Figure 6.17d, Grose et al 2010), with more cloud projected in winter over western Tasmania and in summer over eastern Tasmania, producing a decrease in the range between mean daily minimum and maximum temperatures in these seasons by century end.

Results for the extreme temperature range index are summarised for the A2 and B1 emissions scenarios (including the range of uncertainty in the projections) for three future 30-year periods in Appendix B, shown as a statewide mean indices as well as indices at eight representative locations across Tasmania.

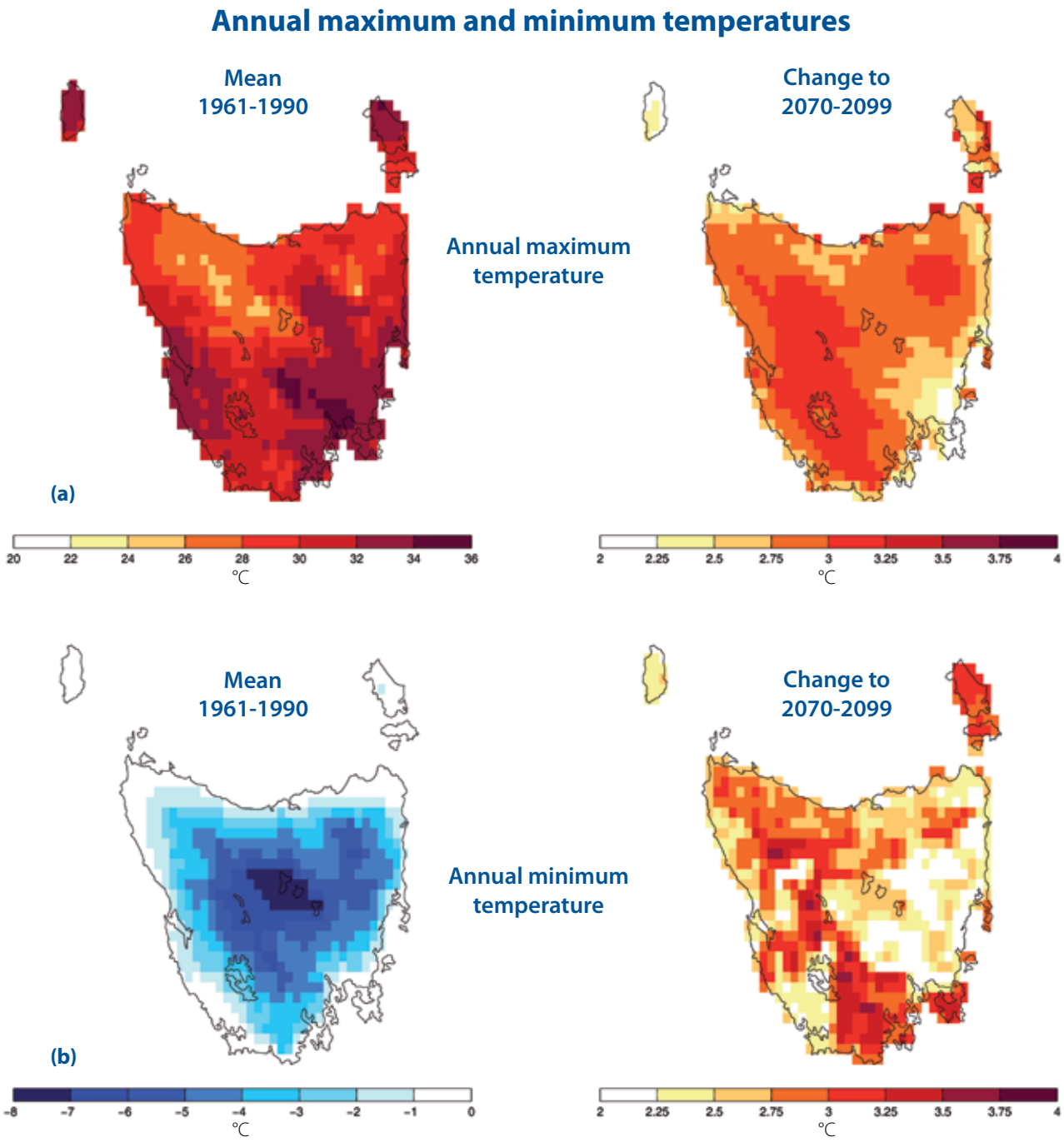

Figure 4.6 Mean annual maximum and minimum temperature magnitudes, showing a) mean annual maximum temperature, and b) mean annual minimum temperature. Left panels show the mean annual temperature magnitudes (in °C) for the baseline 1961-1990 period for each index; right panels show the change in the mean annual temperature magnitudes (in °C) for the future 2070-2099 period relative to the 1961-1990 baseline for each index. All plots show values calculated using the multi-GCM mean of the six downscaled-GCMs for the A2 emissions scenario.

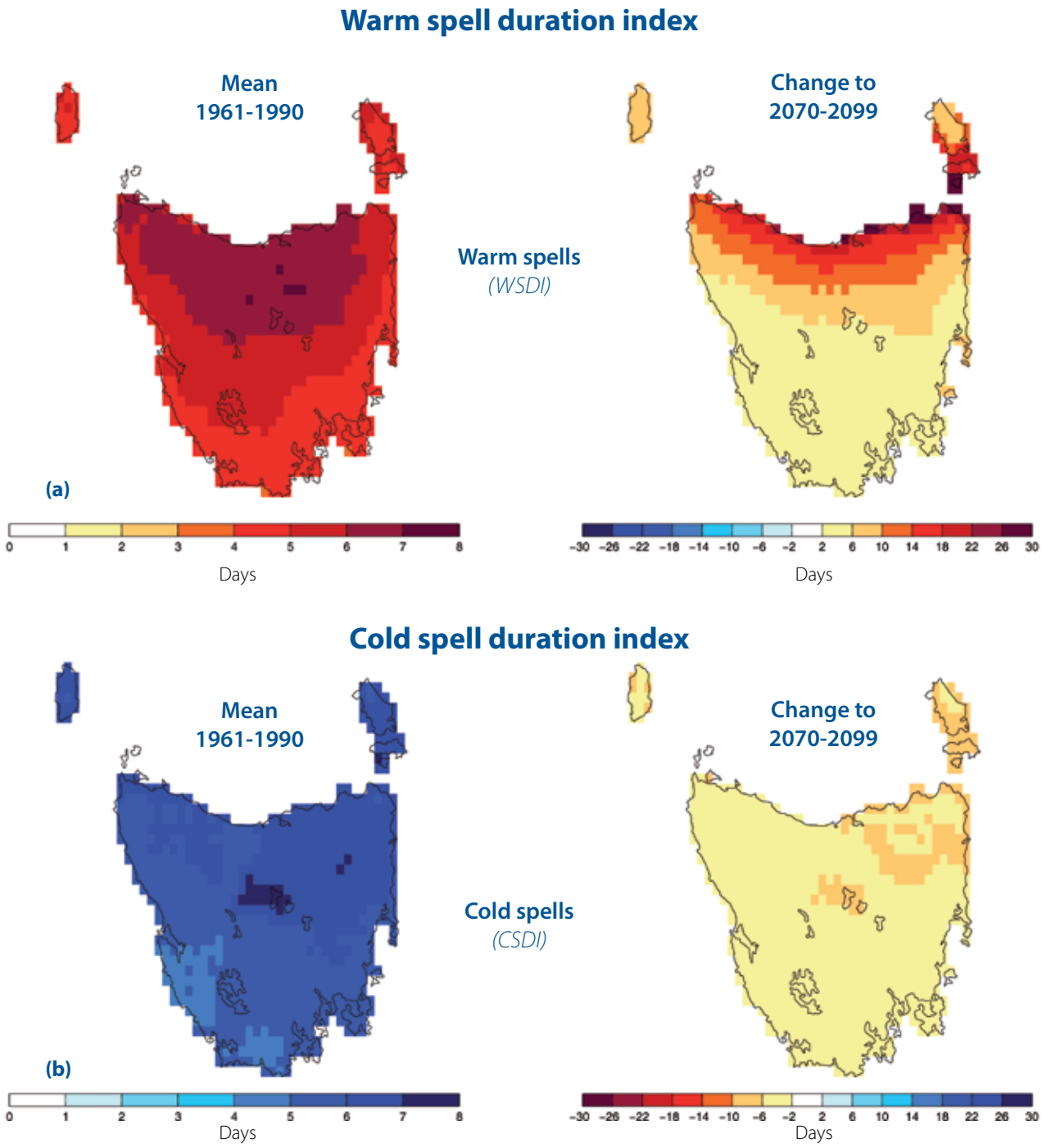

Figure 4.7 Duration of warm and cold spells, showing a) warm-spell duration index (*WSDI*) defined as the annual count of >5 days when daily maximum temperature is >90th percentile from the 1961-1990 baseline, and b) cold-spell duration index (*CSDI*) defined as the annual count of >5 days when daily maximum temperature is <10th percentile from the 1961-1990 baseline. Left panels show the mean annual duration (in days) for the baseline 1961-1990 period for each index; right panels show the change in the mean annual duration (in days) for the future 2070-2099 period relative to the 1961-1990 baseline. All plots show values calculated using the multi-GCM mean of the six downscaled-GCMs for the A2 emissions scenario. Definitions for indices are shown in Table 4.1.

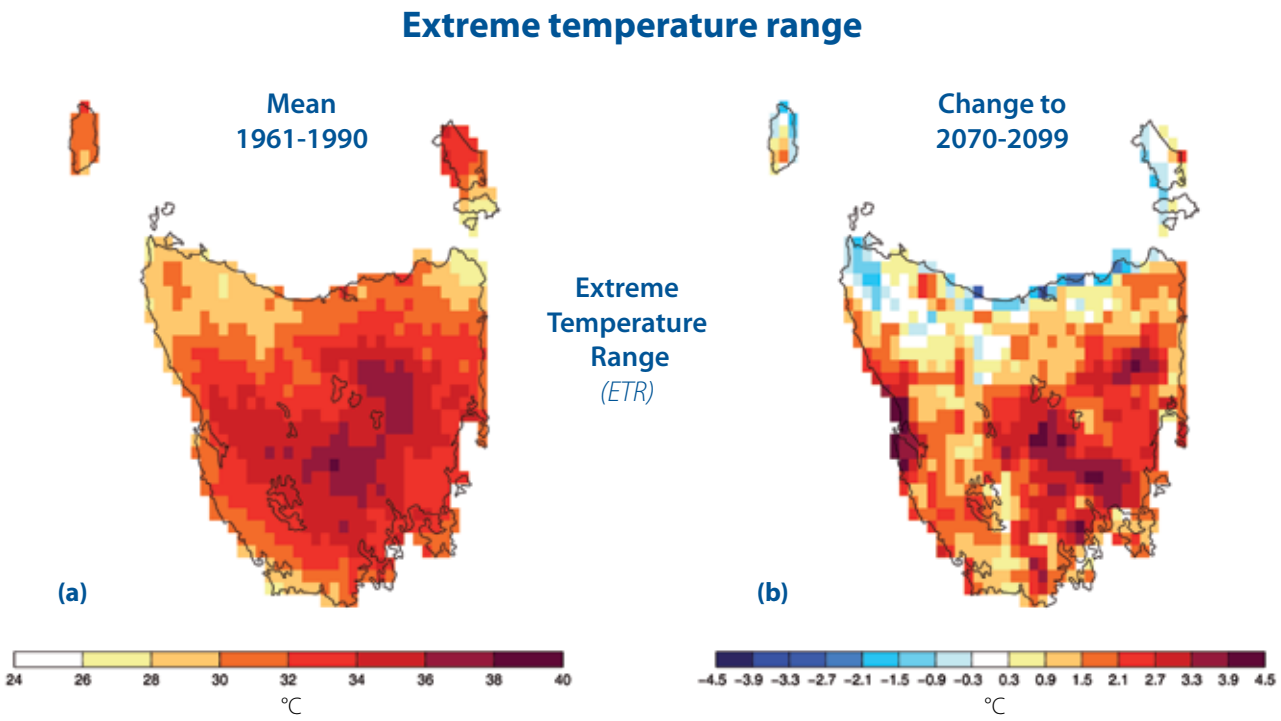

Figure 4.8 Extreme temperature range (*ETR*), showing a) the difference between the highest and lowest temperature values per annum (in °C) for the 1961-1990 baseline period, and b) the mean annual change (in °C) for the 2070-2099 future period relative to the 1961-1990 baseline. All plots show values calculated using the multi-GCM mean of the six downscaled-GCMs for the A2 emissions scenario. Definition for index is shown in Table 4.1.

Diurnal temperature range

Change from 1961-1990 to 2070-2099

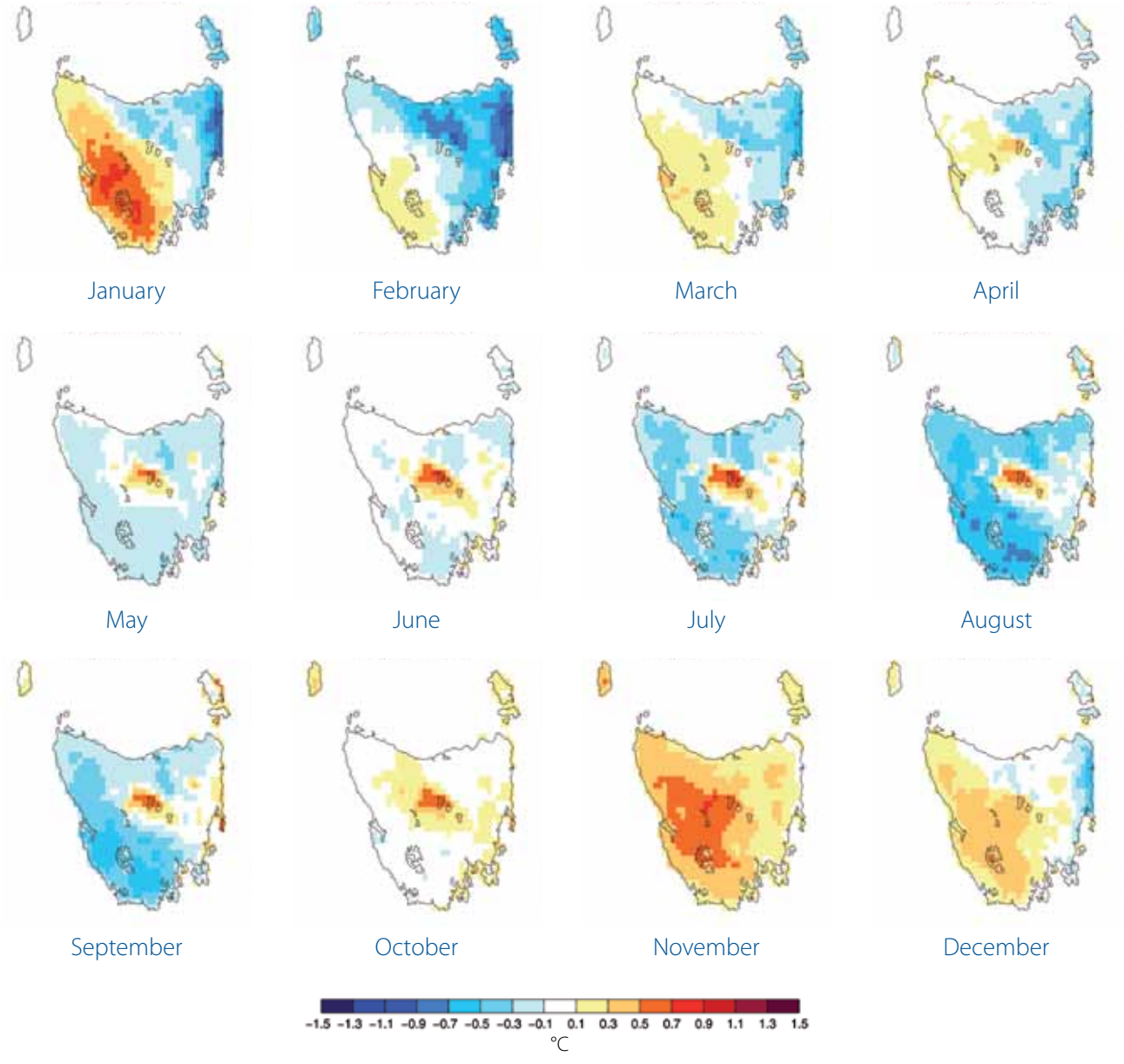

Figure 4.9 Diurnal temperature range (*DTR*), showing changes to the monthly mean difference between daily maximum temperature and daily minimum temperature (in °C) for the 2070-2099 future period relative to the 1961-1990 baseline. All plots show values calculated using the multi-GCM mean of the indices calculated from the six downscaled-GCMs for the A2 emissions scenario. Definition for index is shown in Table 4.1.

4.4 Summary

The results in this section are consistent with findings derived from global-scale and continental-scale studies using observations of the last century and future projections using GCMs. Studies investigating projected changes to temperature extremes globally (for example, Alexander et al 2006) and in the Australian region (Alexander and Arblaster 2009) have noted strong temperature trends and seasonal temperature changes in observations. Alexander et al (2006) noted that, in general, the number of warm days and nights are increasing globally, and Alexander and Arblaster (2009) found that the numbers of frost events are likely to decrease and that maximum daily temperatures are projected to increase across Australia.

The projections for the A2 emissions scenario to the end of the century indicate a reduced incidence of frost days across Tasmania, an increase in the frequency of tropical nights (mainly in the northern and eastern coastal areas) together with an increase in the frequency of summer days and heat waves, particularly in the central north and midlands, the Derwent Valley and the west coast around Macquarie Harbour. The frequency of cold waves is also projected to decrease, notably across the central highlands. The increased incidence of extreme temperature events is likely to be coupled with higher magnitudes, with projected increases in annual maximum temperatures and decreases in annual minimum temperatures across the state.

Changes to the extreme (annual) temperature range and the diurnal (monthly) temperature range are more complex. The extreme temperature range is projected to decrease along the north coast but increase elsewhere across the state. In warmer months (from November to March), the diurnal temperature range is likely to increase in the west but decrease in the east. In the colder months (from May to September), the diurnal temperature range is projected to decrease in the west.

5 Projected changes to extreme precipitation

5.1 Extreme precipitation indices

A summary of extreme precipitation indices developed by the CCI/CLIVAR/JCOMM Expert Team on Climate Change Detection and Indices (ETCCDI) that were introduced in Section 4.1 is included in Table 5.1. The precipitation indices are used in this section to demonstrate projected changes to extreme precipitation events across Tasmania. The list of indices (Table 5.1) shows that precipitation extremes can be categorised by frequency, intensity, duration and variability. As with temperature extremes, the selection of the most useful index will be determined by its application - for example, flood modellers are typically interested in precipitation intensities while farmers may be more interested in the duration of events.

In line with the previous chapter, the ETCCDI indices have been used here to demonstrate projected future changes to the intensity, frequency and duration of extreme precipitation events across Tasmania using the bias-adjusted dynamically downscaled GCM projections. As in Section 4, the projections of each of the extreme precipitation indices are presented as 30-year mean values. The future climate is described using three 30-year periods (2010-2039, 2040-2069 and 2070-2099) relative to the 30-year baseline period (selected as 1961-1990). The projections for each index are summarised in Appendix B as a statewide mean and at eight representative locations across Tasmania for each period. The results are presented as a multi-GCM mean, calculated from each of the six downscaled-GCM simulations independently of each other and these six estimates of the index are averaged (for each 30-year period) to give the central estimate (referred to as a multi-GCM mean in this report). The range of uncertainty associated with a multi-GCM mean index is summarised for each index in Appendix B, presented as a maximum and minimum from the six individual bias-adjusted dynamically downscaled GCM simulations.

5.2 Evaluation of precipitation indices

5.2.1 Performance for precipitation extremes

As with the previous section, the capacity of the dynamically downscaled GCMs to simulate current precipitation extremes with some level of accuracy is important in order to project future conditions reliably. Corney et al (2010) found the bias-adjusted simulations displayed a high level of skill in reproducing the spatial patterns of the mean precipitation climate across the state, producing a correlation of 0.63 with the AWAP gridded observations for the 1961-1990 reference period. However, extreme precipitation events are typically a more localised phenomena, thus present a more difficult challenge to simulate successfully than mean precipitation.

Summary tables in Appendix B present results for each of the extreme precipitation indices for the 1961-1990 baseline period as 30-year means. The precipitation indices have been calculated for both the AWAP interpolated observational dataset and the bias-adjusted dynamically downscaled simulations to enable evaluation of the downscaling performance. There is a good level of agreement between AWAP and the range of the six downscaled simulations for each of the daily precipitation indices at nine representative locations across Tasmania (Table B.1 to Table B.9 in Appendix B, comparing the two columns AWAP and Multi-GCM for 1961-1990). The majority of daily precipitation indices, such as the annual count of days when daily precipitation amount ≥20 mm (R20mm) and the highest daily precipitation amount (R1D), show the downscaled simulations have considerable skill at capturing the magnitudes and frequencies of precipitation extremes for the 1961-1990 baseline period compared to AWAP across the selected locations. In most cases, the range of the downscaled simulations contains the corresponding AWAP value, with the multi-GCM mean index frequently an exact match to the AWAP index. This provides confidence in the ability of the dynamical downscaling and bias-adjustment processes in reproducing the baseline climate for daily precipitation extremes.

However, whereas the daily precipitation simulations show considerable fidelity compared to AWAP for the 1961-1990 baseline period, the downscaled simulations show less skill at capturing the longer duration precipitation indices with the same level of precision. Indices such as the highest total precipitation amount over a consecutive 5-day period (R5D), the average maximum number of consecutive dry days per year when daily precipitation amount <1 mm (CDD) and the average maximum number of consecutive rain days per year when daily precipitation amount ≥1 mm (CWD) each show that the downscaled simulations typically produces an underestimation compared to AWAP across the representative locations.

Extreme precipitation indices

Table 5.1 Summary of extreme precipitation indices developed by the ETCCDI panel. Precise index definitions can be viewed at cccma.seos.uvic.ca/ETCCDI. Extreme precipitation indices were calculated using daily precipitation amounts (***RR***) in millimetres. Rain days (W) defined by daily precipitation amount being ≥1 mm.

Index name	Code	Index definitions	Units
Max 1-day precipitation amount	***R1D***	Highest daily precipitation amount (***RR***)	mm
Max 5-day precipitation amount	***R5D***	Highest total precipitation amount (***RR***) over a consecutive 5-day period	mm
Simple daily intensity index	***SDII***	Ratio of annual total precipitation amount (***RR***) to total annual number of rain days (***W***)	mm/d
Heavy precipitation days	***R10mm***	Annual count of days when daily precipitation amount (***RR***) ≥10 mm	days
Very heavy precipitation days	***R20mm***	Annual count of days when daily precipitation amount (***RR***) ≥20 mm	days
Consecutive dry days	***CDD***	Average of the maximum number of consecutive dry days per year when daily precipitation amount (***RR***) <1 mm	days
Consecutive wet days	***CWD***	Average of the maximum number of consecutive rain days per year (***W***) when daily precipitation amount (***RR***) ≥1 mm	days
Very wet days	***R95p***	Annual count of days when daily precipitation amount (***RR***) >95th percentile of daily precipitation on rain days (***W***) for the 1961-1990 baseline	days
Extremely wet days	***R99p***	Annual count of days when daily precipitation amount (***RR***) >99th percentile of daily precipitation on rain days (***W***) for the 1961-1990 baseline	days
Annual count of wet days	***R1mm***	Annual count of days when daily precipitation amount (***RR***) ≥***nn*** mm, where ***nn*** is user defined (used here to define the count of rain days (***W***) where daily precipitation amount ≥1 mm).	days
Annual total wet-day precipitation	***PRCPTOT***	Annual total of daily precipitation amount (***RR***) in rain days (***W***)	mm

For example, R5D at Strathgordon (Table B.8) shows a value of 155 mm calculated using the AWAP gridded observations for 1961-1990, compared to 135 mm calculated from the multi-GCM mean index from the downscaled simulations. The AWAP estimate in this example is also outside of the range of the downscaled simulations (129/139 mm), implying that the six downscaled simulations consistently underestimate the longer duration extremes.

This underestimation of the longer durations indices suggests that the either the autocorrelation (the temporal sequencing of events) in the downscaled simulations does not fully resemble the observations, or that the bias-adjustment process (see Section 3.4) has not correctly preserved the autocorrelation of events. No account was made in the bias-adjustment process for temporal sequencing as the bias-adjustment factors were calculated using daily precipitation events in the training period (Bennett et al 2010). Limited analysis into autocorrelation has been undertaken for this report. Thus whilst the models have shown a high level of skill in producing credible projections of daily precipitation extremes, the projections using the longer duration indices related to extreme precipitation events have a lower level of accuracy.

5.2.2 Uncertainties and limitations

As with the previous chapter, factors such as the dynamical downscaling process, the topography in the downscaled GCMs, the skill of bias-adjustment process and uncertainties associated with the future emissions scenarios also need to be taken into account when applying the future projected changes to the precipitation extremes presented in this section (also see Section 3.5). As described in previous sections, each index is typically presented as a multi-GCM mean for the A2 and B1 emissions scenarios for prescribed 30-year future periods, providing a central 'best' estimate for each index from the six downscaled simulations for each emissions scenario. The multi-GCM mean for each index (summarised in Table B.1 to Table B.9 in Appendix B) is calculated with an associated range of uncertainty, presented as a maximum and minimum range from the six individual bias-adjusted dynamically downscaled GCM simulations.

Whereas the range of uncertainty for the temperature indices displayed a largely consistent spatial pattern across the state (Section 4.2.2), the picture is more varied for the precipitation indices. The summary tables in Appendix B show the index for heavy precipitation days (R10mm), for example, to have a diverse range of uncertainty across the representative locations (Table B.2 to Table B.9), with some locations displaying a maximum and minimum range of ±2 days (for example, Hobart and Swansea) and others displaying a range of ±4 days (for example, St Helens and Strahan) relative to the multi-GCM mean for the A2 emissions scenario by the end of the century. Extreme precipitation events in particular are typically a localised phenomena, thus this range of uncertainty is not unexpected given the spatial variability evident in both observations and the downscaled simulations of precipitation across Tasmania (Corney et al 2010; Grose et al 2010).

The varied scale of the ranges across the precipitation indices in Appendix B points to a larger range of uncertainty in the projections of precipitation extremes than with extreme temperature. While the six downscaled simulations are largely in agreement, this is not uniform across the downscaled projections, suggesting that uncertainty in the upper end of the extreme precipitation distributions needs to be taken into consideration in conjunction with the central estimate when employing the projections presented in this section.

5.3 Results

The extreme precipitation figures in this section show projections using the A2 emissions scenario only. However, each index has been calculated for both the A2 and B1 emissions scenarios and is summarised in Appendix B. For the precipitation index figures, white-to-green colour bars show the wet extremes (for example, indices using daily total precipitation on an absolute scale, or to signify projected wetting trends) and white-to-brown colour bars show the dry extremes (for example, to signify projected drying trends).

Extreme precipitation distributions

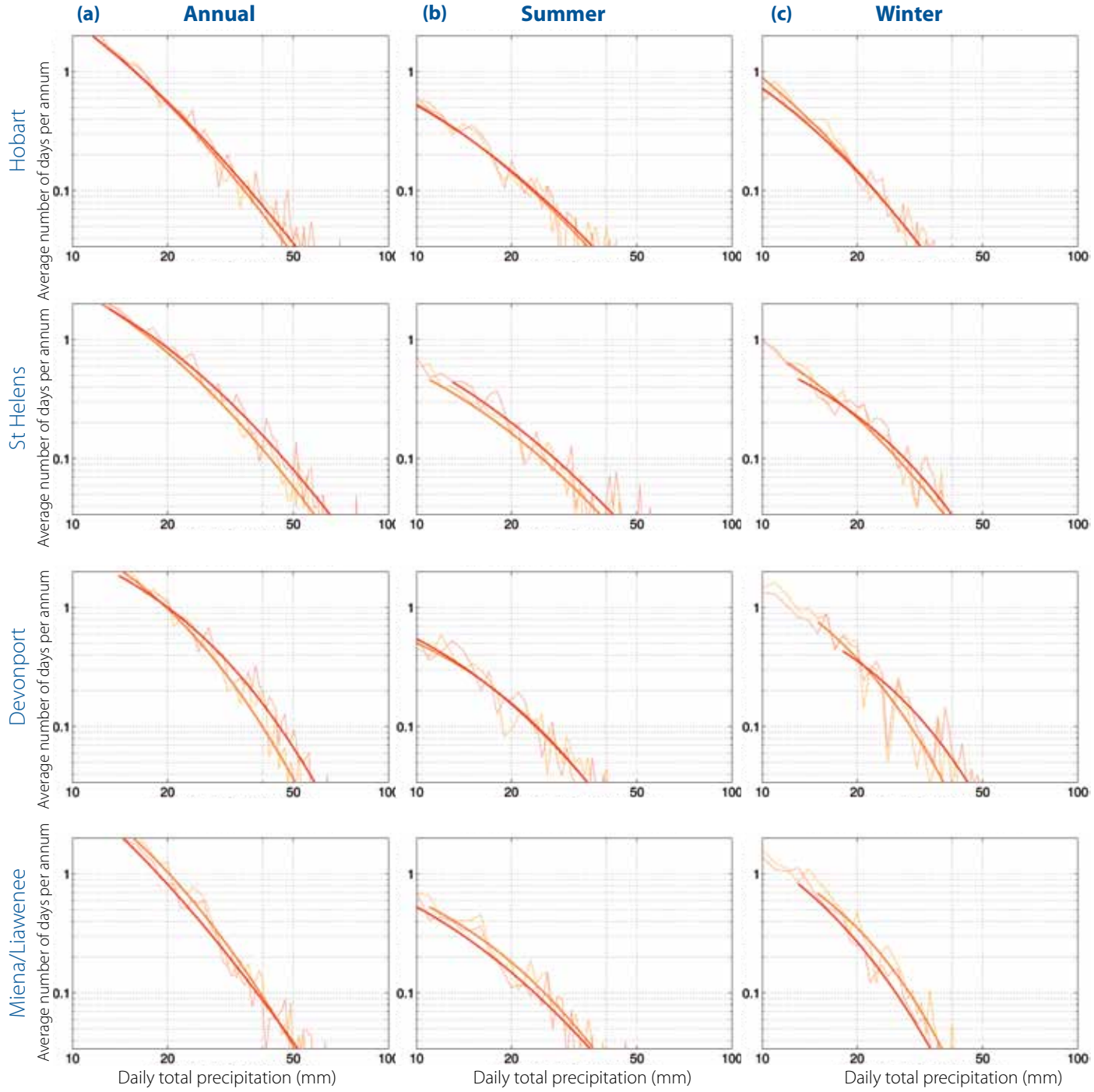

Figure 5.1 a) Annual, b) summer, and c) winter probability density functions (PDFs) of daily precipitation events exceeding 90th percentile, fitted to a generalized Pareto (GP) distribution (presented on a log-scale). PDFs shown at four selected locations across Tasmania for the 1961-1990 baseline period (bold orange lines) and the 2070-2099 future period (bold red lines). Time series of daily precipitation are shown as light red and orange lines. All PDFs show values calculated using the multi-GCM mean of the six downscaled-GCMs for the A2 emissions scenario. Location of sites is shown in Appendix A.

5.3.1 Changes to the frequency of extreme precipitation events

Changes to the frequency of high-intensity extreme precipitation events are more important than mean changes in the context of infrastructure design and flood risk assessment. Extreme precipitation events are often described in terms of exceedance (or non-exceedance) of predetermined threshold values. Figure 5.1 shows projected changes to the probability density functions (PDFs) of annual and seasonal (summer and winter) daily precipitation events exceeding the 90th percentile. The projected changes have also been fitted to a generalized Pareto distribution for 1961-1990 baseline period and the 2070-2099 future period events at selected locations across the state. Unlike the standard bell-curve PDFs shown in Figure 2.2, the plots in Figure 5.1 show threshold exceedances (that is, only the values that are above a given 'extreme' threshold). The annual frequency of daily precipitation events exceeding the 90th percentile (Figure 5.1) is projected to increase at Hobart, St Helens and Devonport, but decrease at Miena/Liawenee in the central highlands. This pattern of change has larger amplitude variations across the summer and winter seasons. In particular, the increased frequency of precipitation extremes in winter at Devonport contributes to the increased annual frequency (Figure 5.1, DJF compared with JJA). In contrast, Miena/Liawenee shows projected decreases to the frequency of extreme precipitation events in both the winter and summer seasons.

The number of very wet precipitation days across the state, defined as the average number of days per annum where daily precipitation totals exceed the 95th percentile of daily precipitation from the 1961-1990 baseline period, is projected to change (Figure 5.2). Across Tasmania, the magnitude of the 95th percentile typically ranges between 10 mm and 40 mm, (Figure 5.2a) for the 1961-1990 baseline period, with the highest values occurring in the wetter western half of the state and in a small region on the east coast.

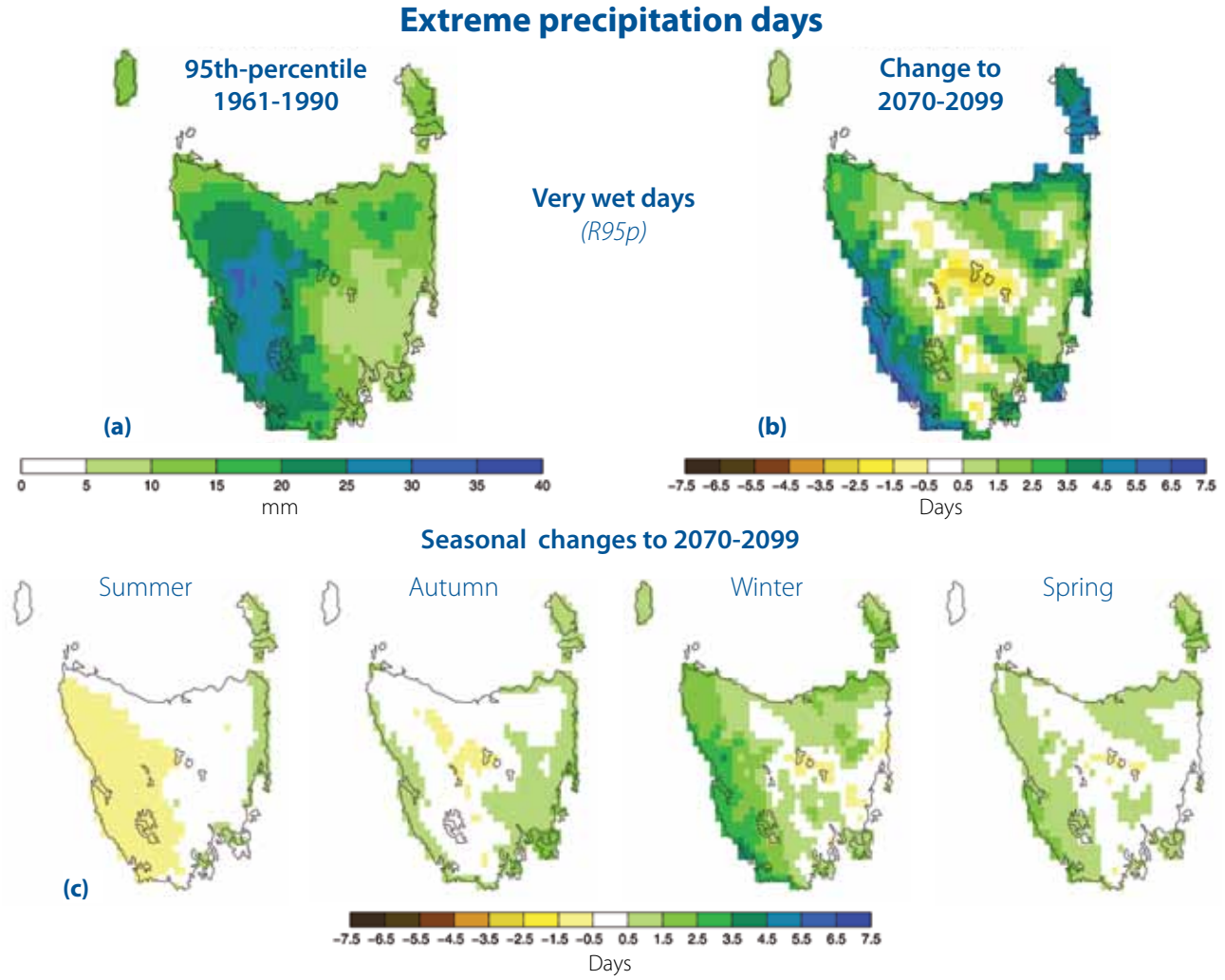

Figure 5.2 Annual and seasonal very wet days (*R95*p), showing a) the magnitude of the annual 95th percentile for the baseline 1961-1990 period (in mm), b) annual mean change in the average number of days per annum for 2070-2099 where daily precipitation totals exceed the 95th percentile of daily precipitation from the 1961-1990 baseline period (in days) and, c) seasonal mean absolute changes in the average number of days per season for 2070-2099 where daily precipitation totals exceed the 95th percentile of daily precipitation from the 1961-1990 baseline period (in days). All plots show values calculated using the multi-GCM mean index from the six downscaled-GCMs for the A2 emissions scenario. Definition for index is shown in Table 5.1.

The frequency of very wet precipitation days exceeding the baseline 95th percentile is projected to increase by 2070-2099 (Figure 5.2) annually across most areas (with the exception of the central plateau and an area extending from it to the north-west). By the end of the century, the frequency of days with precipitation higher than the baseline 95th-percentile are notably greater in the south-west and north-east, with up to five days more per year on average at Strahan, for example (see Table B.7 in Appendix B). These projected increases in western Tasmania are driven predominantly by the increased frequency of winter events (shown in Figure 5.2c), with lesser increases in the autumn and spring seasons. Decreases occur in all seasons in the central highlands, as well as a decrease in summer events in the west of the state.

The overall pattern of very wet days aligns well with the annual and seasonal patterns of projected mean precipitation change (Grose et al 2010) where western Tasmania shows a projected increase in mean precipitation in winter, combined with dryer summers, by the end of the century, while wetter summers are projected for eastern Tasmania. Indeed, the changes to the pattern of very wet days are the major contributor to the projected changes to mean precipitation over Tasmania.

Results for the precipitation frequency indices are summarised for the A2 and B1 emissions scenarios (including the range of uncertainty in the projections) for three future 30-year periods in Appendix B, shown as a statewide mean as well as indices at eight representative locations across Tasmania.

5.3.2 Changes to the intensity of extreme precipitation events

Some regions in Tasmania are more prone to intense precipitation (and the potential for subsequent flooding) than others. Cullenswood, in the eastern coastal region, holds the Tasmanian record for the highest observed one-day total, with 352 mm (Bureau of Meteorology 2010a). Often these are high-intensity events that are outside the normal climate variability are driven by a particular large-scale meteorological driver such as cut-off lows. Pook et al (2010) estimates that at Fingal in the north-east, cut-off lows account for >50% of precipitation totals from April to October (taken from the Bureau of Meteorology observational record at Fingal for 1985 to 2009). In comparison, Launceston receives nearly 50% of its precipitation totals from frontal precipitation events for the same period, despite being less than 100 km from Fingal. Major floods in the north-east in 1929 and in Hobart in 1960 were both associated with cut-off lows. With a projected increase in the number of very wet days across much of Tasmania described in Section 5.3.1, this section determines if the intensity of extreme precipitation events is also likely to increase – in other words, are extreme precipitation events likely to become more intense when they occur.

Figure 5.3a shows mean annual maximum 1-day precipitation amounts for the 1961-1990 baseline period, and relative change annually (Figure 5.3b) and seasonally (Figure 5.3c) for the 2070-2099 future period. The results show a projected increase in the mean maximum 1-day intensities across the whole of Tasmania, with an increase of up to 35% in some coastal regions. Strahan, for example, Table B.7 (Appendix B), shows a projected increase of about 11 mm by the 2070-2099 future period from 49 mm from the 1961-1990 baseline period. Hobart shows a similar ratio of increase for the same period, with about 8 mm increase on 44 mm for the same period.

The increases in the extreme precipitation events are shown as example time series with a likely range of uncertainty (Figure 5.4). The increases in extreme precipitation equate to an approximately 20% increase in intensity at these two locations.

Particularly strong signals of increased intensities are projected in late summer and autumn in the east of the state (Figure 5.3c), with increases in the north and west also found across the majority of seasons. The projected increase in 1-day intensities have a similarity to the spatial pattern of the projected increase in the number of very wet days (see Figure 5.2), highlighting that an increase in both the frequency and intensity of daily extreme precipitation events is likely to occur over almost all regions except the central highlands throughout the 21st century.

To complement the projections of mean maximum 1-day totals, Figure 5.5 shows the mean annual maximum 5-day precipitation totals (in mm) for the 1961-1990 baseline period and relative change for the 2070-2099 future period. Unlike the projected changes to the 1-day totals, the 5-day totals display projected changes with a spatial pattern similar to that of the mean annual total precipitation changes, with a drying trend in the central highlands combined with an increase in the north-eastern, eastern and western coastal regions. The longer duration totals (and the relative projected changes) are more closely linked to mean precipitation totals, indicating that the heavy precipitation events that occur over 5 consecutive days make up a large fraction of the total (annual) precipitation and therefore have a pronounced impact on mean precipitation changes (see Grose et al 2010). Note the lower accuracy associated with the longer duration precipitation indices (see Section 5.2). This result is consistent with the observational records across the state where precipitation events historically tend to be of no more than three days in duration. For example, in the Hobart records for 1893-2010, there are only four events where >=20 mm was observed on three consecutive days, and only three events in the 1931-2009 records at the (old) Launceston Airport site (Bureau of Meteorology 2010c).

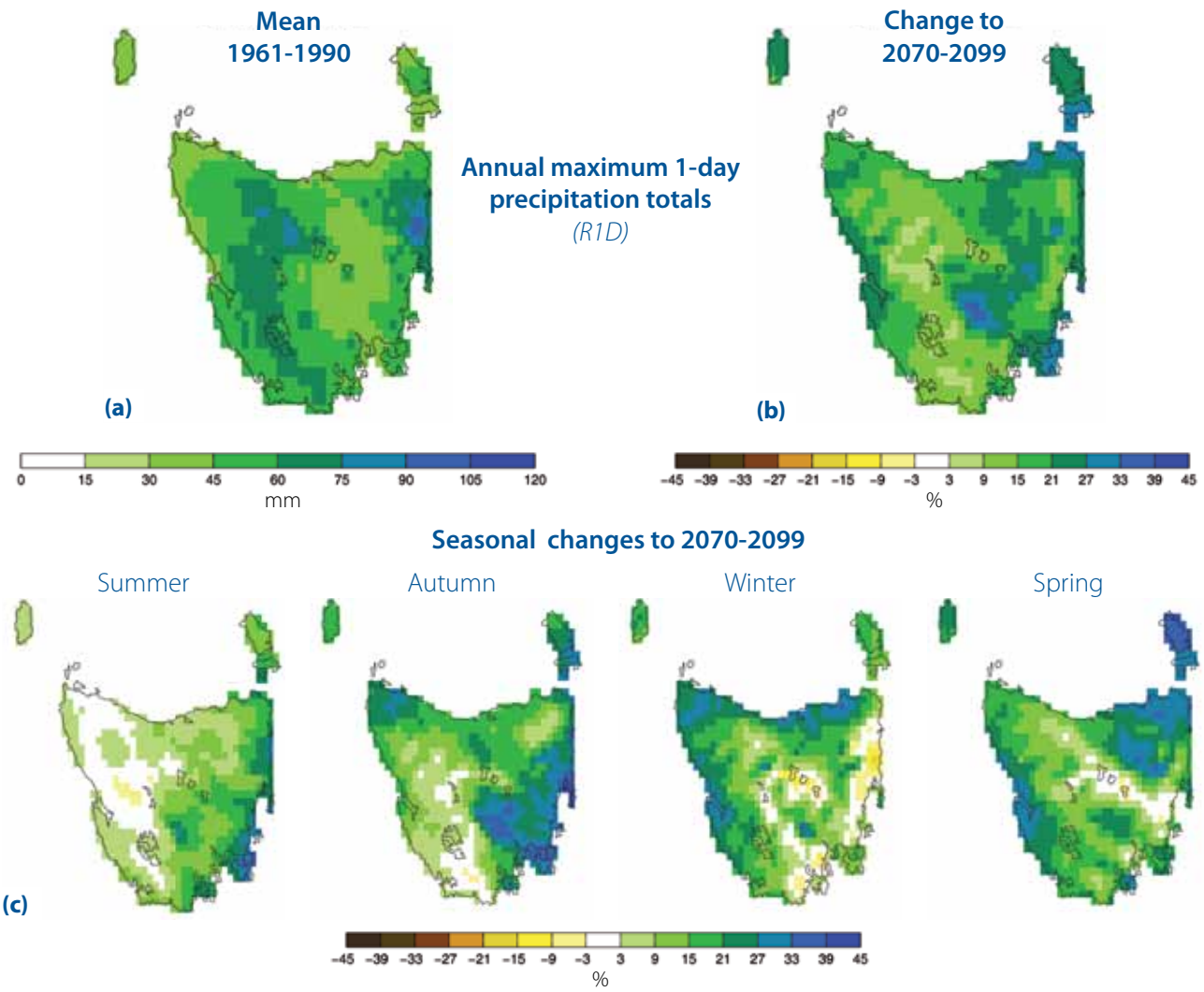

Figure 5.3 Annual and seasonal maximum 1-day precipitation totals (*R1*D), showing a) the mean annual maximum 1-day precipitation totals for the 1961-1990 baseline period (in mm), b) the annual proportional change to 1-day precipitation totals for 2070-2099 relative to the 1961-1990 baseline period (in %), and c) seasonal proportional change to 1-day precipitation totals for 2070-2099 relative to the 1961-1990 baseline period. All plots show values calculated using the multi-GCM mean index from the six downscaled-GCMs for the A2 emissions scenario. Definition for index is shown in Table 5.1.

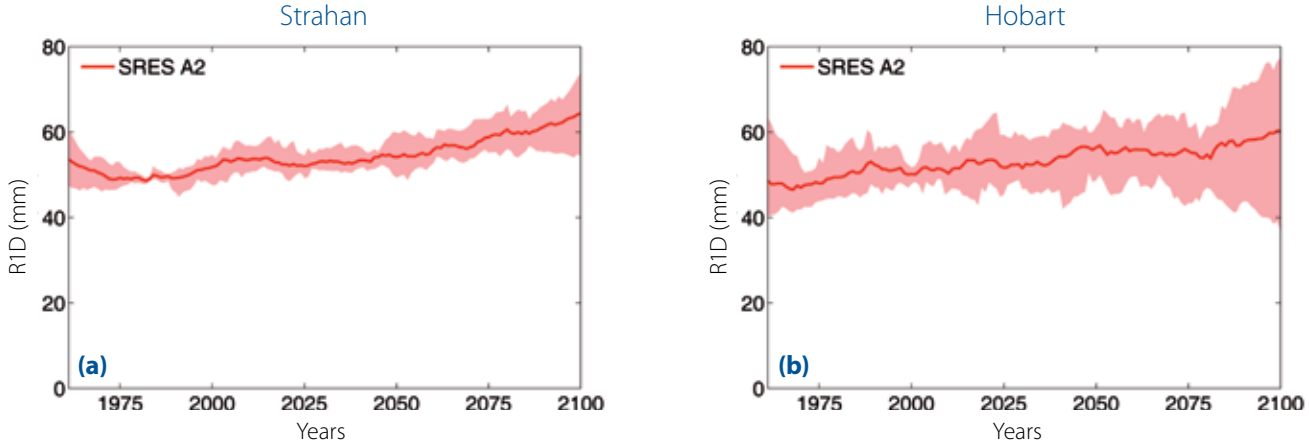

Figure 5.4 Time series of annual maximum 1-day precipitation totals (*R1D*), showing annual maximum 1-day precipitation totals (in mm) at Strahan (left panel) and Hobart (right panel) for 1961-2100. Bold red lines show 11-year running multi-GCM means with the range of the six downscaled-GCMs (light red shading). All plots show values calculated using the multi-GCM mean index from the six downscaled-GCMs for the A2 emissions scenario. Location of sites is shown in Appendix A.

In addition to changes to the intensity of daily and multi-daily precipitation totals, engineers and planners often need information on shorter-duration, higher-intensity events to assist with the design of flood and water infrastructure. The six-minute peak precipitation rate (often referred to as an instantaneous rate) is shown in Figure 5.6. These rates have been sorted from the daily peak six-minute rates stored as part of the downscaled simulations. There are no observations against which to validate or bias-adjust six-minute values from the simulations values, and accordingly the six-minute peak precipitation rates are not bias-adjusted. The results show a notable projected increase in the instantaneous rates (in mm/day) across the state annually for 2070-2099 relative to the 1961-1990 baseline. This signal is particularly strong seasonally in the east of the state, especially in late summer, autumn and spring, with up to a 60% increase in some eastern coastal regions by the end of the century. The results suggest an increase in the intensity of short-duration events that is proportionately greater than that of daily extreme precipitation events in many regions (compare with Figure 5.3).

Results for the precipitation intensity indices are summarised for the A2 and B1 emissions scenarios (including the range of uncertainty in the projections) for three future 30-year periods in Appendix B, shown as a statewide mean as well as indices at eight representative locations across Tasmania.

5.3.3 Changes to the duration of wet and dry spells

In addition to the projected increase in both the frequency and intensity of precipitation events in the previous sections, it is also useful to determine if such events are likely to become longer in duration when they do occur. In this section, the mean annual maximum number of consecutive wet days and dry days are assessed.

For the 1961-1990 baseline period, the longest dry spells are typically in the lower-lying areas in the eastern half of the state (with on average up to 24 consecutive days in any given year, Figure 5.7a). Conversely, the longest wet periods are in the western half (up to 20 consecutive days on average in any given year, Figure 5.7b). This strong east-west divide is driven by the larger proportion of annual precipitation totals in the western half of the state compared to the east, and the dominant synoptic events that bring precipitation (the west coast receives predominantly frontal and stream precipitation, whereas the east and north-east receive a higher proportion of high-intensity, short-duration systems such as cut-off lows) (Risbey et al 2009).

The future projections for the 2070-2099 period suggest there will be a larger fraction of the state with increases of up to 20% and a smaller fraction with some decreases in the annual maximum length of either wet or dry spells as a proportion from the baseline period (Figure 5.7). The greatest changes by the end of the century are projected to be a reduction in the maximum number of consecutive dry days per annum of around two days in the north-east (particularly across Flinders Island) and an increase in the maximum number of consecutive wet days per annum of around two days in the south-west.

Results for the precipitation duration indices are summarised for the A2 and B1 emissions scenarios (including the range of uncertainty in the projections) for three future 30-year periods in Appendix B, shown as a statewide mean as well as indices at eight representative locations across Tasmania.

5.3.4 Changes to the temporal characteristics of extreme precipitation events

To complement the projected changes to precipitation extremes explored throughout this section, it is also important to note that the temporal pattern of precipitation events is also likely to change by the end of the century. Given that an increase in both the frequency and intensity of daily precipitation is projected in many regions of Tasmania through the 21st century, the amount of total precipitation per event is also likely to change. Figure 5.8a shows a varied pattern of increasing and decreasing annual mean precipitation totals by 2070-2099 relative to the 1961-1990 baseline, displaying a drying trend in the central highlands and parts of the north-west with an increase in mean annual total precipitation in north-eastern, eastern and western coastal regions. These changes are likely to be accompanied across Tasmania by a decrease in the mean number of annual rain days (defined here as days with >1 mm of precipitation), shown in Figure 5.8b for the same period, also relative to the 1961-1990 baseline. However, the ratio between mean annual total precipitation and the mean number of annual rain days (that is, the ratio between Figure 5.8a to Figure 5.8b), known as the simple daily intensity index, shows an increase almost everywhere over Tasmania, ranging from 0.25mm/day-1.25 mm/day (see Appendix B). This result implies that the mean precipitation event has increased its intensity sufficiently to cause the average precipitation to increase over much of Tasmania despite the statewide decrease in the number of rain days.

Results for the simple daily intensity index are summarised for the A2 and B1 emissions scenarios (including the range of uncertainty in the projections) for three future 30-year periods in Appendix B, shown as a statewide mean value or index as well as indices at eight representative locations across Tasmania.

Maximum 5–day precipitation totals

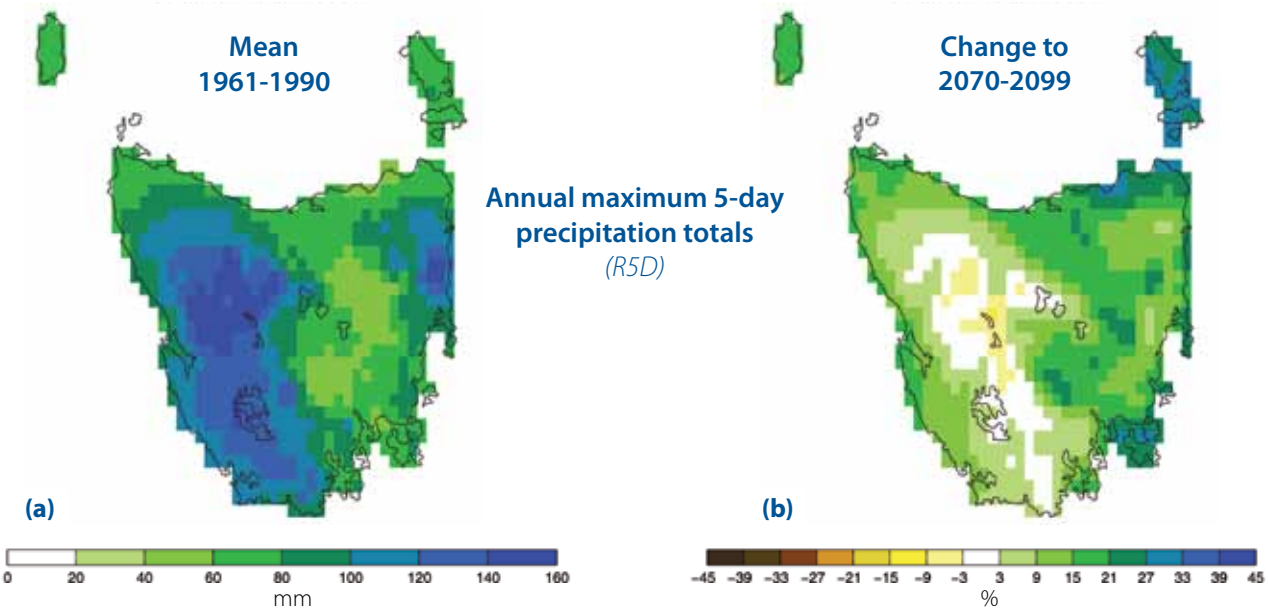

Figure 5.5 Annual maximum 5-day precipitation totals (*R5*D), showing a) the mean annual maximum 5-day precipitation totals for the 1961-1990 baseline period (in mm), and b) the annual proportional change to 1-day precipitation totals for 2070-2099 relative to the 1961-1990 baseline period (in %). All plots show values calculated using the multi-GCM mean of the six downscaled-GCMs for the A2 emissions scenario. Definition for index is shown in Table 5.1.

Short duration precipitation rate

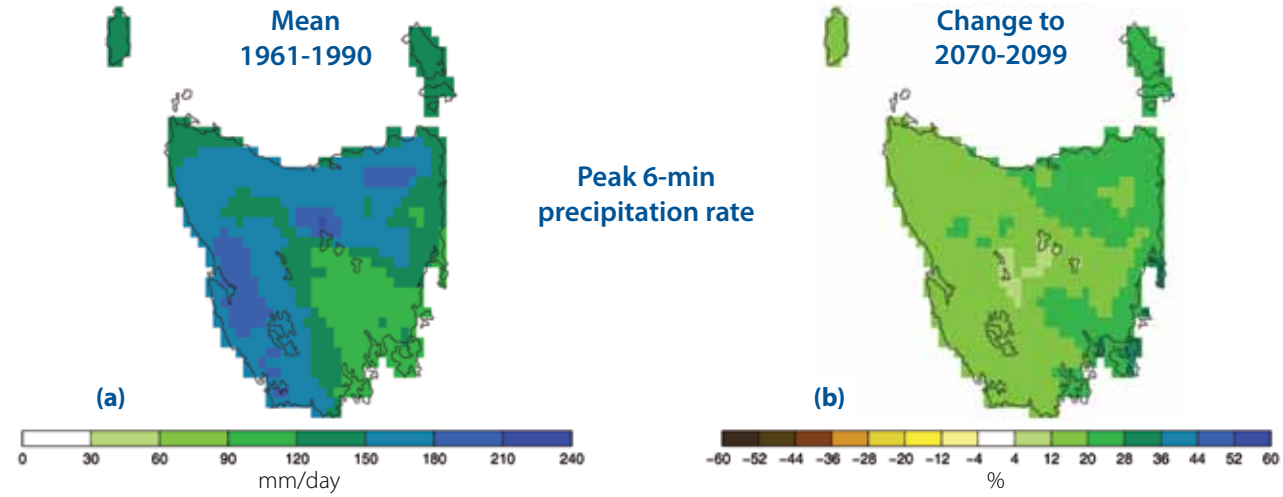

Seasonal changes to 2070-2099

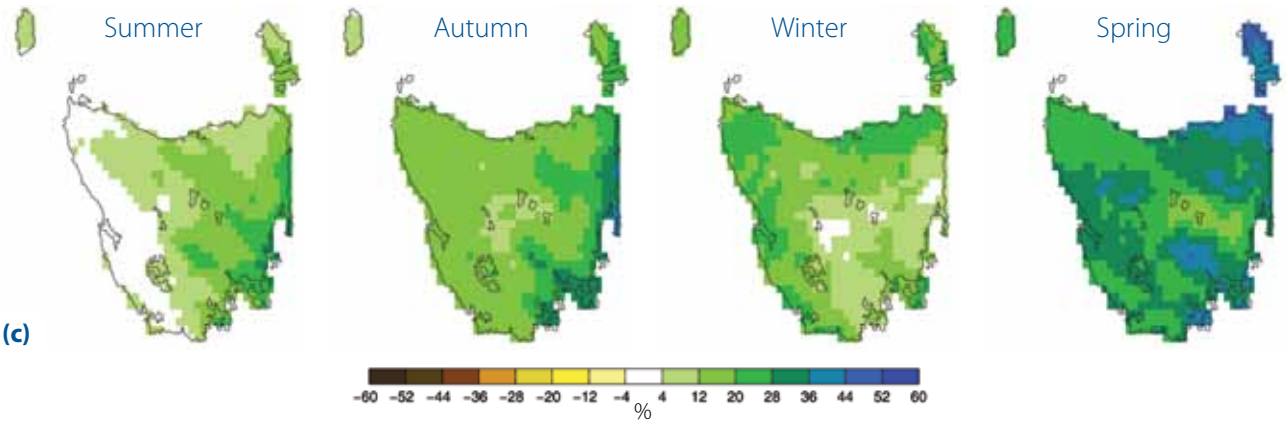

Figure 5.6 Annual and seasonal six-minute peak precipitation rate, showing a) left panel annual mean six-minute peak precipitation rate for 1961-1990 (in mm/day), b) annual mean proportional change (in %), and c) seasonal mean proportional changes (in %) for 2070-2099 relative to the 1961-1990 baseline. All plots show the multi-GCM mean rate from the six downscaled-GCMs for the A2 emissions scenario, calculated using mean monthly maximum values.

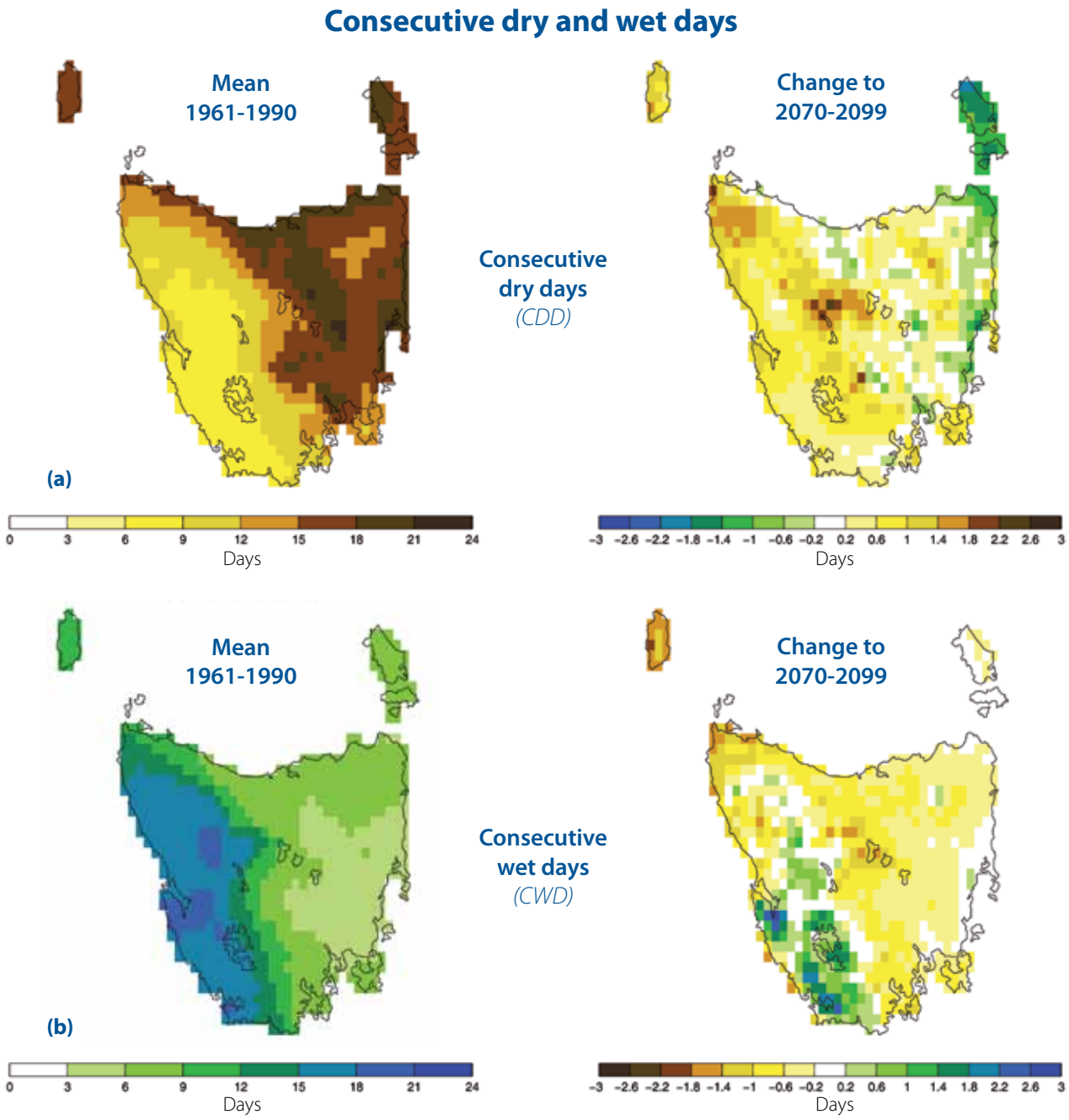

Figure 5.7 Consecutive dry and wet days, showing a) average of maximum number of consecutive dry days per year (*CDD*), and b) average of maximum number of consecutive wet days per year (*CW*D) (in days). Average of the maximum number of consecutive dry/wet days for 1961-1990 shown in left panels (in days) and as absolute changes for 2070-2099 (right panels) relative to the 1961-1990 baseline. All plots show values calculated using the multi-GCM mean of the six downscaled-GCMs for the A2 emissions scenario.

5.4 Summary

Farmers, engineers, planners, emergency managers and the insurance industry are all interested in how extreme precipitation events are likely to change across Tasmania. The results of the downscaled climate projections for Tasmania suggest that there are likely to be substantial changes to the characteristics of extreme precipitation events across many regions. There is a projected increase in the number of very wet days, more intense 1-day precipitation totals and increases in the six-minute precipitation rates, particularly across eastern Tasmania. These increases are likely to increase the risk of flooding in many regions. The west and north-east coastal regions of the state in particular display a pattern of an increasing frequency of extreme precipitation events in winter and early spring, combined with a decrease in summer events that emerges by the end of the 21st century. Therefore, in some regions, more intense and heavy downpours are likely to be interspersed with longer dry periods as the nature of precipitation events changes across Tasmania.

Projected changes to the intensity and frequency of extreme precipitation events (average recurrence intervals) are explored further in Section 7 for 24-hour and 48-hour duration events.

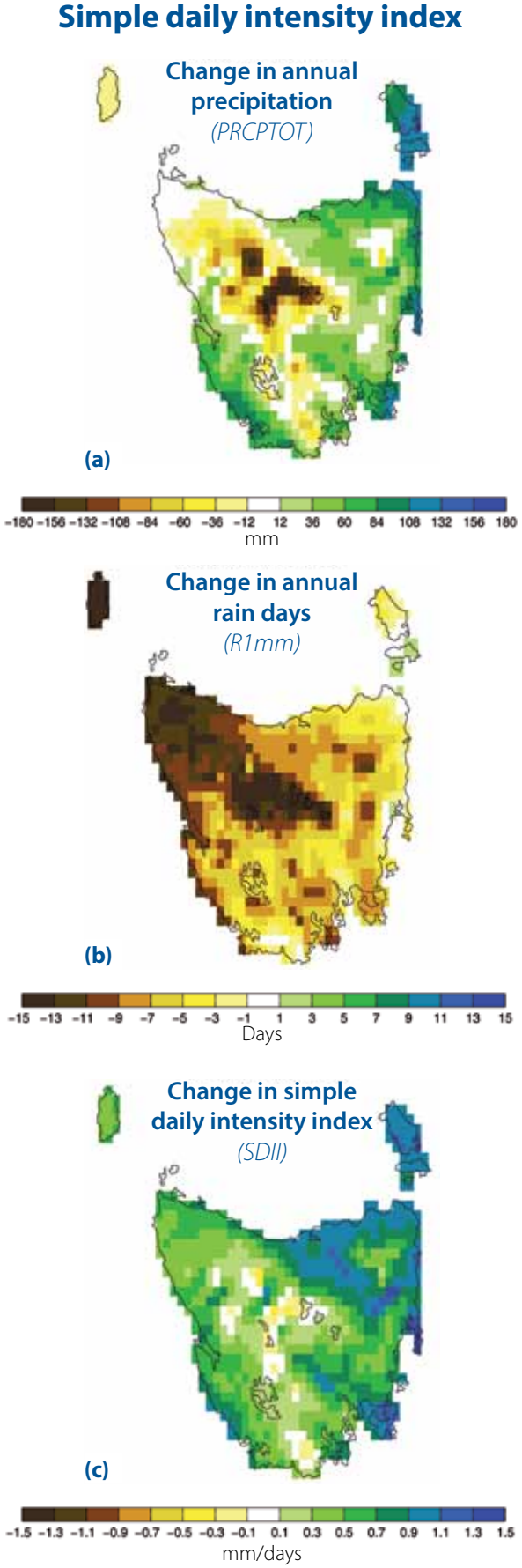

Figure 5.8

Simple daily intensity index (*SDII*), showing a) change in annual total precipitation for 2070-2099 relative to the 1961-1990 baseline period (in mm), b) change in mean annual number of rain days with >1mm of precipitation for 2070-2099 relative to the 1961-1990 baseline period (in days), and c) change in the simple daily intensity index defined as the ratio of annual total precipitation and annual number of rain days (in mm/d) for 2070-2099 relative to the 1961-1990 baseline period. All plots show values calculated using the multi-GCM mean value from the six downscaled-GCMs for the A2 emissions scenario. Definition for index is shown in Table 5.1.

6 Cumulative precipitation totals and meteorological drought

6.1 What are cumulative precipitation totals?

Floods and droughts are two important aspects of extreme hydrological hazard and climate change assessment. While floods often result from short intense precipitation events (depending on the catchment in question and preceding precipitation events), drought is characterised by water deficit, caused by long-term dry climatic conditions where precipitation totals are typically below an observed average.

Understanding precipitation deficit and surplus is crucial for the assessment of either flood or drought. This understanding can be achieved by calculating the total amount of precipitation that has fallen during a selected period, known as the cumulative precipitation total (McKee et al 1993). The amount by which the cumulative precipitation for the selected period is above or below a long-term average (for example an observed or modelled baseline) can then be estimated, indicating either a deficit or a surplus. This is referred to as a cumulative precipitation departure relative to the long-term average.

Whilst the calculation of cumulative precipitation deficits and surpluses are not direct measures of flood or drought, they can be indicative of the likely occurrence of either phenomenon (see Box 4). For example, deficit terms can be used to signify the possibility of drought conditions; surplus terms can be used to suggest the possibility of flood conditions.

6.2 Methods and data

Cumulative precipitation totals provide information on the total amount of precipitation for a time interval and its departure from baseline climatology, expressed either as an absolute or as a relative term. The method used in this study is taken from the Standardised Precipitation Index (SPI) developed by McKee et al (1993) and used by the Bureau of Meteorology to compile monthly drought statements (Bureau of Meteorology 2010d). The monthly drought statements are compiled predominantly for the agricultural community. The method used in this study does not calculate the SPI directly (for example, the totals are not transformed into a standardised normal distribution). The calculation of cumulative precipitation totals is used in this report and is most relevant for examining the combination of extreme precipitation and the occurrence of deficit (drought) and surplus conditions. For an analysis of SPI and how it relates specifically to agriculture, see Holz et al (2010).

Table 6.1 details the cumulative precipitation terms and definitions as used by the Bureau of Meteorology and adopted for use in this section. The six terms can be broadly separated into deficit and surplus conditions: the 'severe deficiency', 'serious deficiency' and 'below average' terms may be used to signify precipitation deficit conditions relative to a baseline total, and the 'average', 'above average' and 'very much above average' terms may be used to identify precipitation surplus conditions relative to a baseline total

For each grid cell, the percentile thresholds for cumulative precipitation deficit and surplus were calculated for the baseline period 1961-1990 for a range of time intervals. The Bureau of Meteorology typically calculates cumulative totals for time intervals of 3-months, 6-months, 12-months, 18-months, 24-months and 36-months. The longer-term precipitation totals (>12-months) automatically account for seasonal variations, and so can indicate deficit and surplus conditions for intervals that may span several years. In this study deficit and surplus percentile thresholds were calculated for time intervals of 6-months, 12-months, 60-months and 120-months

Projected changes to the occurrence of each deficit and surplus condition up to the end of the 21st century (110-years) were then calculated relative to the reference period 1961-1990 threshold values. The categories of future deficit and surplus conditions were then ranked in order of severity. For example, if a cell showed an increase in the incidence of 'below average' conditions and an increase in the incidence of 'serious deficit' conditions, it was designated as 'serious deficit'. In instances where there was a net decrease in deficit conditions, but an increase in one of the other deficit terms, a cell was ascribed to that deficit term. For example, there could be an increase in 'below average' conditions even when there are fewer instances of deficit conditions overall because there was a decrease in 'severe deficiency' or 'serious deficiency' conditions (this occurs at St Helens in Figure 6.3). In this example, a cell would be defined as experiencing increased 'below average' conditions. The same method applies to surplus conditions. This means that considering the patterns of change from one time period to the next is important when interpreting Figure 6.1 and Figure 6.2.

The calculations of future cumulative precipitation totals were based on daily precipitation modelling output derived from the bias-adjusted A2 high-resolution climate projections (Corney et al 2010).

Box 4
Drought

Tasmania does not experience the exceptional dry periods seen in parts of mainland Australia. However, this is not to say that Tasmania does not suffer from drought as it is relative to each location. Regions of Tasmania experience low but highly variable precipitation, therefore extended periods of precipitation totals well below the long-term average are not unlikely. The 1914-15 drought greatly affected Tasmanian crops and livestock, the 1965-68 drought set the scene for disastrous bushfires around Hobart in 1967, and the 'short but sharp' droughts of 1982 and 1983 were caused by record low precipitation in parts of the state (Bureau of Meteorology 2010d). For the 13-year period April 1997-March 2010 and the eight-year period April 2002–March 2010, much of Tasmania has been affected by serious to severe precipitation deficiencies, especially in the north of the state (Bureau of Meteorology 2010e).

The Bureau of Meteorology monitors precipitation deficiencies across the state, however it cannot declare a drought. A declaration of drought (and the provision of financial drought assistance) is the responsibility of the relevant state and federal government departments, such as the federal Department of Agriculture, Fisheries and Forestry, as well as the National Rural Advisory Council. The declaration of drought is a complex issue and depends on more factors than exceptionally low precipitation (Hennessy et al 2008), including the rarity and severity of the drought, and loss of income.

This complexity makes the question of 'What is a drought?' difficult to answer. Drought has several definitions, often depending on severity of the impact. But there are numerous other ways to define drought. For example, BoM gives the definition of a meteorological drought as an expression of the departure from long-term average precipitation totals, which Trenberth et al (2007) describes as a 'prolonged absence or marked deficiency of precipitation'. Meteorological drought is commonly the first indicator of drought (Wilhite and Glantz 1985) as it is the easiest to measure directly from observations. Other definitions can then follow, involving increasingly complex calculations that require complex sets of observations: agricultural drought is when the soil moisture is sufficiently low enough to affect crop growth, hydrological drought is where surface (for example, stream flows, lake levels) and groundwater levels are in deficit, and socio-economic drought is when the acute water shortage begins to affect people directly.

In this regard, mathematical indices are used to define the occurrence and severity of drought by integrating such variables as precipitation, temperature, evapotranspiration and soil moisture. These include, but are not limited to, the Standardised Precipitation Index (SPI) that is based on the probability of precipitation occurring (McKee et al 1993), and the Palmer Drought Severity Index (PDSI), which uses a soil moisture algorithm (Palmer 1965). None of the indices cover all possible definitions of drought and therefore no index is regarded as superior to another.

Most drought indices are designed for the monitoring of current drought conditions based on observations; making future climatic projections about the occurrence, extent or severity of future droughts is a different matter entirely. However, the projections of precipitation deficit conditions for the state in Section 6.2.1, based on the definitions used by BoM, may be used to indicate the likelihood of drought conditions (whether it be meteorological, agricultural, hydrological or socio-economic) occurring in the future through climate change. In addition, Holz et al (2010) calculated SPI values for selected agricultural regions across the state as part of the agriculture component of the project.

Table 6.1 The Australian Bureau of Meteorology cumulative precipitation percentile terms and definitions adapted for future climate projections (source: BoM drought statements).

Term	Definition
Severe deficiency	Precipitation in the lowest 5% of baseline (1961-1990) cumulative totals
Serious deficiency	Precipitation in the lowest 10% of baseline (1961-1990) cumulative totals, but not in the lowest 5%
Below average	Precipitation in the lowest 30% of baseline (1961-1990) cumulative totals, but not in the lowest 10%
Average	Precipitation in the middle 40% of baseline (1961-1990) cumulative totals
Above average	Precipitation in the highest 30% of baseline (1961-1990) cumulative totals, but not in the highest 10%
Very much above average	Precipitation in the highest 10% of baseline (1961-1990) cumulative totals

6.2.1 Deficit conditions and surplus conditions

The multi-GCM mean projections of future occurrence of deficit conditions for the short- to long-time intervals for 2010-2039, 2040-2069 and 2070-2099, relative to the 1961-1990 baseline percentiles, are shown in Figure 6.1. The spatial distribution of the cumulative precipitation totals show that relative to the 1961-1990 period all future periods will have an increase in the occurrence of below-average deficit precipitation, and that for some regions and time intervals there is an increased tendency for serious deficiency and severe deficiency conditions.

The increasing occurrence of 'very much above average' surplus conditions (top 10%) in the south-western, south-eastern and north-eastern regions of the state is particularly strong across all the computed intervals ranging from 6-months to 120-months for the periods 2010-2039, 2040-2069 and 2070-2099 (Figure 6.2). Other regions, such as the central highlands and the north-west, show less detectable change, with a continuation of 'average' conditions projected over the intermediate- to long-term intervals similar to the multi-GCM mean for the same regions (Grose et al 2010).

The precipitation totals for the short to intermediate time intervals suggest the occurrence of surplus conditions are likely to increase relative to the reference period in many regions by the end of the 21st century. Note that the increase in mean annual precipitation (Figure 5.8a) that occurs progressively is also reflected in these figures.

For the future periods, the occurrence of deficit and surplus conditions for most time intervals actually increases and thus Figure 6.1 and Figure 6.2 need to be interpreted together. At first glance, this result seems paradoxical when considered in terms of the annual mean precipitation change for the A2 emissions scenario (see Figure 5.8a). The annual mean precipitation is projected to increase over much of Tasmania. The increase in the occurrence of deficiency conditions shows that the probability distribution is projected to change for future precipitation, with an increase in deficit conditions, a decrease in normal conditions and an increase occurrence of surplus conditions. The probability distribution for cumulative precipitation has broadened and is less peaked around the mean with more of the distribution in the below average or above average part of the distribution relative to the reference period. So while the annual average conditions may actually be wetter over much of Tasmania (for example, the east coast), these changes in the mean conditions are smaller than the changes in the extreme values of the cumulative precipitation, and consequently over much of the state both an increase in deficit and surplus conditions are projected to occur at the same place. The future climate is therefore likely to include more deficit and surplus conditions than in any 30-year historical period.

Deficit precipitation totals

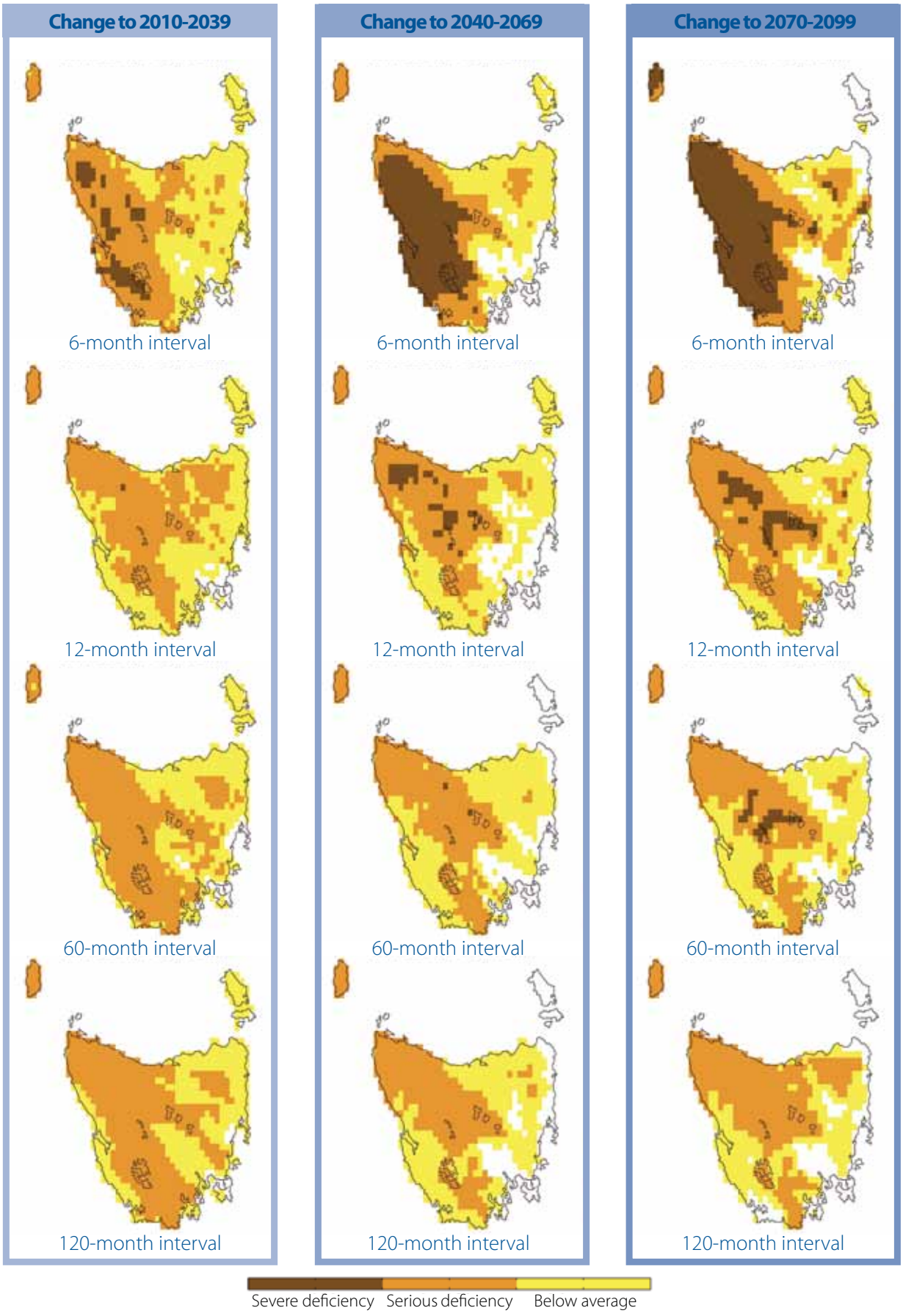

Figure 6.1 Increased occurrences of deficit precipitation totals relative to 1961-1990 baseline percentiles and ranked in order of severity. Accumulation intervals shown are 6-month, 12-month, 60-month and 120-month. Plots display deficits for the periods 2010-2039, 2040-2069 and 2070-2099 relative to 1961-1990 baseline percentiles. All plots show values calculated using the multi-GCM mean deficit precipitation totals from the six downscaled-GCMs for the A2 emissions scenario.

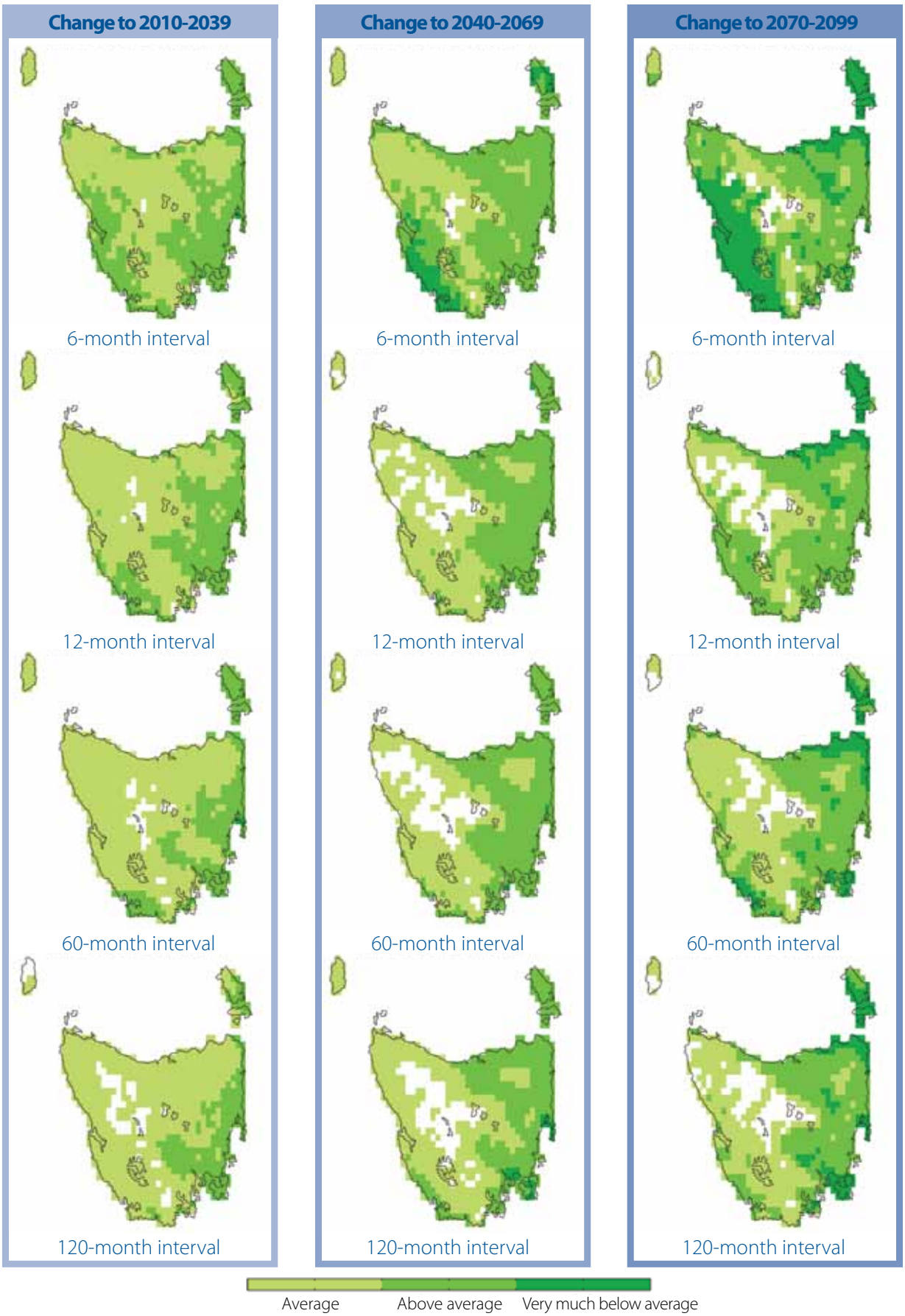

Figure 6.2 Increased occurrences of surplus precipitation totals relative to 1961-1990 baseline percentiles and ranked in order of severity. Accumulation intervals shown are 6-month, 12-month, 60-month and 120-month. Plots display surpluses for the periods 2010-2039, 2040-2069 and 2070-2099 relative to 1961-1990 baseline percentiles. All plots show values calculated using the multi-GCM mean of the surplus precipitation from the six downscaled-GCMs for the A2 emissions scenario.

6.3 Water surplus and deficit occurrence at four example sites

Projected time series of 6-month cumulative precipitation totals for 1961-2100 at four selected locations around the state are shown in Figure 6.3 (left panels). Locations of these sites are given in Appendix A. The 6-month cumulative precipitation totals demonstrate how the projected changes to deficit and surplus conditions may interact at the same location. The percentiles for the cumulative totals must, by definition, always equal 100% at any given time relative to the baseline totals (refer to Table 6.1).

In some regions, for example at Miena in the central highlands (Figure 6.3), the projected increase in deficit conditions towards the end of the century, combined with the decrease in surplus conditions, should lead to increased drought conditions in this area. Contrast this result with Strahan on the west coast where substantial increases in both deficit and surplus conditions may be expected, with a reduction in the occurrence of average or normal conditions. Strahan is in a region that is projected to experience marked changes to the seasonal character of precipitation – less rain in summer, increased rain in winter (Grose et al 2010) – explaining the simultaneous increases and decreases in six-month precipitation totals. This combination of deficit and surplus precipitation trends may appear to be slightly confusing with some regions projected to suffer from more dry periods as well as more wet periods. To aid the interpretation of these trends, Figure 6.3 (right panels) show anomalies of mean monthly precipitation totals and mean monthly number of rain days (>1 mm) for 2070-2099 relative to the 1961-1990 baseline for the same four locations. The explanation for the patterns for the 6-month surplus and deficit conditions are easily reconciled at this time interval with the changing seasonal pattern of precipitation change over the state. The projected decreases in mean summer precipitation in the west of Tasmania (Grose et al 2010), for example, relate to the tendency for more severe and serious deficit conditions. Similarly, increases in mean winter precipitation (Grose et al 2010) in the same region relate to the greater occurrence of surplus conditions (Figure 6.1 and Figure 6.2).

The results show that some regions are likely to experience a notable change to the seasonal variability of precipitation, which may explain the projected future trends shown for the cumulative precipitation totals. For example, at Miena, the projected increase in future deficit conditions is linked to decreases in the total amount of precipitation across all of the seasons. This is matched by a similar decrease in the number of total rain days.

In comparison, at St Helens on the east coast, the projected increase in precipitation surplus conditions, combined with smaller decreased deficit conditions towards the end of the century, can be explained by increased summer and autumn precipitation totals and a decrease in the number of winter and spring rain days. There are also likely to be larger-scale complex causes and drivers behind the projected changes in cumulative precipitation totals, but the projected changes to seasonality and variability caused by climate change are likely to have substantial effects on cumulative precipitation totals.

For the 12-month, 60-month and 120-month intervals the spatial pattern of the increases in the occurrence of precipitation deficits and surpluses (Figure 6.1 and Figure 6.2) is broadly consistent with the changes in the annual mean, particularly for the period 2070-2099. The eastern side of Tasmania is projected to have an increase in mean precipitation, resulting in less extreme levels of deficit conditions and an increased level of surplus conditions relative to other regions in the state. However, even in this location where precipitation is likely to increase on average, deficit conditions have a higher occurrence than in the reference period, caused by the less frequent occurrence of average or normal conditions. Over the central plateau and the north-west, the annual precipitation decreases (see Figure 6.7 in Grose et al) and is reflected here as a lower level of increased surplus conditions (Figure 6.2) and enhanced deficit conditions (Figure 6.1) relative to other regions. Similarly, over the south-west, the high-emissions scenario projects an increase in precipitation and this region shows a lower level of enhanced deficits and a higher level of enhanced surpluses. These results collectively point to a flattening of the probability distribution of the cumulative precipitation, with an enhancement of the tails of distribution. The mean changes in the annual precipitation are smaller (as reported in Grose et al 2010) than these changes in tails of the distributions.

Based on the future projected departures from the baseline climate, the projected increase in precipitation deficit and surplus conditions may lead to more frequent and prolonged drought conditions and more flood events over the 21st century in response to rising greenhouse gases. These results imply that a broader range of precipitation extremes can be expected across the majority of Tasmania on all time scales compared to the reference period. There is similar evidence in other simulations of future precipitation patterns and in the analysis of observations of precipitation (for example, Trenberth et al 2007).

Cumulative precipitation surpluses and deficits

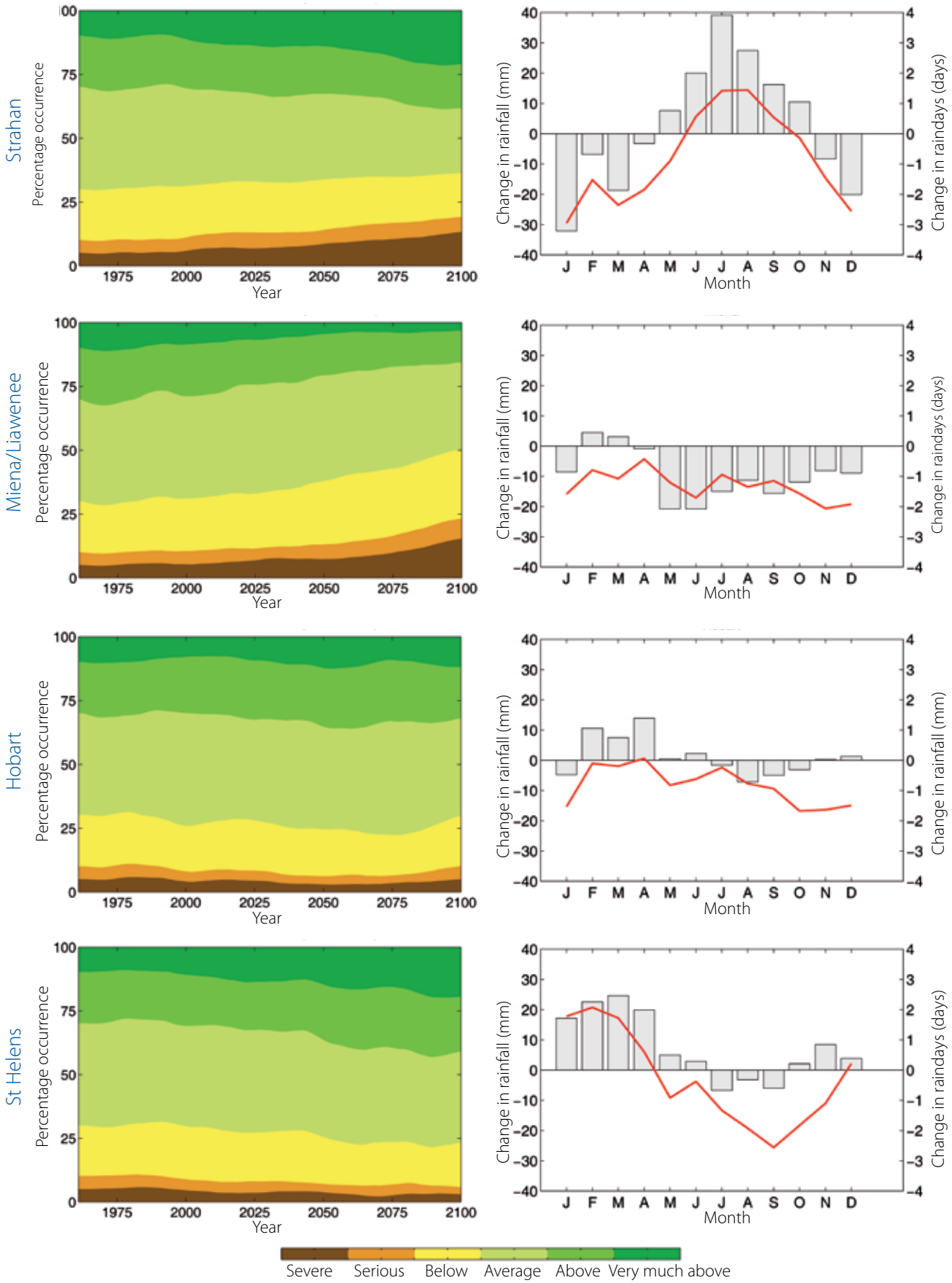

Figure 6.3 Left panel: time series of occurrence of 6-month cumulative precipitation surpluses and deficits for 1961-2100 relative to 1961-1990 baseline at Strahan, Miena, Hobart and St Helens. Right panel: anomalies of mean monthly precipitation totals (grey bars) and mean monthly number of rain days (>1 mm) for 2070-2099 (red lines) relative to the 1961-1990 baseline for the same locations. All plots show values calculated using the multi-GCM mean of the precipitation surpluses from the six downscaled-GCMs for the A2 emissions scenario. Location of sites is shown in Appendix A.

7 Precipitation average recurrence intervals

7.1 Introduction to extreme value theory

Characterisation of extreme values in precipitation is important for decision-makers and engineers involved in the maintenance and design of major infrastructure and for the management of emergencies. Average recurrence intervals (ARIs) are the primary tool used by these groups for informing risk of future events. Extreme value distributions allow for estimates of, for example, a one-in-100 year 24-hour precipitation event from a record that is less than 100-years long. These indices are typically referred to as average recurrence intervals (ARIs). Extreme value theory has been used reliably and extensively in meteorology, climatology and hydrology to estimate the extremes of natural phenomena, including extreme precipitation, temperature and wind speed.

Extreme value distributions are asymptotic functions that allow for the extrapolation of a limited number of observations to values well beyond the range of the given sample (Coles 2001). These can then be used to estimate the probability of rare events (for example, precipitation or temperature extremes) by extrapolating the probability curve through the sparsely populated parts of the distribution. The theory behind extreme value distributions is similar to the Central Limit Theorem (CLT); both infer the limiting distribution of independent, identically distributed, random variables. According to the CLT, the mean value of a sample of identically distributed random variables converges to a standard normal distribution. Similarly, if the maxima of a large number of identically distributed random variables converge to a distribution, this has to be an extreme value distribution (Jagger and Elsner, 2006).

This study uses a statistical model to analyse extreme precipitation events and estimate ARIs using extreme value distributions. The methodology is based on that used by Sanabria and Cechet (2007) for severe wind gusts.

7.2 Methods

7.2.1 Description of the statistical model

The statistical model developed for this study consists of fitting extreme value distributions to the downscaled GCM simulations so that ARIs can be estimated beyond the range of the available model output (or observations). The ARIs are used to assess the maximum 24-hour and 48-hour duration precipitation totals that could be exceeded once, on average, each year. The ARI is the inverse of the complementary cumulative distribution function and thus, a 50-year average recurrence interval event has a probability of exceedance of one-in-every 50 years, or a 2% chance of occurring in any one year.

7.2.2 Selection of independent events

A fundamental condition of extreme value analysis is that events are independent from each other. Precipitation producing weather systems can track slowly across the state, thus the same event may span several days at any given location. It was therefore essential to sort the precipitation simulations into independent events before the extreme value distribution fitting procedure could be employed. This was achieved using the method developed by Stephenson (2004), based on defining the threshold above which the precipitation events were extracted (typically this can be relatively low) and the number of consecutive values below the threshold such that the event may be considered to have ended and a new event may occur. In this report, a threshold of 10 mm has been used to define an event, which is considered to have ended when precipitation has dropped below the 10 mm threshold for three (or more) days. The final value for each independent event is then given by the maximum precipitation value in this period. This process of event selection was repeated across each of the six GCM downscaled simulations.

7.2.3 The generalized Pareto distribution

There are two types of extreme value distributions that may be applicable to climate simulations. These are block-maxima (for example, Generalized Extreme Value) and threshold-exceedance (for example, generalized Pareto) extreme value distributions. The generalized Pareto distribution (GPD) belongs to the set of threshold-exceedance extreme value distributions as it only uses values that exceed a given high threshold, see 'peaks-over-threshold' method in Coles (2001). It has an advantage over a block-maxima approach as it utilises more data than a maxima distribution (which typically selects only one value per annum). Consequently, GPDs have a better distribution in time, allowing for multiple independent events in any single year. As daily simulations were available from the downscaled GCMs, the GPD was selected as the preferred approach for this study.

A number of techniques to fit the GPD have been developed. The most effective techniques are the maximum likelihood (ML) and the probability

weighted moments (PWM) methods. Although in most cases these two methods produce similar results, Palutikof et al (1999) found that the ML method provides more stable parameter estimates over a range of thresholds, and Gillelland and Katz (2005) recommend the ML method because it allows for the incorporation of covariate information more easily than PWM, which is important in the calculation of confidence intervals. Sanabria and Cechet (2007) reported similar results. Subsequently the ML technique was employed in this study.

There are three distinctive regions of the GPD distribution depending on the sign of the shape parameter shp: if shp > 0, the GPD is concave and has no finite bound (Frechet distribution); if shp = 0, the GPD is a straight line with no finite bound (Gumbel distribution); if shp < 0, the GPD is convex with an asymptotic (bounded) limit (Weibull distribution). Curves falling in the third (or upper) category where the GPD is convex have been shown to be appropriate to naturally limited phenomena, including precipitation, wind and temperature (Sanabria and Cechet 2007).

7.2.4 Automated threshold selection

A fundamental problem when fitting a GPD is the selection of an appropriate extreme threshold. The parameters of the GPD are very sensitive to the threshold selection. High threshold values result in only a small sample of the dataset, most likely to be insufficient for a good fit of the GPD. Similarly, low threshold values result in too many samples that are likely to be non-independent. In this study, the automated threshold selection method developed by Sanabria and Cechet (2007) for extreme wind speeds was adapted for precipitation. The procedure was based on the extreme statistical theory introduced by Coles (2001). A similar procedure has also been utilised for selected extreme events in the Western Port and Western Sydney regions of Australia by Abbs and Rafter (2008; 2009).

The automated GPD fitting procedure generates all feasible ARIs for each grid cell in the study area across Tasmania (2856 cells, of which 721 are land cells) using a continuous algorithm with thresholds increasing in steps of 0.25 mm from a selected starting value of 10 mm. At each step, the algorithm iteratively calculates the shape parameter for a number of possible thresholds. The algorithm is automatically stopped when the remaining number of data points available exceeding the threshold falls below 25. The algorithm then searches the set of possible thresholds such that the maximum value of the threshold differences between ARI-500 and ARI-1000 is <12%. This criteria was developed empirically from large-scale testing of the algorithm to avoid thresholds in the shape parameter being selected leading to non-feasible distributions from the maximum likelihood procedure (Sanabria and Cechet 2007). Large differences between ARI-500 and ARI-1000 would be a sign of numerical instability in the estimation of the GPD. The valid threshold that produces the highest ARI-1000 is then selected and the GPD is estimated from all data values greater than the threshold.

As an example of the selection algorithm, Table 7.1 shows a portion of the results produced by the automated algorithm for a grid cell selected at random for 24-hour duration precipitation events. The valid thresholds are shown in the left-hand column (in steps of 0.25 mm), with the second column displaying the number of data points exceeding each threshold. The third column shows the shape parameter 'shp' for each threshold (note that only shp values less than zero are accepted as per the asymptotic (bounded) limit). The fourth column is the asymptotic (bounded) value 'a'. The next two columns show the extreme precipitation ARIs calculated by the GPD for ARI-500 and ARI-1000 (years). The last column shows the difference between the ARI-1000 and ARI-500. For this example, the appropriate threshold is u = 5.5 mm (in bold). This value is the highest feasible (bounded) curve with the highest value of ARI-1000 (179.26 mm), where 'a' is maximised and the shape parameter is negative. All of the data points above this threshold (103 points in this example) are then used to fit the GPD for this grid cell.

Table 7.1 Example of results produced by the automated threshold *u* selection algorithm for a randomly selected grid cell for 24-hour duration precipitation events. The appropriate threshold (u = 65.5 mm, in bold) is the highest feasible (bounded) curve for this grid cell.

u	No>*u*	shp	*a*	ARI–500 (mm)	ARI–1000 (mm)	ARI-diff (mm)
64.00	114	-0.03	675.43	164.37	172.54	8.16
64.25	110	0.00	3500.98	170.01	178.20	8.19
64.50	109	-0.01	729.83	168.92	177.23	8.31
64.75	108	-0.03	643.83	164.21	172.77	8.56
65.00	106	-0.03	606.42	163.86	172.00	8.14
65.25	105	-0.02	871.08	165.45	174.32	8.87
65.50	**103**	**-0.01**	**3900.03**	**170.02**	**179.26**	**9.24**
65.75	102	-0.01	1389.71	166.81	176.65	9.84
66.00	100	-0.01	1221.17	166.54	175.96	9.42
66.25	97	-0.02	732.75	165.39	172.12	6.73
66.50	94	-0.03	500.71	164.01	169.30	5.29
66.75	94	-0.02	796.49	165.62	172.72	7.10
67.00	93	-0.02	1020.70	166.19	174.42	8.24

7.2.5 Confidence intervals

To assess the uncertainty inherent in the extreme value distribution fitting, confidence intervals were calculated. For a given probability, the confidence interval shows the range of values in which the value of the ARI lies.

Gillelland and Katz (2005) found that the Profile Likelihood method for the calculation of confidence values to extreme value temperature datasets produced more accurate results as it considers the asymmetry of the data. As precipitation data is also highly asymmetric, the Profile Likelihood method, as developed in Gillelland and Katz (2009), was used. In this study, confidence intervals between 5% and 95% probability were estimated. This interval defines where the true value of the ARI can be found in 90% of cases. Figure 7.1 shows an example ARI plot of 24-hour duration precipitation at a single location in Tasmania (Fingal) with calculated 5th and 95th confidence intervals. Both the upper and lower bounds for the ARI are shown asymmetrically with respect to the calculated ARI. Note that the confidence interval substantially increases in magnitude as the ARI values increase, indicating a higher degree of uncertainty when making inferences substantially beyond the probability range of the observations.

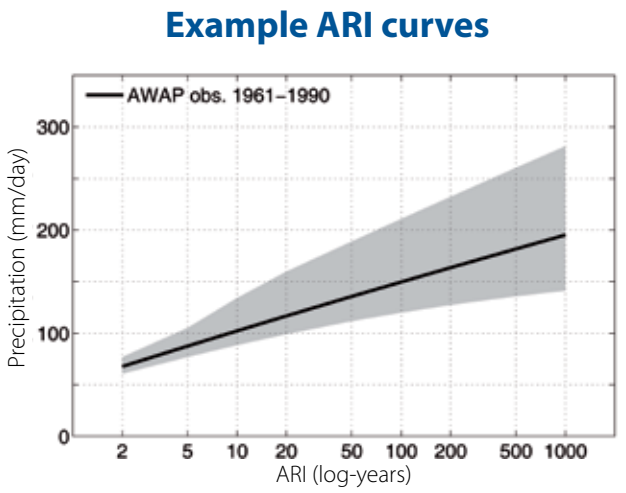

Figure 7.1
Example 24-hour duration precipitation ARIs at Fingal (black line) with 90% confidence interval (grey shading), calculated using a generalized Pareto distribution. ARIs estimated using AWAP gridded observations of daily precipitation for 1961-1990, for ARIs ranging from ARI-2 to ARI-1000 years. ARIs are expressed in mm/d.

7.2.6 Uncertainties and limitations

Some important considerations of the statistical model method developed for this study should be noted:

- The shape of extreme value distributions is necessarily theoretical, and the actual shape of extreme events distributions could differ from it;
- The short length of simulations may not be representative of the real extremes at any given location (for example, the average recurrence interval for extreme precipitation may be much greater than the length of each of the simulations);
- Each grid cell is treated as independent from its neighbouring cell(s). Precipitation events, while typically localised, are likely to be more regional or catchment-wide. The dynamical downscaling process maintains spatial relationships inherent in extreme precipitation events, meaning that this problem is minimised for these projections. However, it is possible that an event that occurs above the GPD selection threshold will occur below the GPD selection threshold for a neighbouring cell, leading to artificial differences in the GPDs calculated for the two cells;
- The statistical model utilises the downscaled GCM simulations that may have as yet, unknown limitations for extremes;
- In addition, other factors such as the dynamical downscaling process, topography in the downscaled GCMs (Section 3.3) and uncertainties in the future emissions also need to be considered.

These considerations can be broadly separated into two kinds of uncertainty: aleatory and epistemic, as suggested in Sanabria and Dhu (2005). This research has considered both, where possible. Aleatory uncertainty includes the natural variability and inherent randomness of complex natural phenomena. This type of uncertainty can be modelled (for example, using random sampling), but cannot be reduced in size. In this section, aleatory uncertainty of extreme precipitation is modelled using extreme value distributions with corresponding confidence intervals. Epistemic uncertainty, on the other hand, is the result of inadequate data and incomplete climate model development due to limitations in knowledge of the physics of the simulated phenomena. This kind of uncertainty can be reduced with improvement to the GCMs, advances in knowledge of the physics and refinement of the climate simulations for extremes. In this section, epistemic uncertainty is dealt with by estimating the ARIs using both individual downscaled GCMs and an ensemble of all six downscaled-GCMs.

Both the aleatory and epistemic uncertainties should to be taken into account when interpreting the results of the ARI estimates presented in this section, especially at the local or individual grid cell level.

7.3 Evaluation of ARI estimates

The performance of the automated extreme value GPD fitting procedure in modelling the magnitude and frequency of extreme 24-hour and 48-hour duration precipitation events was investigated using the non-bias-adjusted (see Section 3.4) downscaled GCM simulations across Tasmania. The procedure was applied to each of the six downscaled-GCM simulations for the A2 emissions scenario and the AWAP gridded dataset on an identical 0.1-degree grid resolution across the state. The performance of the simulations was then evaluated against the AWAP gridded data using the reference period of 1961-1990.

The 24-hour duration ARI-200 (in years) is primarily used as a representation of the ARI validation process in this section. However, all ARIs (ranging from ARI-2 to ARI-1000, for 24-hour and 48-hour durations) were also used in the validation process for this report.

The performance of the individual downscaled GCMs was assessed by comparing the spatial patterns of the ARI magnitudes across the state. Figure 7.2 compares 24-hour duration ARI-200 magnitudes for the validation period 1961-1990, generated for each of the six downscaled-GCM simulations for the A2 emissions scenarios. Note that for this reference period, all of the downscaled GCMs use the same 30-year climatology for the reference period (Corney et al 2010). Figure 7.3 shows the corresponding 90% CI for each GCM (shown as an absolute range between the 5th and 95th CIs).

The magnitudes of ARI-200 for the six single downscaled GCMs were shown to be fairly consistent between each other, both spatially and in magnitude (Figure 7.2). The majority of the downscaled GCMs show areas such as the North-Western Tiers, the northern plateau and the north-eastern coastal region of the state as typically producing the highest precipitation magnitudes across Tasmania.

Similarly, in Figure 7.3, the 90% CI ranges were also found to be relatively consistent across the downscaled GCMs, with no simulation producing ARI magnitudes greatly inconsistent with any other. This was found to be the case for all ARI magnitudes ranging from ARI-2 to ARI-1000 for the 24-hour duration events (not shown).

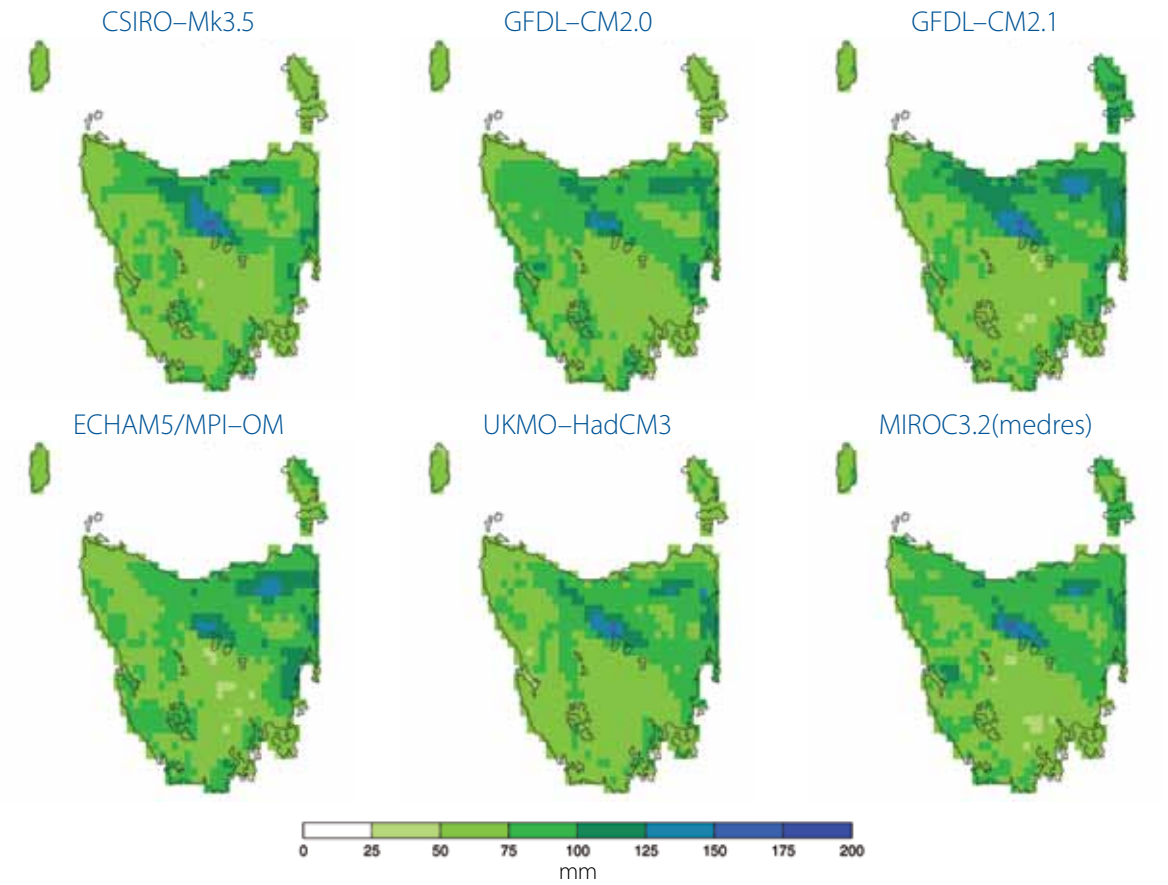

Figure 7.2 Magnitudes of 24-hour duration ARI-200 (years) for 1961-1990 calculated using a generalized Pareto distribution for the six downscaled-GCMs across Tasmania for the A2 emissions scenario simulations. ARIs are expressed in millimetres.

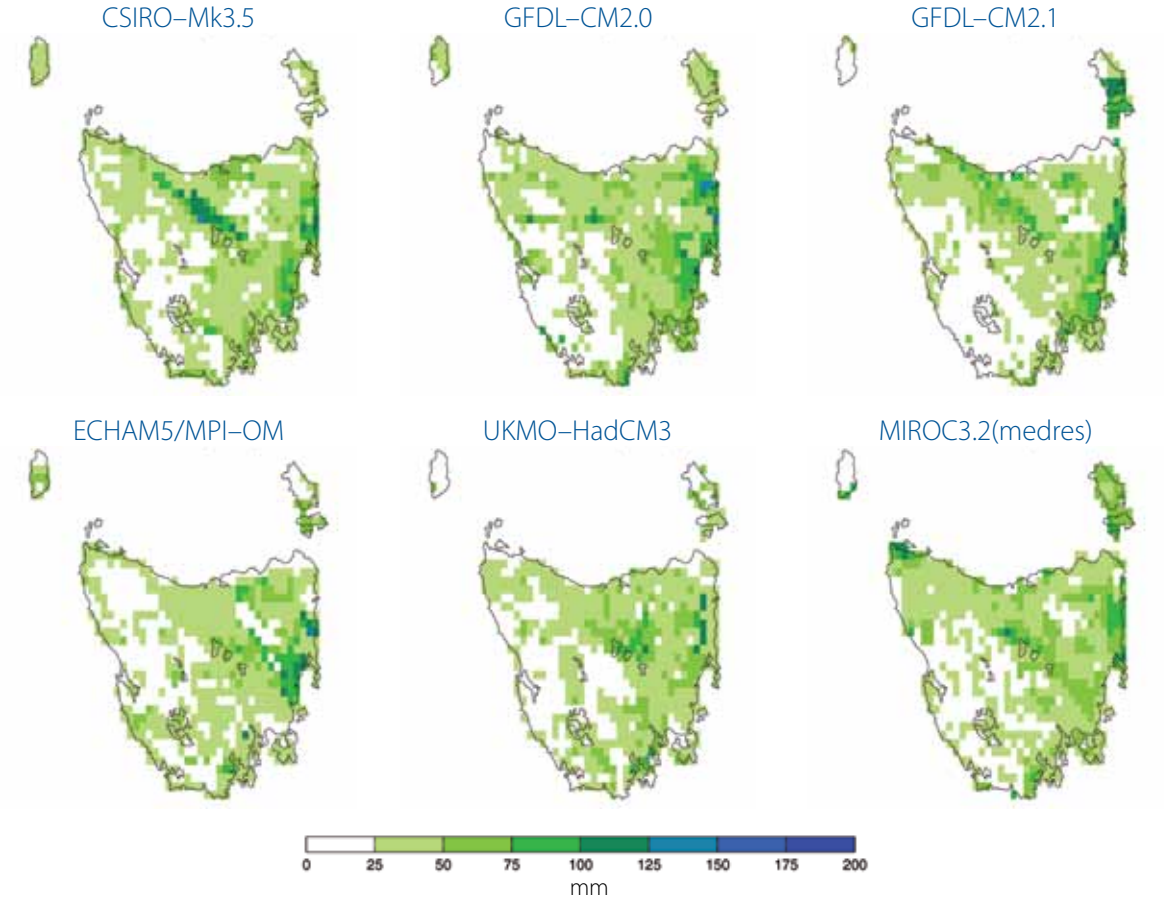

Figure 7.3 As for Figure 7.2, but showing the 90% confidence intervals, expressed in mm.

Overall, the ARI-200 estimates from each of the single downscaled GCM simulations show a good degree of similarity with the ARI-200 estimated from the AWAP dataset (Figure 7.4a). The ARI-200 from the downscaled GCM simulations has a magnitude in the same range and a similar spatial pattern as the ARI-200 from AWAP. The ARI-200 from the six individual downscaled GCMs show similar spatial features over eastern Tasmania and in the north as the ARI-200 from AWAP, and both estimates have smaller magnitudes over the southern and central highlands. An overall qualitative consistency across the ARIs estimated from the six downscaled-GCMs and AWAP was noted, which is particularly noteworthy considering the multiple tiers of calculations required to estimate ARIs combined with the dynamical downscaling process, and the use of the AWAP dataset, which has its own biases and errors.

However, results from the single downscaled GCM simulations (Figure 7.2) with ARI-200 magnitudes from the AWAP dataset (Figure 7.4a) reveals an underestimation of the ARI magnitudes in many regions by the downscaled GCMs, particularly in areas of significantly varied topography. The largest discrepancy was the high magnitudes in AWAP in southern Tasmania, a relatively sparse data region with substantial topographical features conducive to extreme precipitation events. Some variation between neighbouring cells was also noted, a result of the sensitivity of the automated GPD fitting procedure to the threshold selection procedure and the number of available events in the distribution from each downscaled GCM simulation. Therefore, given the relatively limited number of extreme events in each downscaled GCM simulation per 30-year period, it was decided to repeat the automated GPD fitting procedure using an ensemble of the six single downscaled GCM simulations for the A2 emissions scenario. This was possible due to the relative consistency found across the six single downscaled GCM simulations. The ensemble method provides a larger sample size of extreme precipitation events from which to estimate the ARI magnitudes (for example, the six GCMs produced a distribution of 180 years of 24-hour simulations for the 1961-1990 validation period).

Figure 7.4b shows the estimated magnitudes of ARI-200 using the multi-GCM ensemble of six downscaled-GCMs for the A2 emissions scenario. This shows an improvement compared to the single downscaled GCM magnitudes. This result illustrates the benefits of using multiple models to improve the accuracy of the estimates of the ARI magnitudes and to reduce model biases (for example, Ebert 2001). Figure 7.4c and Table 7.2 show that some differences remain, with some regions displaying magnitudes from the multi-GCM ensemble that were too high (mainly in the south-west and western regions and in the mid-northern area around Launceston), while other regions displayed magnitudes that were too low (notably the north-eastern area of the state around St Helens) compared to the ARIs estimated from the AWAP dataset. Table 7.2 also shows that the number of independent events used in the automated GPD fitting procedure (here estimated using events exceeding 10 mm and a standard event window of +/- 3 days) to be consistently higher in the downscaled GCM ensemble when compared to the AWAP gridded observations (typically + 10% to 20%). In spite of these differences, the multi-GCM ensemble ARIs were all found to lie within the 90% confidence interval of the ARIs estimated from the AWAP gridded observations for these locations.

7.4 Results

The automated GPD fitting procedure produced a suite of future projections for 24-hour and 48-hour duration precipitation events for a range of ARIs (from ARI-2 to ARI-1000). Figure 7.5 shows a panel of the projected proportional changes (as a percentage change) relative to the magnitudes of ARI-10 to ARI-500 (years) for 2010-2039, 2040-2069 and 2070-2099 relative to the 1961-1990 baseline period for the multi-GCM ensemble, for 24-hour and 48-hour duration events respectively. ARI estimates from the AWAP gridded observations are shown for the baseline period. The results for ARI-200 for 24-hour and 48-hour duration events are summarised (as both absolute and percentage changes) in Table 7.3 and Table 7.4 respectively, at representative locations across Tasmania.

Considerable changes are projected to the magnitudes of extreme precipitation events. The size and character of changes is found to vary across Tasmania, although in general the majority of the state displays a projected increase in the ARI magnitudes by the end of the century. The projected changes indicate an increase in the intensity of both the 24-hour and 48-hour duration precipitation events.

The trend in the 24-hour duration events is strongest in the eastern and northern regions. The projected change in the magnitudes of the ARIs in the north-east is particularly noteworthy as it is this region that has the highest observed precipitation magnitudes in Tasmania (Bureau of Meteorology 2010a).

This emerging pattern of increased magnitudes is explored further at four representative locations across Tasmania in Figure 7.7. The left panels show the absolute magnitudes of the 24-hour duration ARI-2 to ARI-1000 (years) for 1961-1990 and 2070-2099 with corresponding 90% CI ranges. The right panels show the same absolute magnitudes of the 24-hour duration ARIs (CI ranges not shown) for the three future periods of 2010-2039, 2040-2069 and 2070-2099 relative to the AWAP gridded observations for 1961-1990.

Table 7.2 Comparison of magnitudes of the annual mean number of independent events and 24-hour duration ARI-200 (years) estimated from AWAP gridded observations and the multi-GCM ensemble for 1961-1990, at eight representative locations across Tasmania. Independent events estimated using events exceeding 10 mm and a standard event window of +/- 3 days. ARIs estimated using a generalized Pareto distribution. Multi-GCM ensemble ARIs estimated using the six downscaled-GCMs for the A2 emissions scenario. ARIs are expressed in mm. Location of sites is shown in Appendix A.

Location	Annual mean number of independent events		ARI-200 (mm)	
	AWAP (1961-1990)	Multi-GCM ensemble (1961-1990)	AWAP (1961-1990)	Multi-GCM ensemble (1961-1990)
Hobart	13.3	14.3	100 (76/128)	97 (87/106)
Swansea	10.8	12.4	122 (91/162)	121 (97/158)
St Helens	16.4	18.5	145 (107/210)	119 (110/128)
Launceston	14.6	15.8	66 (51/85)	94 (77/119)
Devonport	19.3	22.0	97 (76/131)	84 (83/87)
Strahan	34.0	39.7	68 (65/73)	101 (93/109)
Strathgordon	34.2	40.6	97 (93/105)	80 (72/88)
Miena/Liawenee	20.3	22.4	98 (78/134)	73 (59/93)

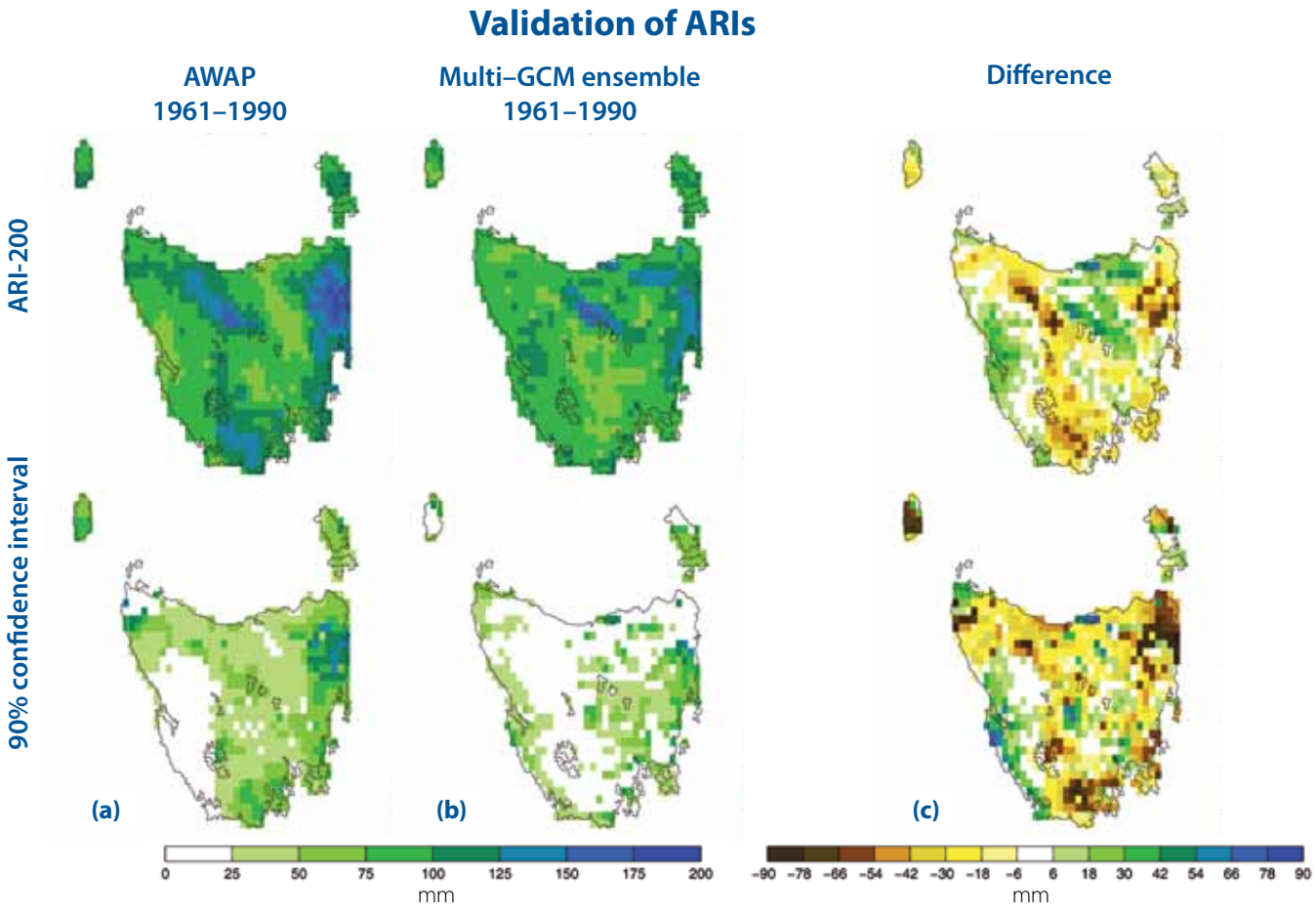

Figure 7.4 Magnitudes of 24-hour duration ARI-200 (years) (top panels) with 90% confidence intervals (bottom panels) for 1961-1990, displaying a) AWAP gridded observations, b) multi-GCM ensemble, and c) the difference between a) and b), estimated using a generalized Pareto distribution. Multi-GCM ensemble ARIs estimated using the six downscaled-GCMs across Tasmania for the A2 emissions scenario. ARIs and differences are expressed in mm.

The plots display substantial increases to the ARI magnitudes relative to the reference period (at St Helens in particular in this example) over the coming century.

It is interesting to note that the projected changes are not uniform increases across the three future periods of 2010-2039, 2040-2069 and 2070-2099. Figure 7.7 (right panels) and Table 7.3 suggest the change to the 24-hour duration ARI magnitudes may actually decrease at some locations in the latter part of the 21st century (2070-2099) when compared to the middle part of the century (2040-2069). Miena/ Liawenee in the central highlands is an example of this phenomenon, and in this case is consistent with the relatively large projected decline in annual precipitation over the central highlands. Other regions, such as the eastern and north-east coastal areas, including Swansea and St Helens, display a jump in the magnitude of extreme 24-hour duration precipitation events in the 2070-2099 period. This is likely to be the impact of strengthening greenhouse gas signal on extreme rainfall rising above natural variations.

7.5 Summary

The projected changes of the ARI estimates indicate an increase in the magnitudes of the 24-hour and 48-hour duration precipitation events across the state by the end of the 21st century. The percentage changes in the average recurrence intervals are broadly consistent with the underlying climate drivers of weather in Tasmania. The largest increases in the average recurrence intervals occur in the north-east (in some regions as much as 90%, Table 7.3), precisely where the most variable and intense precipitation already occur in both the observations used in AWAP gridded dataset and downscaled simulations of the current climate (for example, Grose et al 2010).

The broad consistency between the AWAP estimates of the ARI and those from the simulations for the reference period are striking (Figure 7.4), and consequently give confidence that the future projections are broadly realistic changes on the current observed climate. The implication of the projected changes to the future Tasmanian climate is that more frequent and more intense precipitation events will cause the recurrence intervals to decrease.

Figure 7.5 Magnitudes of 24-hour duration ARI-10 to ARI-500 (years) for 1961-1990 (left most panels) estimated from AWAP gridded observations (expressed in mm), with mean ARIs estimated from multi-GCM ensemble shown as the percentage change (right three panels) for 2010-2039, 2040-2069 and 2070-2099, relative to the AWAP 1961-1990 baseline using a generalized Pareto distribution. Multi-GCM ensemble ARIs estimated using the six downscaled-GCMs across Tasmania for the A2 emissions scenario.

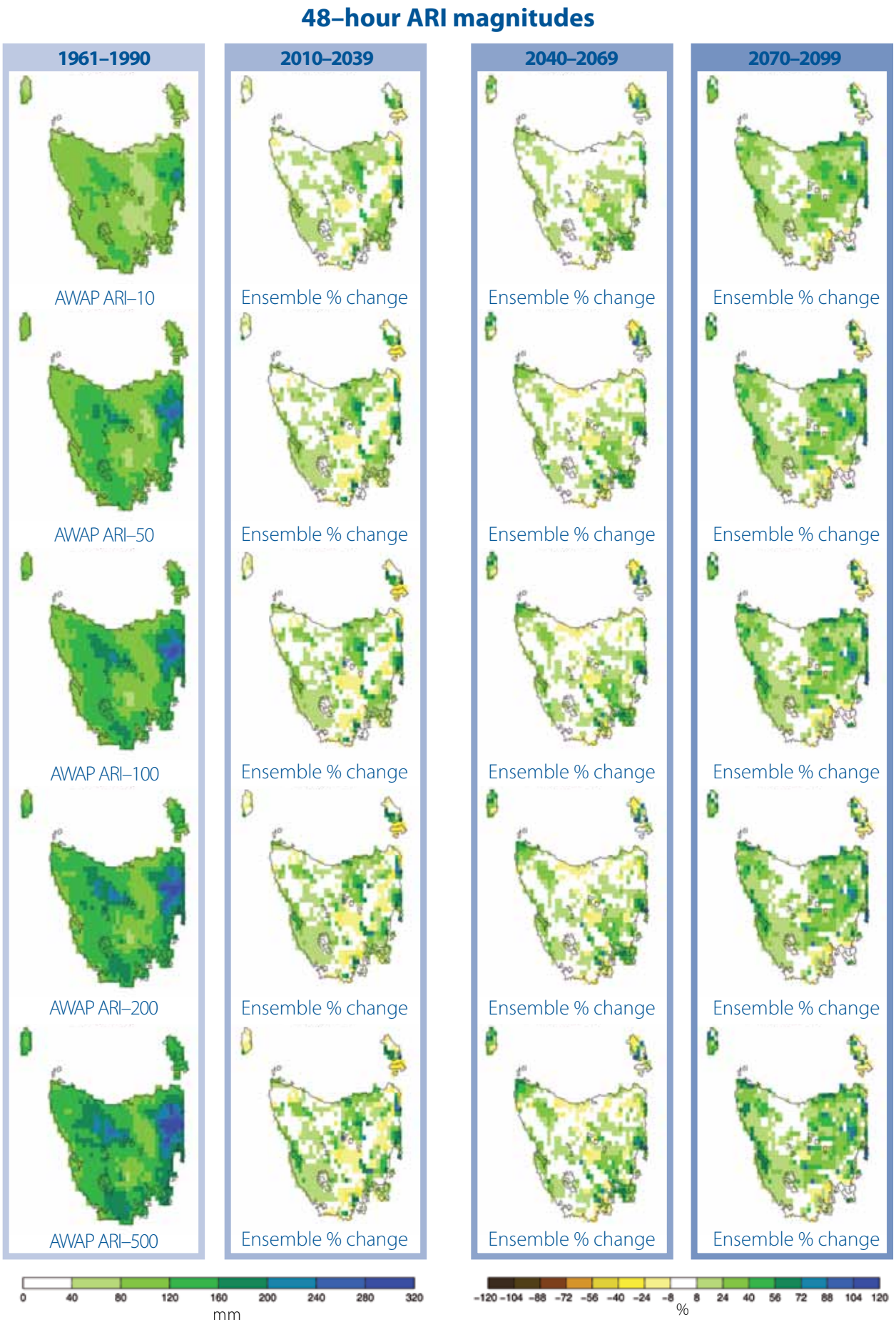

Figure 7.6 As for Figure 7.5, but showing the 48-hour duration ARI magnitudes.

Table 7.3 Magnitudes of 24-hour duration ARI-200 (years) for 1961-1990 estimated from AWAP gridded observations (5th/95th CIs in brackets), with projected multi-GCM ensemble change for 2010-2039, 2040-2069 and 2070-2099, at eight representative locations across Tasmania. ARIs estimated using a generalized Pareto distribution. Multi-GCM ensemble ARIs estimated using the six downscaled-GCMs for the A2 emissions scenario. ARIs are expressed in mm. Delta ARI-200 values are expressed in millimetres and as a percentage change (in square brackets []), relative to the AWAP 1961-1990 baseline. Location of sites is shown in Appendix A

	ARI–200 (mm)	Delta ARI–200 (mm)		
Location	AWAP (1961–1990)	Multi–GCM ensemble (2010–2039)	Multi–GCM ensemble (2040–2069)	Multi–GCM ensemble (2070–2099)
Hobart	100 (76/128)	31 [31%]	40 [40%]	30 [30%]
Swansea	122 (91/162)	16 [13%]	14 [11%]	112 [92%]
St Helens	145 (107/210)	10 [7%]	40 [27%]	68 [47%]
Launceston	66 (51/85)	3 [4%]	34 [51%]	34 [52%]
Devonport	97 (76/131)	4 [4%]	23 [24%]	36 [37%]
Strahan	68 (65/73)	6 [9%]	8 [12%]	18 [26%]
Strathgordon	97 (93/105)	21 [21%]	30 [31%]	36 [37%]
Miena/Liawenee	98 (78/134)	50 [51%]	30 [30%]	5 [5%]

Table 7.4 As for Table 7.3, but showing 48-hour duration ARI-200 (years) estimates.

	ARI–200 (mm)	Delta ARI–200 (mm)		
Location	AWAP (1961–1990)	Multi–GCM ensemble (2010–2039)	Multi–GCM ensemble (2040–2069)	Multi–GCM ensemble (2070–2099)
Hobart	134 (100/178)	29 [22%]	-6 [-4%]	-54 [-41%]
Swansea	177 (133/237)	58 [33%]	127 [72%]	56 [32%]
St Helens	200 (152/368)	192 [96%]	58 [29%]	135 [68%]
Launceston	92 (73/135)	56 [61%]	16 [17%]	42 [46%]
Devonport	127 (102/157)	21 [16%]	17 [14%]	28 [22%]
Strahan	119 (99/150)	42 [35%]	20 [17%]	58 [49%]
Strathgordon	144 (130/163)	6 [4%]	21 [15%]	14 [10%]
Miena/Liawenee	151 (112/231)	-20 [-14%]	-27 [-18%]	-16 [-11%]

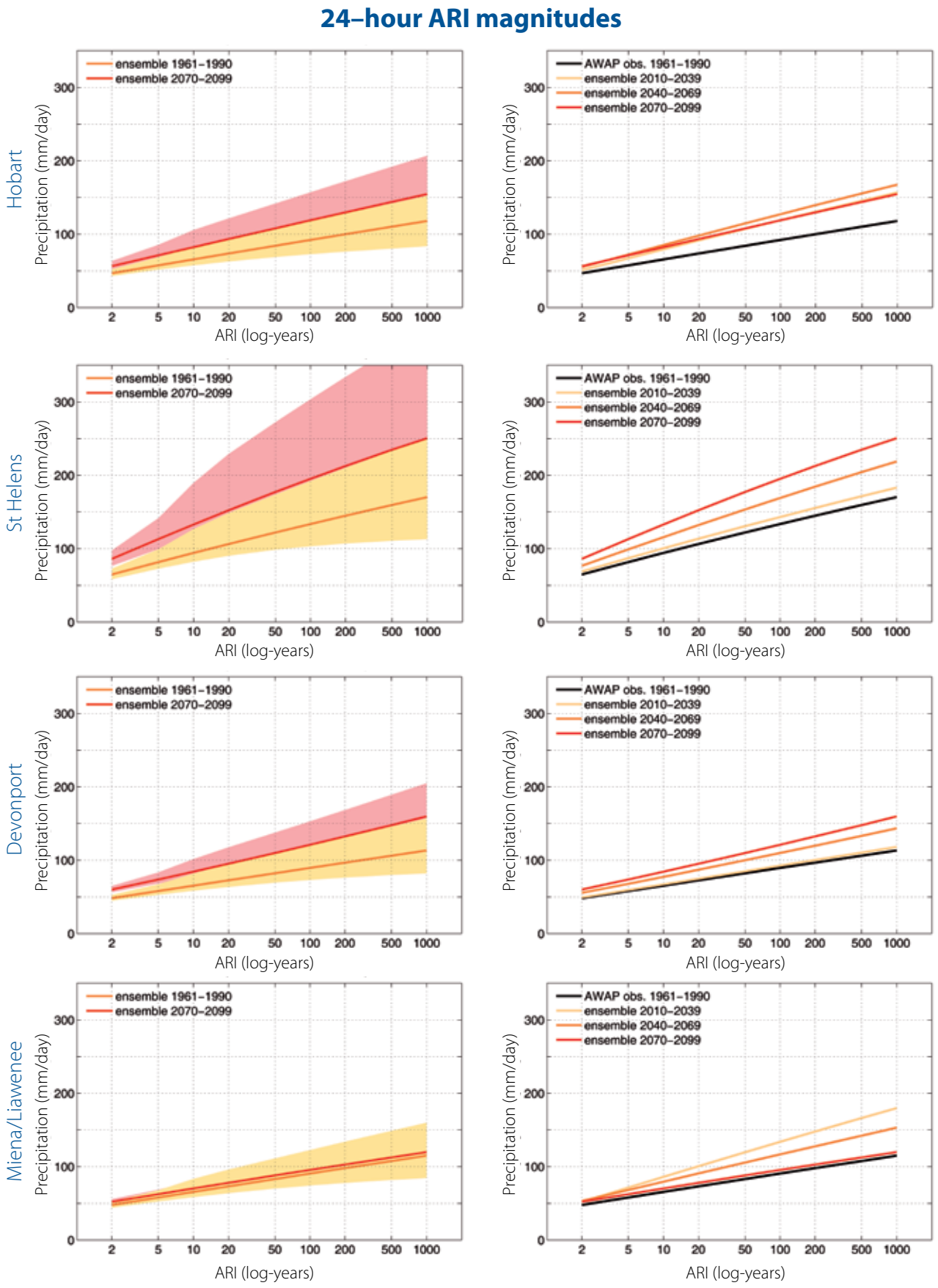

Figure 7.7 Left panels: Projected magnitudes of 24-hour duration ARI-2 to ARI-1000 (years) for 2070-2099 (red lines) compared to 1961-1990 (dark orange lines) using multi-GCM ensembles at four representative locations across Tasmania, calculated using a generalized Pareto distribution. 90% confidence intervals shown for 1961-1990 (light orange shading) and 2070-2099 (light red shading). Right panels: as for left panels, but showing a comparison of the projected changes to the 24-hour duration ARI estimates for 1961-1990 (black lines), 2010-2039 (light orange lines), 2010-2039 (dark orange lines) and 2070-2099 (red lines). Multi-GCM ensemble ARIs estimated using the six downscaled-GCMs for the A2 emissions scenario. ARIs are expressed in mm. Location of sites is shown in Appendix A.

References

Abbs D and Rafter T 2008, *The Effect of Climate Change on Extreme Rainfall Events in the Western Port Region*, CSIRO Marine and Atmospheric Research, Melbourne, Australia.

Abbs D and Rafter T 2009, *Impact of Climate Variability and Climate Change on Rainfall Extremes in Western Sydney and Surrounding Areas. Report to the Sydney Metro Catchment Management Authority and Partners*, CSIRO Marine and Atmospheric Research, Melbourne, Australia.

ACE CRC 2008, *Position Analysis: Climate change, sea-level rise and extreme events: impacts and adaptation issues,* Antarctic Climate & Ecosystems Cooperative Research Centre (ACE CRC), PA01-0809011.

Alexander LV, Zhang X, Peterson TC, Caesar J, Gleason B, Klein Tank AMG, Haylock M, Collins D, Trewin B, Rahim F, Tagipour A, Kumar Kolli R, Revadekar JV, Griffiths G, Vincent L, Stephenson DB, Burn J, Aguilar E, Brunet M, Taylor M, New M, Zhai P, Rusticucci M, and Vazquez Aguirre JL 2006, Global observed changes in daily climate extremes of temperature and precipitation, *Journal of Geophysical Research-Atmospheres* 111: D05109, DOI:10.1029/2005JD006290.

Alexander LV and Arblaster JM 2009, 'Assessing trends in observed and modelled climate extremes over Australia in relation to future projections', *International Journal of Climatology* 29(3): 417–435, DOI: 10.1002/joc.1730.

Bennett JC, Ling FLN, Graham B, Grose MR, Corney SP, White CJ, Holz GK, Post DA, Gaynor SM & Bindoff NL 2010, *Climate Futures for Tasmania: water and catchments technical report,* Antarctic Climate & Ecosystems Cooperative Research Centre, Hobart.

Bureau of Meteorology 2008, *Tasmania's Weather Tales: One Hundred Years of Weather and Climate Services in Tasmania and Antarctic*, Bureau of Meteorology, ISBN 0642706026.

Bureau of Meteorology 2010a, *Drought Statement*, Bureau of Meteorology, http://www.bom.gov.au/climate/drought/drought.shtml (Retrieved 2010-04-16).

Bureau of Meteorology 2010b, *Climate Education,* Bureau of Meteorology, http://www.bom.gov.au/lam/climate/index.htm (Retrieved 2010-04-16).

Bureau of Meteorology 2010c, *Rainfall and Temperature Extremes,* Bureau of Meteorology, http://www.bom.gov.au/climate/extreme/records.shtml (Retrieved 2010-05-18).

Bureau of Meteorology 2010d, *Australian High Quality Climate Site Networks, Bureau of Meteorology*, http://www.bom.gov.au/cgi-bin/climate/hqsites/site_networks.cgi (Retrieved 2010-11-12).

Bureau of Meteorology 2010e, *Monthly Weather Review – Tasmania, July 2010*, Bureau of Meteorology, http://www.bom.gov.au/cgi-bin/climate/mwr/. ISSN 1836-2982.

Cechet RP, Sanabria A, Divi CB, Thomas C, Yang T, Arthur C, Dunford M, Nadimpalli K, Power L, White CJ, Bennett JC, Corney SP, Holz GK, Grose MR, Gaynor SM & Bindoff NL in prep, *Climate Futures for Tasmania: severe wind hazard and risk technical report*, Antarctic Climate & Ecosystems Cooperative Research Centre, Hobart, Tasmania.

Christensen JH, Hewitson B, Busuioc A, Chen A, Gao X, Held I, Jones R, Kolli RK, Kwon W-T, Laprise R, Magaña Rueda V, Mearns L, Menéndez CG, Räisänen J, Rinke A, Sarr A & Whetton P 2007, 'Regional climate projections', in *Climate Change 2007: The Physical Science Basis. Contribution of Working Group I to the Fourth Assessment Report of the Intergovernmental Panel on Climate Change*, [Solomon S, Qin D, Manning M, Chen Z, Marquis M, Averyt KB, Tignor M & Miller HL (eds)], Cambridge University Press, Cambridge, United Kingdom and New York, NY, USA.

Coles S 2001, *An Introduction to Statistical Modelling of Extreme Value*, Springer series in statistics, London.

Corney SP, Katzfey JJ, McGregor JL, Grose MR, Bennett JC, White CJ, Holz GK, Gaynor SM & Bindoff NL 2010, *Climate Futures for Tasmania: climate modelling technical report,* Antarctic Climate & Ecosystems Cooperative Research Centre, Hobart.

CSIRO and Bureau of Meteorology 2007, *Climate change in Australia: impacts, adaptation and vulnerability. Technical Report*, 140pp.

CSIRO 2009, *Water availability for Tasmania. Report one of seven to the Australian Government from the CSIRO Tasmania Sustainable Yields Project,* CSIRO Water for a Healthy Country Flagship, Australia.

Diffenbaugh NS, Pal JS, Trapp RJ and Giorgi F 2005, 'Fine-scale processes regulate the response of extreme events to global climate change', *Proceedings of the National Academy of Science USA*, 102(44), 15774–15778.

Easterling DR, Chagnon S, Karl TR, Meehl J and Parmesan C 2000, 'Climate extremes: observations, modeling and impacts,' *Science*, 289(5487), 2068-2074.

Ebert EE 2001, 'Ability of a poor man's ensemble to predict the probability and distribution of precipitation', *Monthly Weather Review*, 129, 2461-2480.

Frich P, Alexander LV, Della-Marta P, Gleason B, Haylock M, Klein Tank AMG and Peterson T 2002, 'Observed coherent changes in climatic extremes during the second half of the twentieth century', *Climate Research* 19: 193–212.

Gillelland E and Katz RW 2005, *Analysing Seasonal to Interannual Extreme Weather and Climate Variability with the Extremes Toolkit,* National Center for Atmospheric Research (NCAR), Boulder CO, USA.

Gillelland E and Katz RW 2009, *Extremes Toolkit (extRemes): Weather and Climate Applications of Extreme Value Statistics*, National Center for Atmospheric Research (NCAR), Boulder CO, USA.

Griffiths GM, Chambers LE, Haylock MR, Manton MJ, Nicholls N, Baek HJ, Choi Y, Della-Marta PM, Gosai A, Iga N, Lata R, Laurent V, Maitrepierre L, Nakamigawa H, Ouprasitwong N, Solofa D, Tahani L, Thuy DT, Tibig L, Trewin B, Vediapan K and Zhai P 2005, 'Change in mean temperature as a predictor of extreme temperature change in the Asia–Pacific region', *International Journal of Climatology,* 25(10), 1301-1330.

Groisman PY, Karl TR, Easterling DR, Knight RW, Jamason PF, Hennessy KJ, Suppiah R, Page CM, Wibig J, Fortuniak K, Razuvaev VN, Douglas A, Førland E and Zhai PM 1999, 'Changes in the probability of heavy precipitation: Important indicators of climatic change', *Climatic Change,* 42, 243–283.

Grose MR, Barnes-Keoghan I, Corney SP, White CJ, Holz GK, Bennett JC, Gaynor SM & Bindoff NL 2010, *Climate Futures for Tasmania: general climate impacts technical report,* Antarctic Climate & Ecosystems Cooperative Research Centre, Hobart.

Haylock MR, Peterson T, Abreu de Sousa JR, Alves LM, Ambrizzi T, Baez J, Barbosa JI, Barros VR, Berlato MA, Bidegain M, Coronel G, Corradi V, Grimm AM, Jaildo dos Anjos R, Karoly D, Marengo JA, Marino MB, Meira PR, Miranda GC, Molion L, Moncunill DF, Nechet D, Ontaneda G, Quintana J, Ramirez E, Rebello E, Rusticucci M, Santos JL, Varillas IT, Villanueva JG, Vincent L and Yumiko M 2006, 'Trends in total and extreme South America rainfall 1960-2000 and links with sea surface temperature', *Journal of Climate*, 19: 1490-512.

Haynes K, Tibbits A and Lowe T, 'Local knowledge and gender: re-evaluating the 1967 Hobart bushfire fatalities', *Risk Frontiers Quarterly Newsletter*, Volume 7, Issue 2, 2008.

Hennessy K, Lucas C, Nicholls N, Suppiah R and Ricketts J 2005, *Climate change impacts on fire-weather in south-east Australia*, CSIRO, Australia, 88 pp.

Hennessy K, Fawcett R, Kirono D, Mpelasoka F, Jones D, Bathols J, Whetton P, Stafford Smith M, Howden M, Mitchell C and Plummer N 2008, *Drought: exceptional circumstances, An assessment of the impact of climate change on the nature and frequency of exceptional climatic events,* CSIRO and Bureau of Meteorology, 33pp., http://www.bom.gov.au/droughtec.

Holz GK, Grose MR, Bennett JC, Corney SP, White CJ, Phelan D, Potter K, Kriticos D, Rawnsley R, Parsons D, Lisson S, Gaynor SM & Bindoff NL 2010, *Climate Futures for Tasmania: impacts on agricultural technical report,* Antarctic Climate & Ecosystems Cooperative Research Centre, Hobart.

IPCC 2007a, *Climate Change 2007: The Physical Science Basis, Contribution of Working Group I to the Fourth Assessment Report of the Intergovernmental Panel on Climate Change* [Solomon S, Qin D, Manning M, Chen Z, Marquis M, Averyt KB, Tignor M and Miller HL (eds)], Cambridge University Press, Cambridge, United Kingdom and New York, NY, USA.

IPCC 2007b, 'Summary for Policy Makers', in *Climate Change 2007: Impacts, Adaptation and Vulnerability, Contribution of Working Group II to the Fourth Assessment Report of the Intergovernmental Panel on Climate Change* [Parry ML, Canziani OF, Palutikof JP, van der Linden PJ and Hanson CE (eds)], Cambridge University Press, Cambridge, UK, and New York, pp. 7-22, http://www.ipcc.ch.

Jagger TH and Elsner JB 2006, 'Climatology Models for Extreme Hurricane Winds near the United States', *Journal of Climate*, Vol. 19, 3220-3236.

Jones DA, Wang W and Fawcett R 2009, 'High-quality spatial climate data-sets for Australia', *Australian Meteorological and Oceanographic Journal*, 58: 233-248.

Kharin VV, Zwiers FW and Zhang X 2005, 'Intercomparison of near surface temperature and precipitation extremes in AMIP-2 simulations, reanalyses and observations', *Journal of Climate*, 18: 5201-5223.

Kharin VV, Zwiers FW, Zhang X, and Hegerl GC 2007, 'Changes in temperature and precipitation extremes in the IPCC ensemble of global coupled model simulations', *Journal of Climate*, 20, 1419--1444.

Kiktev D, Sexton D, Alexander L and Folland C 2003, 'Comparison of modelled and observed trends in indicators of daily climate extremes', *Journal of Climate*, 16: 3560-71.

Le Quéré C, Raupach MR, Canadell JG, Marland G, Bopp L, Ciais P, Conway TJ, Doney SC, Feely RA, Foster P, Friedlingstein P, Gurney K, Houghton RA, House JI, Huntingford C, Levy PE, Lomas MR, Majkut J, Metzl N, Ometto JP, Peters GP, Prentice IC, Randerson JT, Running SW, Sarmiento JL, Schuster U, Sitch S, Takahashi T, Viovy N, van der Werf GR and Woodward FI 2009, 'Trends in the sources and sinks of carbon dioxide', *Nature Geoscience*, 2: 831-836.

McGregor JL and Dix MR 2008, 'An updated description of the Conformal Cubic Atmospheric Model', *High Resolution Simulation of the Atmosphere and Ocean* [Hamilton K and Ohfuchi W. (eds)], Springer, pp. 51-76.

McInnes KL, Macadam I, Hubbert GD and O'Grady JG 2009, 'A Modelling Approach for Estimating the Frequency of Sea Level Extremes and the Impact of Climate Change in Southeast Australia', *Natural Hazards*, 51, 115–137, DOI 10.1007/s11069-009-9383-2.

McInnes KL, O'Grady JG, Hemer M, Macadam I, Abbs DJ, White CJ, Bennett JC, Corney SP, Holz GK, Grose MR, Gaynor SM & Bindoff NL in prep, *Climate Futures for Tasmania: extreme tide and sea level events technical report*, Antarctic Climate & Ecosystems Cooperative Research Centre, Hobart.

McIntosh PC, Pook MJ and McGregor J 2005, *Study of future and current climate: a scenario for the Tasmanian region (stages 2 & 3),* CSIRO Marine and Atmospheric Research, Hobart, Tasmania.

McKee TB, Doesken NJ and Kleist J 1993, 'The relationship of drought frequency and duration to time scales', Eighth Conference on Applied Climatology, *American Meteorological Society*, Jan 17-23, 1993, Anaheim CA, pp. 179-186.

McMichael AJ, Campbell-Lendrum D, Ebi K, Githeko A, Scheraga J and Woodward A (eds) 2003, *Climate Change and Human Health: Risks and Responses,* WHO, Geneva, Switzerland, 322pp.

Meehl GA, Stocker TF, Collins WD, Friedlingstein P, Gaye AT, Gregory JM, Kitoh A, Knutti R, Murphy JM, Noda A, Raper SCB, Watterson IG, Weaver AJ and Zhao Z-C 2007, 'Global Climate Projections' in *Climate Change 2007: The Physical Science Basis. Contribution of Working Group I to the Fourth Assessment Report of the Intergovernmental Panel on Climate Change* [Solomon S, Qin D, Manning M, Chen Z, Marquis M, Averyt KB, Tignor M & Miller HL (eds)], Cambridge University Press, Cambridge, United Kingdom and New York, NY, USA.

Nakićenović N & Swart R (eds) 2000, *Special Report on Emissions Scenarios. A Special Report of Working Group III of the Intergovernmental Panel on Climate Change*. Cambridge University Press, Cambridge, United Kingdom and New York, NY, USA.

Nicholls N and Alexander L 2007, 'Has the climate become more variable or extreme? Progress 1992-2006', *Progress in Physical Geography,* 31, 77-87.

Palmer WC 1965, *Meteorological Drought, Research Paper 45*, US Department of Commerce, Weather Bureau, Washington, DC, 58 pp [Available from NOAA Library and Information Services Division, Washington, DC 20852].

Palutikof JP, Brabson BB, Lister DH and Adcock ST 1999, 'A Review of Methods to Calculate Extreme Wind Speeds', *Meteorological Applications,* 6, 119-132.

Pook MJ, Risbey J, and McIntosh P 2010, East coast lows, atmospheric blocking and rainfall: a Tasmanian perspective, *IOP Conference Series: Earth and Environmental Science* 11: 012011

Raupach MR, Briggs PR, Haverd V, King EA, Paget M and Trudinger CM 2008, *Australian Water Availability Project (AWAP), final report for Phase 3*, CSIRO Marine and Atmospheric Research component, CSIRO Marine and Atmospheric Research, Canberra, Australia, 67pp.

Reynolds RW 1988, 'A real-time global sea surface temperature analysis', *Journal of Climate*, 1, 12.

Risbey JS, Pook MJ, McIntosh PC, Wheeler MC and Hendon HH 2009, 'On the remote drivers of rainfall variability in Australia', *Monthly Weather Review*, 137, 3233-3253.

Sanabria LA and Dhu T 2005, 'A Methodology for Consistent Modelling of Natural Hazards', *Proceedings of the International Congress on Modelling and Simulation (MODSIM05),* December 2005, University of Melbourne, Australia.

Sanabria LA, and RP Cechet 2007, *A Statistical Model of Severe Winds*, Geoscience Australia, Canberra, Record 2007/12, 60pp.

Stephenson A 2004, *A User's Guide to the 'EVD' Package (Version 2.1),* Department of Statistics, Macquarie University, Australia.

Sun Y, Solomon S, Dai A and Portmann R 2006, 'How often does it rain?', *Journal of Climate*, 19: 916–934.

Svensson C and Jones DA 2004, 'Dependence between sea surge, river flow and precipitation in south and west Britain', *Hydrology and Earth System Sciences, 8*: 973-992.

Tebaldi C, Hayhoe K, Arblaster JM and Meehl GA 2006, 'Going to the extremes: an intercomparison of model-simulated historical and future changes in extreme events', *Climatic Change*, 79: 185–211.

The Copenhagen Diagnosis 2009: *Updating the World on the Latest Climate Science*. Allison I, Bindoff NL, Bindschadler RA, Cox PM, de Noblet N, England MH, Francis JE, Gruber N, Haywood AM, Karoly DJ, Kaser G, Le Quéré C, Lenton TM, Mann ME, McNeil BI, Pitman AJ, Rahmstorf S, Rignot E, Schellnhuber HJ, Schneider SH, Sherwood SC, Somerville RCJ, Steffen K, Steig EJ, Visbeck M and Weaver AJ 2009, The University of New South Wales Climate Change Research Centre (CCRC), Sydney, Australia.

Timbal B, Arblaster J, Braganza K, Fernandez E, Hendon H, Murphy B, Raupach M, Rakich C, Smith I, Whan K and Wheeler M 2010, *Understanding the anthropogenic nature of the observed rainfall decline across South Eastern Australia,* CAWCR Technical Report No. 026.

Trenberth KE, Jones PD, Ambenje P, Bojariu R, Easterling D, Klein Tank A, Parker D, Rahimzadeh F, Renwick JA, Rusticucci M, Soden B and Zhai P 2007, 'Observations: Surface and Atmospheric Climate Change', *Climate Change 2007: The Physical Science Basis, Contribution of Working Group I to the Fourth Assessment Report of the Intergovernmental Panel on Climate Change* [Solomon S, Qin D, Manning M, Chen Z, Marquis M, Averyt KB, Tignor M and Miller HL (eds)], Cambridge University Press, Cambridge, United Kingdom and New York, NY, USA.

White CJ 2007, *The use of joint probability analysis to predict flood frequency in estuaries and tidal rivers*, PhD thesis, School of Civil Engineering and the Environment, University of Southampton, UK. [Available from Soton ePrints: http://eprints.soton.ac.uk/63847/].

Wilhite DA and Glantz MH 1985, 'Understanding the drought phenomenon: The role of definitions', *Water International*, 10(3), 111–120.

Williams A, Karoly DJ and Tapper N 2001, 'The sensitivity of Australian fire to climate change', *Climatic Change*, 49, 171-191.

Appendices

Appendix A1
Selected representative locations across Tasmania

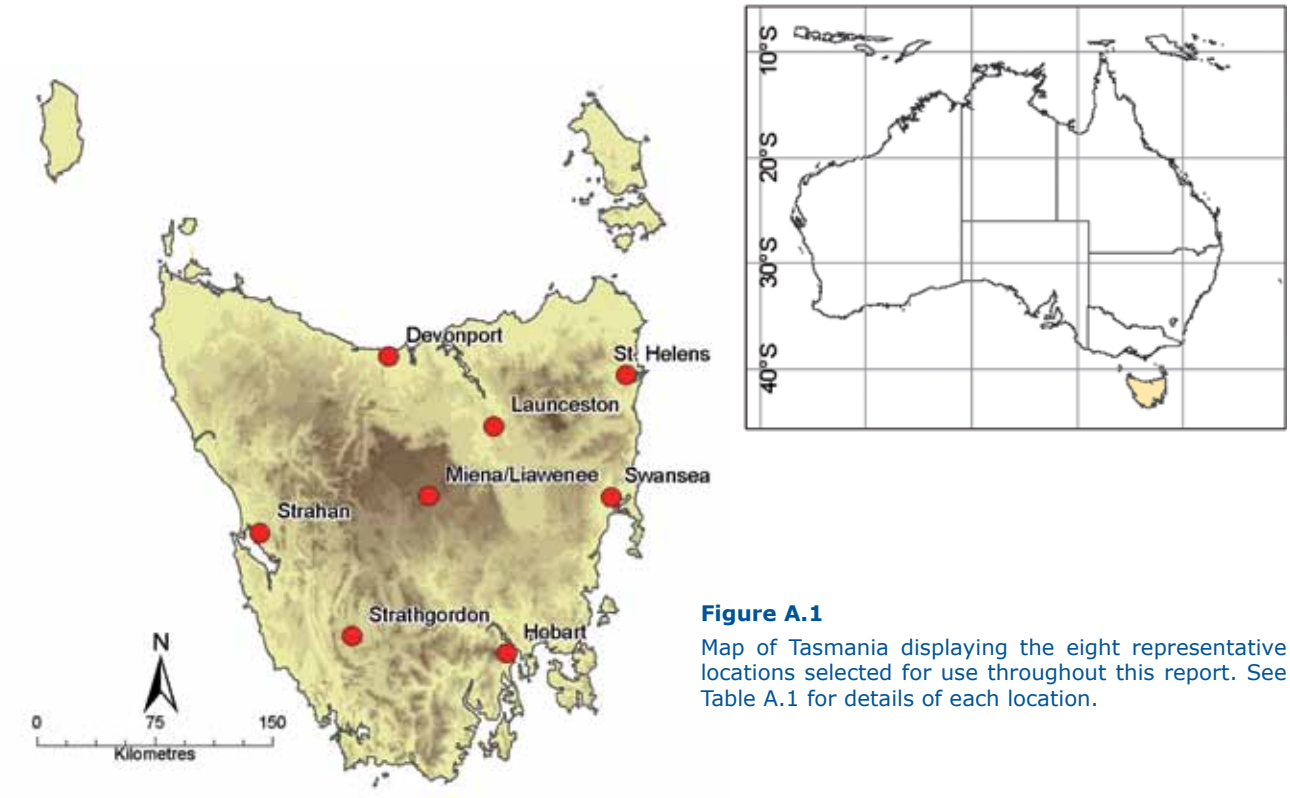

Figure A.1
Map of Tasmania displaying the eight representative locations selected for use throughout this report. See Table A.1 for details of each location.

Table A.1 Details of the eight representative locations across Tasmania selected for use throughout this report.

Location	Grid cell Lat/Long at centroid	Elevation (zs) from 0.1-degree downscaled GCMs (in metres)
Hobart	42.9° S/147.3° E	225.4
Swansea	42.0° S/148.1° E	87.3
St Helens	41.3° S/148.2° E	91.7
Launceston	41.6° S/147.2° E	154.7
Devonport	41.2° S/146.4° E	38.4
Strahan	42.2° S/145.4° E	125.0
Strathgordon	42.8° S/146.1° E	377.0
Miena/Liawenee	42.0° S/146.7° E	1032.0

Appendix A2
Tasmania elevation map

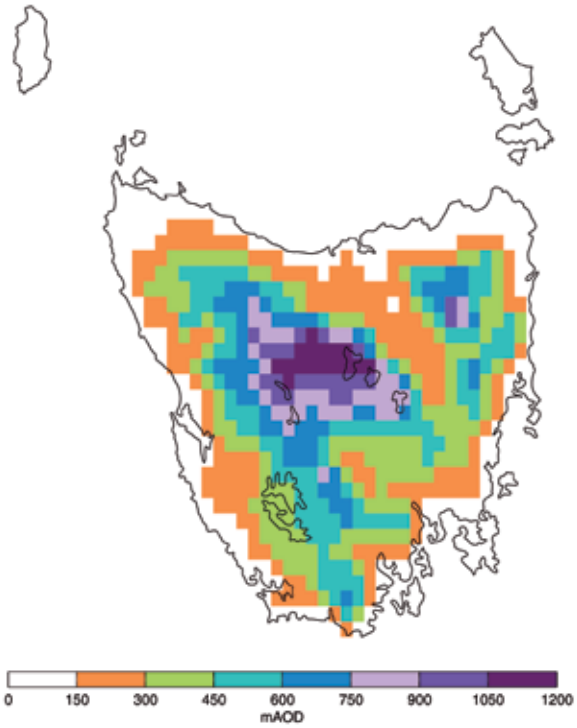

Figure A.2

Elevation map (*zs*) of Tasmania taken from the 0.1-degree downscaled GCMs (in metres) calculated using a 250 m digital elevation model (DEM).

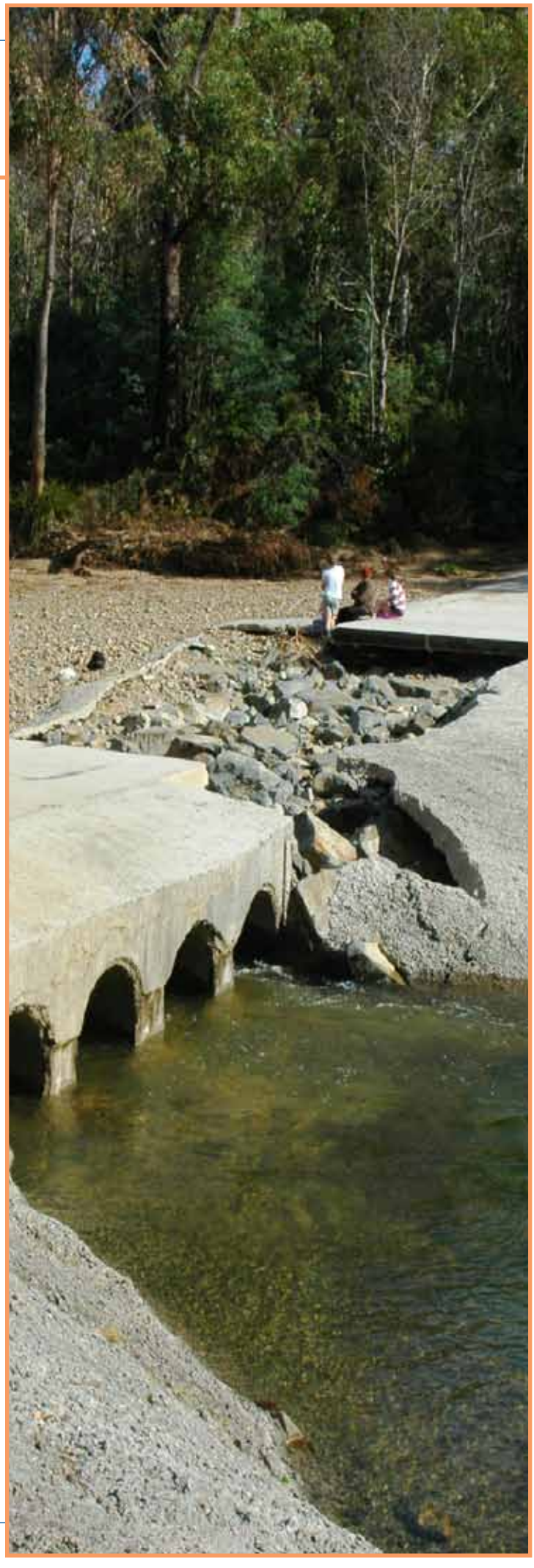

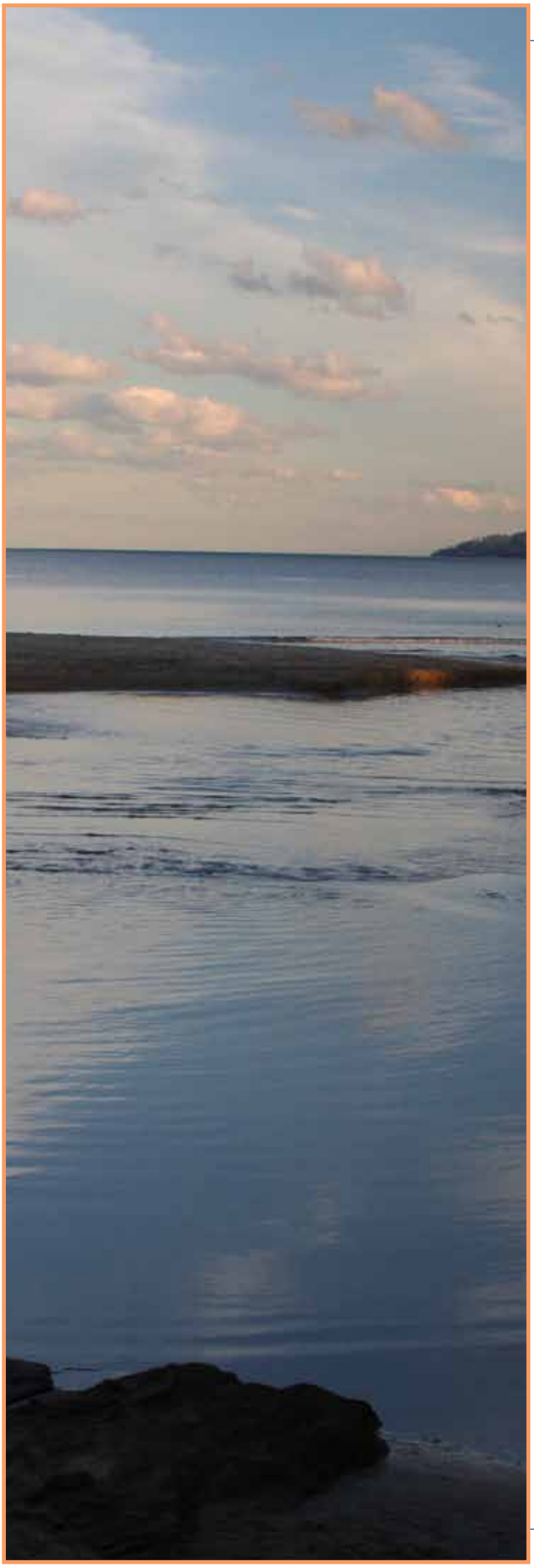

Appendix B1
Summary extreme indices tables

List of tables:

Statewide indices

Table B.1 Summary statewide mean values (721 land cells) for the ETCCDI extreme temperature and precipitation indices. Baseline values for each index show AWAP (gridded observations) and the multi-GCM mean of the six bias-adjusted downscaled GCMs with minimum/maximum range of the six GCMs (in brackets) for 1961-1990. Future projections show the multi-GCM mean delta of the six bias-adjusted downscaled GCMs (expressed in absolute units) with minimum/maximum range of the six GCMs (in brackets) for 2010-2039, 2040-2069 and 2070-2099, relative to the 1961-1990 baseline. All indices expressed as an annual mean. Cells labelled '-' n/a for index.

			Change relative to Baseline						
Index ID	**1961-1990 Baseline**		**2010-2039 Multi-GCM**		**2040-2069 Multi-GCM**		**2070-2099 Multi-GCM**		**Units**
Extreme temperature indices									
	AWAP	**Multi-GCM**	**SRES B1**	**SRES A2**	**SRES B1**	**SRES A2**	**SRES B1**	**SRES A2**	
FD	26	27 (26/28)	-9 (-10/-8)	-9 (-10/-8)	-12 (-15/-11)	-15 (-16/-14)	-16 (-18/-15)	-20 (-21/-20)	days
SU	12	12 (11/12)	4 (2/5)	4 (3/4)	7 (5/9)	10 (9/12)	11 (9/13)	20 (18/24)	days
ID	0	0 (0/0)	0 (0/0)	0 (0/0)	0 (0/0)	0 (0/0)	0 (0/0)	0 (0/0)	days
TR	0	0 (0/0)	0 (0/0)	0 (0/0)	0 (0/1)	1 (0/1)	1 (0/1)	2 (1/3)	days
HW	0	0 (0/0)	0 (0/0)	0 (0/0)	0 (0/0)	0 (0/0)	0 (0/0)	0 (0/1)	events
CW	0	0 (0/0)	0 (0/0)	0 (0/0)	0 (0/0)	0 (0/0)	0 (0/0)	0 (0/0)	events
TN10p	-	-	-4 (-5/-3)	-4 (-5/-3)	-5 (-7/-4)	-7 (-8/-5)	-7 (-8/-6)	-9 (-9/-8)	%
TX10p	-	-	-4 (-5/-3)	-4 (-5/-3)	-6 (-7/-4)	-7 (-8/-5)	-7 (-8/-6)	-9 (-9/-8)	%
TN90p	-	-	4 (2/5)	5 (3/6)	7 (6/9)	10 (8/13)	10 (8/13)	19 (16/22)	%
TX90p	-	-	3 (1/4)	3 (2/4)	5 (3/6)	7 (6/8)	7 (6/9)	13 (11/15)	%
WSDI	6	6 (5/6)	1 (1/1)	1 (1/2)	2 (2/2)	3 (3/4)	3 (2/4)	8 (6/9)	days
CSDI	7	6 (5/6)	-2 (-2/-2)	-2 (-2/-2)	-3 (-3/-3)	-3 (-4/-3)	-3 (-4/-3)	-4 (-4/-4)	days
ETR	32	32 (31/35)	2 (1/4)	0 (-2/1)	1 (0/2)	1 (0/2)	1 (0/3)	2 (1/3)	℃
Extreme precipitation indices									
	AWAP	**Multi-GCM**	**SRES B1**	**SRES A2**	**SRES B1**	**SRES A2**	**SRES B1**	**SRES A2**	
R1mm	160	158 (156/160)	-2 (-4/1)	-2 (-5/2)	-4 (-6/-1)	-4 (-8/1)	-6 (-9/-2)	-8 (-13/-1)	days
R10mm	42	42 (41/43)	0 (-1/2)	0 (-1/2)	-1 (-2/1)	-1 (-2/1)	-1 (-3/1)	-1 (-2/2)	days
R20mm	14	14 (14/15)	1 (0/1)	0 (0/1)	1 (0/1)	1 (0/2)	1 (0/2)	2 (1/3)	days
R95p	-	-	1 (-1/3)	0 (-1/3)	1 (-1/2)	1 (-1/4)	1 (-1/3)	2 (0/5)	days
R99p	-	-	0 (0/1)	0 (0/1)	0 (0/1)	1 (0/1)	1 (0/2)	1 (0/3)	days
R1D	51	52 (49/55)	2 (0/4)	3 (2/5)	4 (3/7)	5 (3/7)	5 (3/6)	9 (6/13)	mm
R5D	105	93 (88/98)	3 (0/6)	5 (3/9)	4 (1/7)	4 (1/7)	4 (2/8)	9 (4/15)	mm
CDD	17	14 (13/14)	0 (0/0)	0 (0/0)	0 (0/0)	0 (0/0)	0 (0/0)	0 (0/1)	days
CWD	14	10 (10/11)	0 (-1/0)	0 (0/0)	0 (-1/0)	0 (-1/0)	0 (-1/0)	0 (-1/0)	days
SDII	8	8 (8/8)	0 (0/0)	0 (0/0)	0 (0/0)	0 (0/0)	0 (0/0)	1 (0/1)	mm/d
PRCPTOT	1292	1281 1250/1303)	3 (-30/60)	0 (-21/56)	-2 (-41/33)	-2 (-48/66)	-7 (-55/64)	17 (-27/102)	mm

Hobart indices

Table B.2 As for Table B.1, but for Hobart (42.9° S/147.3° E).

Index ID	1961-1990 Baseline		Change relative to Baseline: 2010-2039 Multi-GCM		2040-2069 Multi-GCM		2070-2099 Multi-GCM		Units
Extreme temperature indices									
	AWAP	**Multi-GCM**	**SRES B1**	**SRES A2**	**SRES B1**	**SRES A2**	**SRES B1**	**SRES A2**	
FD	5	5 (4/5)	-2 (-2/-3)	-3 (-2/-3)	-3 (-3/-3)	-4 (-3/-4)	-4 (-4/-4)	-4 (-4/-5)	days
SU	18	18 (17/19)	4 (3/7)	4 (5/4)	8 (5/9)	10 (10/12)	11 (9/14)	21 (20/24)	days
ID	0	0 (0/0)	0 (0/0)	0 (0/0)	0 (0/0)	0 (0/0)	0 (0/0)	0 (0/0)	days
TR	0	0 (0/0)	0 (0/0)	0 (0/0)	0 (0/0)	0 (0/1)	0 (0/1)	1 (0/1)	days
HW	0	0 (0/0)	0 (0/0)	0 (0/0)	0 (0/0)	0 (0/0)	0 (0/0)	0 (0/0)	events
CW	0	0 (0/0)	0 (0/0)	0 (0/0)	0 (0/0)	0 (0/0)	0 (0/0)	0 (0/0)	events
TN10p	-	-	-4 (-6/-4)	-4 (-6/-3)	-6 (-8/-5)	-7 (-9/-6)	-7 (-9/-6)	-9 (-9/-8)	%
TX10p	-	-	-4 (-5/-3)	-4 (-5/-3)	-5 (-7/-4)	-6 (-8/-5)	-7 (-8/-6)	-8 (-9/-8)	%
TN90p	-	-	4 (3/5)	5 (3/5)	7 (6/9)	10 (8/13)	10 (8/14)	18 (16/22)	%
TX90p	-	-	2 (1/3)	2 (2/3)	4 (2/5)	5 (5/6)	5 (5/6)	9 (9/10)	%
WSDI	5	4 (4/4)	0 (0/1)	1 (1/1)	1 (1/1)	1 (1/2)	1 (1/2)	3 (2/3)	days
CSDI	8	6 (5/6)	-2 (-2/-1)	-2 (-2/-2)	-2 (-3/-2)	-3 (-3/-2)	-3 (-3/-2)	-4 (-4/-4)	days
ETR	33	34 (33/36)	2 (1/4)	-1 (-3/0)	2 (2/1)	1 (-1/4)	2 (-1/7)	3 (2/5)	°C
Extreme precipitation indices									
	AWAP	**Multi-GCM**	**SRES B1**	**SRES A2**	**SRES B1**	**SRES A2**	**SRES B1**	**SRES A2**	
R1mm	118	118 (115/119)	-3 (-5/0)	-3 (-5/0)	-4 (-6/-2)	-3 (-8/5)	-6 (-7/0)	-5 (-7/2)	days
R10mm	18	18 (18/18)	0 (-1/2)	0 (-1/1)	0 (-1/2)	0 (0/3)	0 (-1/2)	0 (0/2)	days
R20mm	5	5 (5/5)	0 (0/1)	1 (0/1)	0 (0/1)	1 (0/2)	0 (0/1)	1 (0/1)	days
R95p	-	-	0 (-1/2)	0 (-2/1)	0 (-1/2)	0 (-1/3)	0 (-1/2)	1 (-1/3)	days
R99p	-	-	0 (-1/1)	0 (0/1)	0 (0/1)	1 (0/2)	0 (0/2)	1 (0/2)	days
R1D	44	49 (44/56)	3 (1/0)	4 (4/5)	5 (3/5)	7 (6/6)	7 (7/8)	8 (1/8)	mm
R5D	73	78 (69/87)	1 (1/-2)	9 (12/13)	3 (0/6)	8 (10/6)	5 (7/4)	7 (2/10)	mm
CDD	18	16 (15/17)	0 (-1/0)	0 (-1/0)	0 (-1/-1)	0 (-1/0)	0 (0/0)	-1 (-1/0)	days
CWD	8	6 (6/7)	0 (0/-1)	0 (0/-1)	0 (-1/-1)	0 (-1/-1)	-1 (-1/-1)	-1 (-1/-1)	days
SDII	6	6 (6/6)	0 (0/0)	0 (0/0)	0 (0/0)	0 (0/0)	0 (0/0)	0 (0/1)	mm/d
PRCPTOT	681	678 (666/690)	0 (-27/38)	8 (-19/46)	0 (-20/35)	24 (-9/91)	-3 (-19/37)	17 (-30/90)	mm

Swansea indices

Table B.3 As for Table B.1, but for Swansea (42.0° S/148.1° E).

Index ID	1961-1990 Baseline		Change relative to Baseline: 2010-2039 Multi-GCM		2040-2069 Multi-GCM		2070-2099 Multi-GCM		Units
Extreme temperature indices									
	AWAP	**Multi-GCM**	**SRES B1**	**SRES A2**	**SRES B1**	**SRES A2**	**SRES B1**	**SRES A2**	
FD	9	8 (7/10)	-4 (-4/-4)	-4 (-5/-4)	-5 (-6/-5)	-6 (-6/-6)	-6 (-6/-7)	-7 (-7/-8)	days
SU	17	17 (17/18)	5 (2/9)	6 (5/7)	10 (6/13)	13 (12/14)	14 (11/18)	27 (22/33)	days
ID	0	0 (0/0)	0 (0/0)	0 (0/0)	0 (0/0)	0 (0/0)	0 (0/0)	0 (0/0)	days
TR	0	0 (0/0)	0 (0/0)	0 (0/0)	0 (0/1)	0 (0/1)	0 (0/1)	2 (1/2)	days
HW	0	0 (0/0)	0 (0/0)	0 (0/0)	0 (0/0)	0 (0/0)	0 (0/0)	0 (0/0)	events
CW	0	0 (0/0)	0 (0/0)	0 (0/0)	0 (0/0)	0 (0/0)	0 (0/0)	0 (0/0)	events
TN10p	-	-	-3 (-4/-2)	-4 (-5/-2)	-5 (-6/-3)	-6 (-8/-5)	-6 (-8/-5)	-8 (-9/-7)	%
TX10p	-	-	-4 (-5/-3)	-4 (-5/-3)	-6 (-8/-4)	-7 (-8/-5)	-7 (-9/-6)	-9 (-9/-8)	%
TN90p	-	-	4 (3/5)	5 (3/5)	7 (6/10)	10 (9/12)	11 (9/14)	19 (17/22)	%
TX90p	-	-	2 (2/3)	3 (2/4)	4 (3/6)	6 (5/7)	6 (5/9)	12 (10/14)	%
WSDI	5	5 (4/5)	1 (1/1)	1 (1/1)	1 (0/2)	2 (2/2)	2 (2/3)	4 (3/5)	days
CSDI	8	6 (5/6)	-2 (-2/-2)	-2 (-2/-2)	-3 (-3/-3)	-3 (-4/-3)	-3 (-4/-3)	-4 (-4/-4)	days
ETR	34	34 (31/36)	2 (2/4)	0 (0/2)	2 (2/3)	2 (2/4)	3 (1/4)	3 (2/6)	°C
Extreme precipitation indices									
	AWAP	**Multi-GCM**	**SRES B1**	**SRES A2**	**SRES B1**	**SRES A2**	**SRES B1**	**SRES A2**	
R1mm	93	89 (88/90)	0 (-2/5)	0 (-2/4)	0 (-1/3)	1 (-3/7)	0 (-2/1)	1 (0/2)	days
R10mm	16	15 (15/16)	1 (1/2)	1 (1/1)	1 (1/2)	2 (1/4)	1 (1/2)	3 (1/3)	days
R20mm	6	6 (5/6)	1 (0/1)	1 (0/1)	1 (0/2)	1 (0/2)	1 (0/1)	1 (0/3)	days
R95p	-	-	1 (-1/3)	1 (0/3)	2 (0/4)	2 (0/5)	2 (-1/2)	3 (0/4)	days
R99p	-	-	0 (0/1)	0 (0/1)	1 (0/1)	1 (-1/1)	0 (0/1)	1 (-1/2)	days
R1D	52	59 (54/64)	1 (-5/3)	7 (3/22)	8 (6/9)	9 (2/11)	4 (1/3)	12 (2/30)	mm
R5D	90	89 (81/99)	3 (-4/5)	13 (6/26)	13 (0/17)	16 (5/22)	5 (6/5)	13 (2/40)	mm
CDD	24	20 (20/21)	0 (0/-1)	-1 (-2/0)	0 (0/-1)	-1 (-3/1)	0 (-1/0)	-1 (-2/-1)	days
CWD	7	5 (5/5)	0 (0/0)	0 (0/1)	0 (0/1)	0 (0/1)	0 (0/0)	0 (0/1)	days
SDII	7	7 (7/7)	0 (0/0)	0 (0/1)	1 (0/1)	1 (0/1)	0 (0/1)	1 (0/2)	mm/d
PRCPTOT	609	590 (580/599)	30 (-7/45)	36 (17/63)	50 (23/102)	65 (4/121)	37 (6/67)	89 (18/162)	mm

St Helens indices

Table B.4 As for Table B.1, but for St Helens (41.3° S/148.2° E).

Index ID	1961-1990 Baseline		Change relative to Baseline: 2010-2039 Multi-GCM		2040-2069 Multi-GCM		2070-2099 Multi-GCM		Units
Extreme temperature indices									
	AWAP	**Multi-GCM**	**SRES B1**	**SRES A2**	**SRES B1**	**SRES A2**	**SRES B1**	**SRES A2**	
FD	7	7 (6/7)	-3 (-4/-3)	-3 (-4/-3)	-4 (-5/-4)	-5 (-5/-5)	-5 (-5/-6)	-6 (-6/-7)	days
SU	13	13 (12/14)	4 (2/6)	4 (3/4)	8 (4/12)	11 (10/11)	12 (9/15)	24 (19/30)	days
ID	0	0 (0/0)	0 (0/0)	0 (0/0)	0 (0/0)	0 (0/0)	0 (0/0)	0 (0/0)	days
TR	0	0 (0/0)	0 (0/0)	0 (0/0)	0 (0/0)	0 (0/1)	0 (0/1)	2 (1/3)	days
HW	0	0 (0/0)	0 (0/0)	0 (0/0)	0 (0/0)	0 (0/0)	0 (0/0)	0 (0/0)	events
CW	0	0 (0/0)	0 (0/0)	0 (0/0)	0 (0/0)	0 (0/0)	0 (0/0)	0 (0/0)	events
TN10p	-	-	-4 (-5/-2)	-4 (-5/-3)	-5 (-7/-4)	-7 (-8/-5)	-7 (-8/-6)	-9 (-9/-8)	%
TX10p	-	-	-5 (-6/-4)	-5 (-5/-4)	-6 (-8/-5)	-7 (-8/-6)	-8 (-9/-7)	-9 (-10/-9)	%
TN90p	-	-	5 (3/6)	5 (4/6)	8 (6/10)	11 (9/13)	12 (10/15)	20 (18/23)	%
TX90p	-	-	3 (1/4)	3 (2/4)	5 (2/8)	7 (6/9)	8 (5/11)	15 (13/17)	%
WSDI	5	5 (5/5)	1 (0/2)	1 (0/1)	2 (1/3)	3 (2/3)	3 (2/5)	7 (6/10)	days
CSDI	7	6 (6/7)	-2 (-3/-2)	-2 (-2/-3)	-3 (-4/-3)	-4 (-4/-4)	-4 (-4/-4)	-5 (-5/-5)	days
ETR	31	31 (30/34)	2 (1/2)	1 (-1/4)	1 (0/2)	3 (2/3)	1 (0/1)	1 (0/1)	°C
Extreme precipitation indices									
	AWAP	**Multi-GCM**	**SRES B1**	**SRES A2**	**SRES B1**	**SRES A2**	**SRES B1**	**SRES A2**	
R1mm	124	121 (119/122)	-1 (-3/6)	-2 (-4/5)	-4 (-7/1)	-1 (-8/6)	-4 (-7/0)	-3 (-5/-1)	days
R10mm	25	24 (24/25)	1 (-1/3)	1 (-2/4)	1 (-3/5)	2 (-2/4)	1 (-3/3)	2 (-2/6)	days
R20mm	9	9 (8/9)	0 (0/1)	0 (0/1)	0 (-1/1)	1 (-1/2)	1 (-1/3)	2 (0/4)	days
R95p	-	-	1 (-1/5)	1 (-2/5)	1 (-3/5)	1 (-2/5)	1 (-3/4)	2 (-2/7)	days
R99p	-	-	0 (-1/1)	1 (-1/2)	1 (0/2)	1 (0/2)	1 (0/2)	1 (0/3)	days
R1D	65	68 (60/74)	0 (-3/1)	3 (4/5)	7 (9/19)	5 (-1/10)	1 (-6/2)	11 (8/24)	mm
R5D	111	104 (97/113)	1 (-7/3)	7 (-1/11)	14 (2/22)	10 (-6/19)	2 (-14/4)	13 (6/37)	mm
CDD	21	16 (15/18)	0 (-1/0)	0 (0/-1)	0 (0/0)	0 (0/-1)	0 (1/-1)	0 (0/-1)	days
CWD	8	7 (7/7)	0 (0/0)	0 (0/1)	0 (-1/1)	0 (-1/0)	0 (-1/0)	0 (0/0)	days
SDII	7	7 (7/7)	0 (0/0)	0 (0/1)	1 (0/1)	1 (0/1)	0 (0/1)	1 (0/2)	mm/d
PRCPTOT	897	866 (853/875)	24 (-27/118)	31 (-21/122)	38 (-32/144)	62 (-63/141)	28 (-68/133)	91 (-10/218)	mm

Launceston indices

Table B.5 As for Table B.1, but for Launceston (41.6° S/147.2° E).

Index ID	1961-1990 Baseline		Change relative to Baseline: 2010-2039 Multi-GCM		2040-2069 Multi-GCM		2070-2099 Multi-GCM		Units
Extreme temperature indices									
	AWAP	Multi-GCM	SRES B1	SRES A2	SRES B1	SRES A2	SRES B1	SRES A2	
FD	29	30 (28/33)	-10 (-12/-11)	-11 (-13/-10)	-15 (-18/-15)	-20 (-21/-20)	-20 (-21/-21)	-27 (-27/-27)	days
SU	29	29 (28/31)	9 (3/15)	9 (6/11)	18 (10/23)	24 (20/26)	26 (23/33)	46 (41/53)	days
ID	0	0 (0/0)	0 (0/0)	0 (0/0)	0 (0/0)	0 (0/0)	0 (0/0)	0 (0/0)	days
TR	0	0 (0/0)	0 (0/0)	0 (0/0)	0 (0/0)	0 (0/0)	0 (0/1)	1 (1/2)	days
HW	1	1 (0/1)	0 (0/0)	0 (0/0)	1 (0/1)	1 (1/1)	1 (0/1)	1 (1/1)	events
CW	0	0 (0/0)	0 (0/0)	0 (0/0)	0 (0/0)	0 (0/0)	0 (0/0)	0 (0/0)	events
TN10p	-	-	-3 (-5/-2)	-3 (-5/-2)	-5 (-7/-3)	-6 (-8/-5)	-7 (-8/-6)	-8 (-9/-8)	%
TX10p	-	-	-4 (-5/-3)	-4 (-4/-3)	-5 (-7/-4)	-6 (-8/-5)	-7 (-9/-6)	-9 (-9/-8)	%
TN90p	-	-	4 (3/5)	5 (3/6)	7 (6/9)	10 (9/12)	10 (9/12)	18 (16/20)	%
TX90p	-	-	3 (0/5)	3 (1/4)	6 (3/8)	7 (5/8)	8 (6/10)	14 (11/16)	%
WSDI	7	7 (6/7)	2 (0/3)	2 (1/2)	3 (3/4)	4 (4/5)	4 (4/5)	9 (9/9)	days
CSDI	8	6 (6/7)	-2 (-2/-2)	-2 (-2/-2)	-3 (-3/-3)	-4 (-4/-3)	-4 (-4/-4)	-5 (-5/-5)	days
ETR	35	35 (33/38)	2 (3/2)	1 (1/1)	0 (0/0)	2 (2/4)	1 (1/1)	1 (2/3)	°C
Extreme precipitation indices									
	AWAP	Multi-GCM	SRES B1	SRES A2	SRES B1	SRES A2	SRES B1	SRES A2	
R1mm	100	98 (95/100)	-2 (-3/2)	-2 (-3/3)	-3 (-3/-2)	-3 (-5/0)	-5 (-4/-4)	-6 (-8/-1)	days
R10mm	19	18 (18/19)	1 (0/3)	0 (0/1)	1 (1/2)	1 (0/2)	1 (1/3)	3 (2/3)	days
R20mm	4	4 (4/4)	1 (0/1)	0 (0/1)	1 (0/1)	1 (0/2)	1 (0/2)	2 (1/3)	days
R95p	-	-	1 (0/4)	0 (-1/3)	1 (0/2)	1 (-1/4)	1 (0/3)	3 (1/4)	days
R99p	-	-	0 (0/1)	1 (0/1)	1 (0/1)	1 (0/2)	1 (0/2)	2 (1/3)	days
R1D	33	34 (31/36)	1 (2/5)	4 (4/4)	4 (5/4)	3 (1/4)	2 (1/5)	8 (6/12)	mm
R5D	61	53 (51/55)	3 (0/10)	6 (4/13)	4 (5/4)	2 (-6/5)	4 (2/5)	9 (3/15)	mm
CDD	24	20 (19/22)	1 (-1/1)	-1 (-1/-1)	0 (0/0)	-1 (-1/0)	0 (1/-1)	0 (0/0)	days
CWD	7	5 (5/6)	0 (0/0)	0 (0/0)	0 (0/0)	0 (0/0)	0 (0/-1)	0 (0/0)	days
SDII	7	7 (6/7)	0 (0/0)	0 (0/0)	0 (0/1)	0 (0/1)	0 (0/1)	1 (1/1)	mm/d
PRCPTOT	629	618 (608/628)	13 (-12/60)	9 (-10/42)	14 (-3/38)	20 (-25/67)	13 (-15/67)	46 (11/92)	mm

Devonport indices

Table B.6 As for Table B.1, but for Devonport (41.2° S/146.4° E).

Index ID	1961-1990 Baseline		Change relative to Baseline: 2010-2039 Multi-GCM		2040-2069 Multi-GCM		2070-2099 Multi-GCM		Units
Extreme temperature indices									
	AWAP	**Multi-GCM**	**SRES B1**	**SRES A2**	**SRES B1**	**SRES A2**	**SRES B1**	**SRES A2**	
FD	6	5 (4/5)	-3 (-3/-3)	-3 (-3/-4)	-4 (-4/-4)	-4 (-4/-4)	-4 (-4/-5)	-5 (-4/-5)	days
SU	10	8 (8/9)	5 (2/7)	5 (4/5)	9 (7/12)	13 (11/13)	15 (12/19)	31 (28/36)	days
ID	0	0 (0/0)	0 (0/0)	0 (0/0)	0 (0/0)	0 (0/0)	0 (0/0)	0 (0/0)	days
TR	0	0 (0/0)	0 (0/0)	0 (0/0)	0 (0/1)	1 (1/1)	1 (1/1)	4 (4/5)	days
HW	0	0 (0/0)	0 (0/0)	0 (0/0)	0 (0/0)	0 (0/0)	0 (0/0)	0 (0/0)	events
CW	0	0 (0/0)	0 (0/0)	0 (0/0)	0 (0/0)	0 (0/0)	0 (0/0)	0 (0/0)	events
TN10p	-	-	-4 (-5/-2)	-4 (-5/-2)	-5 (-7/-3)	-6 (-8/-5)	-7 (-8/-6)	-9 (-9/-8)	%
TX10p	-	-	-4 (-6/-3)	-4 (-5/-4)	-6 (-8/-5)	-7 (-9/-6)	-7 (-9/-7)	-9 (-10/-8)	%
TN90p	-	-	5 (2/6)	5 (3/6)	8 (6/9)	11 (9/14)	11 (9/14)	19 (16/21)	%
TX90p	-	-	4 (2/6)	5 (4/5)	7 (5/10)	10 (9/11)	11 (9/13)	19 (18/21)	%
WSDI	6	6 (6/7)	2 (1/3)	3 (2/4)	4 (3/6)	7 (5/8)	7 (4/10)	19 (15/21)	days
CSDI	7	6 (6/6)	-2 (-3/-1)	-2 (-3/-2)	-3 (-3/-2)	-4 (-4/-3)	-4 (-4/-4)	-5 (-5/-4)	days
ETR	31	31 (29/32)	-1 (-2/0)	-2 (-3/-2)	-1 (-1/1)	-1 (-2/0)	-1 (-1/1)	-1 (-1/-1)	℃
Extreme precipitation indices									
	AWAP	**Multi-GCM**	**SRES B1**	**SRES A2**	**SRES B1**	**SRES A2**	**SRES B1**	**SRES A2**	
R1mm	112	111 (107/113)	-2 (-3/2)	-2 (-2/1)	-3 (-3/-2)	-3 (-4/0)	-5 (-5/-4)	-7 (-7/-2)	days
R10mm	29	28 (28/29)	0 (-2/1)	-1 (-2/-1)	-1 (-2/0)	0 (-2/1)	-1 (-2/1)	0 (-1/2)	days
R20mm	9	8 (8/9)	1 (0/1)	1 (-1/1)	1 (0/1)	1 (1/2)	2 (0/3)	2 (1/4)	days
R95p	-	-	1 (-1/3)	0 (-1/1)	1 (0/2)	1 (0/3)	1 (-1/3)	2 (0/4)	days
R99p	-	-	0 (0/1)	0 (0/1)	1 (0/1)	1 (0/2)	1 (0/1)	2 (1/3)	days
R1D	47	47 (44/50)	1 (1/0)	2 (4/1)	4 (4/5)	2 (2/2)	3 (2/2)	9 (7/10)	mm
R5D	89	71 (67/78)	2 (0/-1)	3 (2/0)	5 (5/4)	1 (-3/-1)	6 (6/6)	13 (10/15)	mm
CDD	24	20 (19/22)	0 (-1/0)	0 (-1/-1)	0 (-1/1)	0 (-1/-1)	0 (-1/-2)	0 (-1/0)	days
CWD	8	6 (6/6)	0 (-1/0)	0 (0/0)	0 (-1/0)	0 (-1/0)	-1 (-1/-1)	-1 (-1/-1)	days
SDII	8	8 (8/8)	0 (0/0)	0 (0/0)	0 (0/0)	0 (0/0)	0 (0/1)	1 (1/2)	mm/d
PRCPTOT	866	851 (833/873)	0 (-32/40)	-8 (-19/12)	9 (-13/28)	11 (-21/59)	0 (-20/55)	40 (7/77)	mm

Strahan indices

Table B.7 As for Table B.1, but for Strahan (42.2° S/145.4° E).

Index ID	1961-1990 Baseline		Change relative to Baseline: 2010-2039 Multi-GCM		2040-2069 Multi-GCM		2070-2099 Multi-GCM		Units
Extreme temperature indices									
	AWAP	**Multi-GCM**	**SRES B1**	**SRES A2**	**SRES B1**	**SRES A2**	**SRES B1**	**SRES A2**	
FD	6	5 (5/6)	-3 (-3/-3)	-3 (-3/-3)	-3 (-3/-3)	-4 (-4/-4)	-4 (-4/-4)	-5 (-4/-5)	days
SU	19	19 (18/19)	5 (2/7)	5 (5/6)	9 (6/10)	12 (10/14)	12 (11/13)	23 (22/25)	days
ID	0	0 (0/0)	0 (0/0)	0 (0/0)	0 (0/0)	0 (0/0)	0 (0/0)	0 (0/0)	days
TR	0	0 (0/0)	0 (0/0)	0 (0/0)	0 (0/0)	0 (0/1)	0 (0/1)	1 (1/2)	days
HW	0	0 (0/0)	0 (0/0)	0 (0/0)	0 (0/0)	0 (0/0)	0 (0/0)	1 (1/1)	events
CW	0	0 (0/0)	0 (0/0)	0 (0/0)	0 (0/0)	0 (0/0)	0 (0/0)	0 (0/0)	events
TN10p	-	-	-4 (-5/-3)	-4 (-5/-2)	-6 (-7/-4)	-7 (-8/-5)	-7 (-8/-6)	-8 (-9/-8)	%
TX10p	-	-	-4 (-5/-3)	-3 (-5/-2)	-5 (-6/-3)	-6 (-8/-4)	-6 (-8/-5)	-8 (-9/-7)	%
TN90p	-	-	3 (2/4)	4 (2/6)	6 (5/8)	9 (6/14)	9 (7/12)	17 (13/22)	%
TX90p	-	-	2 (0/2)	2 (2/3)	4 (3/4)	5 (4/6)	5 (4/6)	10 (8/10)	%
WSDI	5	5 (4/5)	1 (0/0)	1 (1/1)	1 (1/1)	2 (2/2)	2 (2/2)	3 (4/4)	days
CSDI	6	5 (5/6)	-2 (-2/-2)	-1 (-2/-1)	-2 (-2/-2)	-2 (-3/-2)	-3 (-3/-3)	-3 (-4/-3)	days
ETR	32	33 (32/35)	4 (1/4)	0 (-1/-1)	2 (1/3)	1 (1/2)	2 (0/3)	3 (2/4)	°C
Extreme precipitation indices									
	AWAP	**Multi-GCM**	**SRES B1**	**SRES A2**	**SRES B1**	**SRES A2**	**SRES B1**	**SRES A2**	
R1mm	209	213 (211/215)	-3 (-5/0)	-3 (-5/0)	-5 (-7/-3)	-6 (-8/0)	-7 (-11/-4)	-9 (-22/0)	days
R10mm	77	76 (75/77)	0 (-2/2)	-1 (-2/4)	0 (-2/1)	-2 (-5/4)	-2 (-7/3)	-2 (-4/3)	days
R20mm	23	23 (22/25)	2 (0/2)	1 (2/1)	2 (1/2)	2 (1/3)	3 (2/4)	5 (4/7)	days
R95p	-	-	2 (-2/3)	1 (-1/3)	2 (0/3)	2 (-1/5)	3 (0/5)	5 (2/7)	days
R99p	-	-	1 (0/2)	1 (0/2)	1 (0/1)	1 (0/2)	2 (0/4)	3 (1/3)	days
R1D	49	49 (49/50)	3 (-1/7)	4 (2/7)	4 (1/6)	4 (2/7)	7 (4/11)	11 (7/15)	mm
R5D	115	106 (103/108)	6 (1/15)	7 (5/13)	4 (-1/8)	5 (3/12)	10 (6/21)	14 (10/20)	mm
CDD	11	9 (9/10)	0 (0/1)	0 (0/0)	0 (-1/0)	1 (0/1)	0 (0/1)	1 (1/1)	days
CWD	19	16 (15/18)	0 (-1/0)	0 (-1/-1)	0 (-1/-1)	0 (-1/-1)	0 (-1/-1)	0 (-2/1)	days
SDII	10	10 (9/10)	0 (0/0)	0 (0/0)	0 (0/0)	0 (0/1)	0 (0/1)	1 (0/1)	mm/d
PRCPTOT	2001	2022 (1963/2052)	17 (-9/72)	17 (33/89)	14 (-32/39)	1 (-11/118)	18 (-55/106)	41 (47/177)	mm

Strathgordon indices

Table B.8 As for Table B.1, but for Strathgordon (42.8° S/146.1° E).

Index ID	1961-1990 Baseline		Change relative to Baseline: 2010-2039 Multi-GCM		2040-2069 Multi-GCM		2070-2099 Multi-GCM		Units
Extreme temperature indices									
	AWAP	**Multi-GCM**	**SRES B1**	**SRES A2**	**SRES B1**	**SRES A2**	**SRES B1**	**SRES A2**	
FD	16	15(14/16)	-5 (-6/-5)	-5 (-5/-5)	-7 (-8/-6)	-8 (-10/-8)	-9 (-11/-8)	-12 (-13/-12)	days
SU	14	14 (14/15)	4 (1/5)	4 (4/5)	7 (5/9)	10 (10/13)	11 (9/12)	21 (18/25)	days
ID	0	0 (0/0)	0 (0/0)	0 (0/0)	0 (0/0)	0 (0/0)	0 (0/0)	0 (0/0)	days
TR	0	0 (0/0)	0 (0/0)	0 (0/0)	0 (0/0)	0 (0/0)	0 (0/0)	0 (0/0)	days
HW	0	0 (0/0)	0 (0/0)	0 (0/0)	0 (0/0)	0 (0/1)	0 (0/0)	1 (0/1)	events
CW	0	0 (0/0)	0 (0/0)	0 (0/0)	0 (0/0)	0 (0/0)	0 (0/0)	0 (0/0)	events
TN10p	-	-	-3 (-5/-3)	-3 (-4/-2)	-4 (-6/-3)	-5 (-6/-4)	-6 (-7/-5)	-7 (-8/-6)	%
TX10p	-	-	-3 (-5/-2)	-3 (-4/-2)	-5 (-7/-3)	-6 (-8/-4)	-6 (-8/-5)	-8 (-9/-7)	%
TN90p	-	-	4 (3/5)	4 (4/5)	7 (6/8)	10 (7/13)	10 (7/12)	18 (15/22)	%
TX90p	-	-	2 (1/3)	2 (2/3)	4 (3/4)	5 (5/6)	5 (4/5)	9 (9/11)	%
WSDI	5	5 (5/6)	0 (0/0)	0 (0/0)	1 (1/1)	1 (1/2)	1 (1/1)	3 (2/3)	days
CSDI	7	5 (5/6)	-1 (-2/-2)	-1 (-1/-2)	-2 (-2/-2)	-2 (-3/-3)	-3 (-3/-3)	-3 (-3/-4)	days
ETR	34	34 (32/36)	3 (3/3)	0 (-2/-1)	1 (1/2)	1 (0/1)	1 (0/4)	2 (1/4)	°C
Extreme precipitation indices									
	AWAP	**Multi-GCM**	**SRES B1**	**SRES A2**	**SRES B1**	**SRES A2**	**SRES B1**	**SRES A2**	
R1mm	224	223 (221/224)	-1 (-5/2)	-1 (-6/3)	-1 (-5/0)	-4 (-8/1)	-2 (-10/3)	-5 (-17/2)	days
R10mm	81	82 (80/84)	-1 (-1/0)	-2 (-1/2)	-2 (-4/0)	-3 (-4/-1)	-4 (-6/0)	-5 (-7/-1)	days
R20mm	33	34 (33/35)	1 (1/2)	0 (-1/1)	1 (0/1)	0 (0/0)	1 (0/2)	1 (1/3)	days
R95p	-	-	1 (-2/3)	0 (-2/3)	0 (-2/2)	0 (-1/2)	1 (-1/3)	2 (0/5)	days
R99p	-	-	1 (0/2)	0 (0/1)	0 (-1/2)	0 (0/1)	1 (0/3)	2 (1/2)	days
R1D	65	65 (63/66)	1 (1/3)	2 (1/3)	3 (3/6)	5 (4/9)	7 (2/14)	8 (7/10)	mm
R5D	155	135 (129/139)	7 (4/12)	5 (3/9)	1 (-7/8)	2 (6/4)	7 (4/19)	6 (-3/11)	mm
CDD	11	8 (8/9)	0 (0/0)	0 (0/0)	0 (0/0)	0 (0/0)	0 (0/0)	0 (0/1)	days
CWD	22	16 (15/17)	0 (-1/1)	0 (0/0)	0 (0/0)	0 (1/1)	1 (-1/2)	1 (0/3)	days
SDII	10	11 (10/11)	0 (0/0)	0 (0/0)	0 (0/0)	0 (0/0)	0 (0/0)	0 (0/0)	mm/d
PRCPTOT	2296	2321 (2261/2354)	15 (-8/72)	-1 (-8/79)	-6 (-48/10)	-38 (-74/16)	0 (-92/113)	-17 (-65/100)	mm

Miena/Liawenee indices

Table B.9 As for Table B.1, but for Miena/Liawenee (42.0° S/146.7° E).

Index ID	1961-1990 Baseline		Change relative to Baseline: 2010-2039 Multi-GCM		2040-2069 Multi-GCM		2070-2099 Multi-GCM		Units
Extreme temperature indices									
	AWAP	**Multi-GCM**	**SRES B1**	**SRES A2**	**SRES B1**	**SRES A2**	**SRES B1**	**SRES A2**	
FD	118	121 (119/124)	-23 (-25/-21)	-23 (-24/-19)	-34 (-41/-32)	-42 (-48/-39)	-44 (-54/-41)	-63 (-72/-57)	days
SU	4	4 (3/4)	2 (0/2)	1 (1/2)	3 (3/4)	4 (4/6)	5 (4/5)	9 (8/11)	days
ID	0	0 (0/1)	0 (0/0)	0 (0/0)	0 (0/0)	0 (0/0)	0 (0/0)	0 (0/0)	days
TR	0	0 (0/0)	0 (0/0)	0 (0/0)	0 (0/0)	0 (0/0)	0 (0/0)	0 (0/0)	days
HW	0	0 (0/0)	0 (0/0)	0 (0/0)	0 (0/0)	0 (0/0)	0 (0/0)	0 (0/0)	events
CW	2	2 (2/2)	-1 (-1/-1)	-1 (-1/-1)	-1 (-1/-1)	-1 (-1/-1)	-2 (-1/-2)	-2 (-2/-2)	events
TN10p	-	-	-3 (-5/-2)	-3 (-4/-2)	-5 (-7/-4)	-6 (-7/-5)	-6 (-8/-5)	-8 (-9/-7)	%
TX10p	-	-	-4 (-6/-3)	-4 (-5/-4)	-6 (-7/-5)	-7 (-8/-5)	-7 (-8/-6)	-9 (-9/-8)	%
TN90p	-	-	4 (2/4)	4 (3/5)	7 (6/9)	10 (9/11)	10 (8/12)	18 (16/21)	%
TX90p	-	-	2 (1/3)	3 (1/3)	5 (3/5)	6 (5/7)	7 (5/8)	12 (10/13)	%
WSDI	7	6 (6/7)	1 (0/1)	1 (1/1)	1 (1/2)	2 (2/3)	2 (2/2)	5 (5/6)	days
CSDI	8	7 (7/7)	-3 (-3/-2)	-3 (-3/-3)	-4 (-4/-3)	-4 (-5/-4)	-4 (-5/-4)	-5 (-5/-5)	days
ETR	33	33 (32/36)	5 (3/4)	1 (0/1)	3 (2/3)	2 (1/4)	4 (2/5)	3 (0/5)	°C
Extreme precipitation indices									
	AWAP	**Multi-GCM**	**SRES B1**	**SRES A2**	**SRES B1**	**SRES A2**	**SRES B1**	**SRES A2**	
R1mm	155	153 (150/157)	-4 (-5/-5)	-6 (-10/-1)	-10 (-14/-11)	-12 (-16/-6)	-14 (-15/-12)	-17 (-25/-10)	days
R10mm	32	32 (31/33)	-1 (-3/1)	-2 (-4/0)	-3 (-5/-1)	-3 (-6/-1)	-4 (-6/-3)	-5 (-8/-2)	days
R20mm	9	8 (8/9)	0 (0/0)	0 (-1/0)	-1 (-1/0)	-1 (-2/0)	-1 (-1/-1)	-1 (-1/0)	days
R95p	-	-	0 (-2/1)	-1 (-4/1)	-2 (-3/0)	-2 (-5/0)	-2 (-4/-1)	-3 (-6/0)	days
R99p	-	-	0 (-1/0)	0 (-1/1)	0 (-1/0)	0 (-1/0)	-1 (-1/0)	0 (-1/1)	days
R1D	46	49 (46/54)	3 (-7/13)	4 (-2/5)	3 (3/2)	4 (1/8)	3 (-3/6)	8 (2/19)	mm
R5D	92	83 (79/88)	4 (-8/13)	5 (-5/10)	-1 (0/-2)	2 (-6/3)	-1 (-6/4)	5 (-5/20)	mm
CDD	16	13 (13/14)	0 (0/0)	0 (0/0)	1 (1/1)	1 (-1/1)	1 (0/1)	1 (0/3)	days
CWD	11	8 (8/9)	0 (-1/0)	-1 (-1/0)	-1 (-1/-1)	-1 (-1/-1)	-1 (-1/-1)	-1 (-2/-1)	days
SDII	7	7 (7/7)	0 (0/0)	0 (0/0)	0 (0/0)	0 (0/0)	0 (0/0)	0 (0/0)	mm/d
PRCPTOT	1026	1026 (1005/1044)	-33 (-75/18)	-41 (-91/35)	-75 (-114/-40)	-77 (-135/-10)	-107 (-140/-47)	-119 (-185/-8)	mm

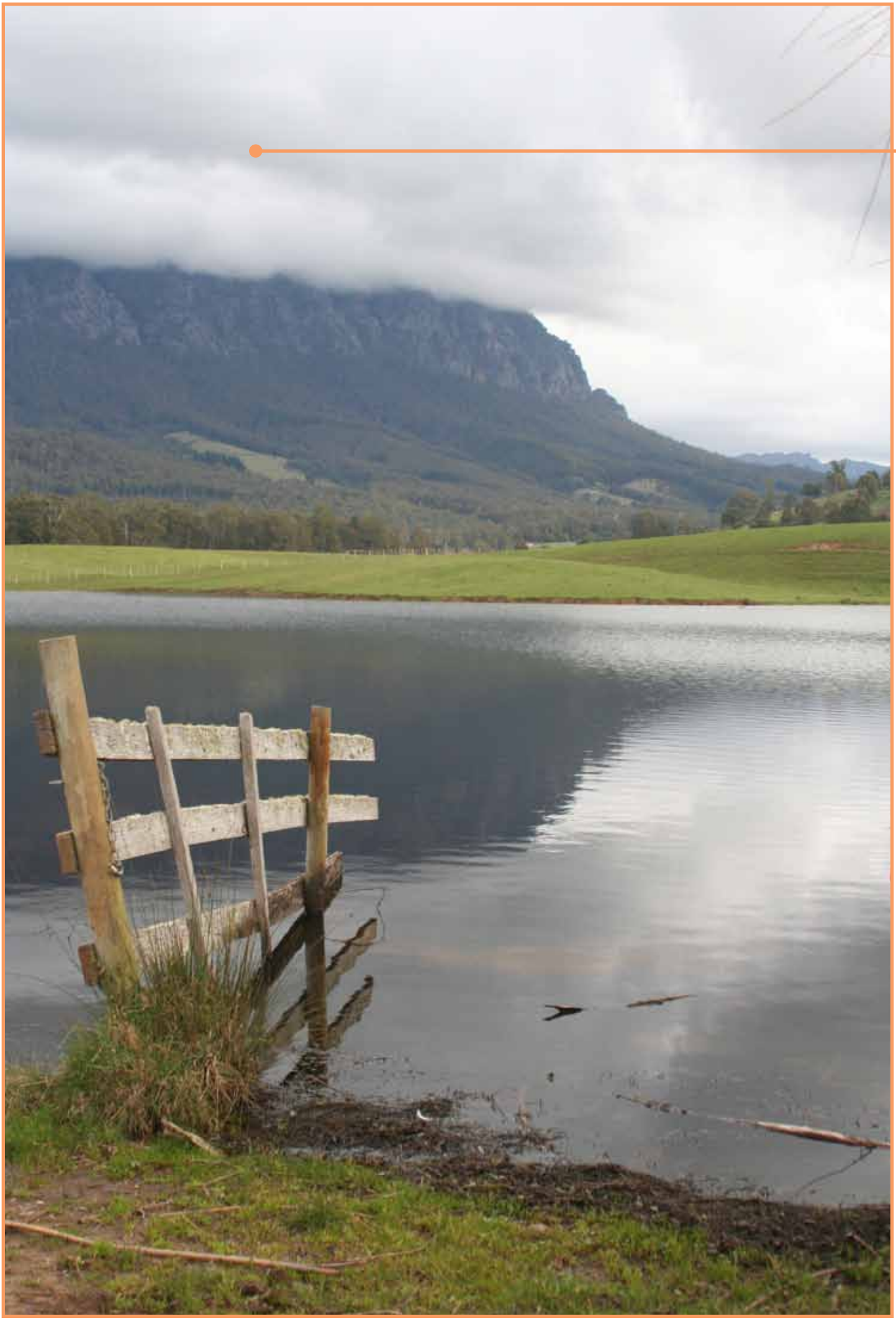

Project Acknowledgements

The Climate Futures for Tasmania project was funded primarily by the State Government of Tasmania, the Australian Government's Commonwealth Environment Research Facilities Program and Natural Disaster Mitigation Program. The project also received additional funding support from Hydro Tasmania.

Scientific leadership and contributions were made from a consortium of organisations including: Antarctic Climate & Ecosystems Cooperative Research Centre, Tasmanian Department of Primary Industries, Parks, Water and Environment, Tasmanian State Emergency Service, Hydro Tasmania Consulting, Geoscience Australia, Bureau of Meteorology, CSIRO, Tasmanian Partnership for Advanced Computing, Tasmanian Institute of Agricultural Research and the University of Tasmania.

The generation of the Climate Futures for Tasmania climate simulations was commissioned by the Antarctic Climate & Ecosystems Cooperative Research Centre (ACE CRC), as part of its Climate Futures for Tasmania project. The climate simulations are freely available through the Tasmanian Partnership for Advanced Computing digital library at www.tpac.org.au.

Climate Futures for Tasmania is possible with support through funding and research of a consortium of state and national partners.

Climate Futures for Tasmania is possible with support through funding and research of a consortium of state and national partners.

ANTARCTIC CLIMATE & ECOSYSTEMS CRC

Australian Government
Department of Sustainability, Environment, Water, Population and Communities

Tasmania
Explore the possibilities

Australian Government
Attorney-General's Department

STATE EMERGENCY SERVICE TASMANIA

Australian Government
Bureau of Meteorology

Hydro Tasmania
The power of natural thinking

Australian Government
Geoscience Australia

CSIRO

UTAS

tiar
TASMANIAN INSTITUTE OF AGRICULTURAL RESEARCH

TPAC